Geochronology and geochemistry of calcite-filled fractures, southern Ontario: Insight into Cretaceous deformation

Jennifer Spalding

Supervisor: David Schneider, University of Ottawa

A thesis submitted to the Faculty of Graduate and Postdoctoral Studies in partial fulfillment of the requirements for the degree of

Master of Science in Earth Sciences

University of Ottawa

Ottawa, Canada

January 2018

© Jennifer Spalding, Ottawa, Canada, 2018

Abstract

The St. Lawrence Platform is located along the northern shoreline of Lake Ontario, currently in an intra-cratonic setting exposing relatively flat-lying middle Ordovician sedimentary strata. The purpose of this study is to gain insight on recent brittle deformation events that have deformed the bedrock. Based on structural field observations, broadly trending E-W extensional joints are the youngest stress recorded in the bedrock. These joints are partially filled and sealed with calcite mineralization and were strategically sampled to gain insight on the source and timing of fluid flow. Trace element geochemistry and stable isotope (δ18O and δ13C) analysis on calcite mineralization indicate that their compositions are analogous to the host rock, thus, fluids originate from connate fluids that were released from pore space during deformation. In addition, U-Pb geochronology via LA-ICP-MS methods yield a model age of 101 ± 6 Ma (MSWD: 2.3). The date of calcite crystallization is contemporaneous with the establishment of North America's modern compressive stress field, and is linked to a Cretaceous tectonic plate reorganization event that was global in scale. This study demonstrates that calcite veins can serve as a tool to date brittle deformation in limestone, which could have direct applications in hydrocarbon exploration, paleohydrology, and the consideration for locating sites to host deep geological repositories.

Résumer

La plate-forme du Saint-Laurent est située au nord-est du lac Ontario, dans une région intra-cratonique qui expose la stratigraphie sédimentaire horizontale de l'Ordovicien moyen. Le but de cette étude est de comprendre l'événement le plus récent et qui a généré la déformation cassante dans le substrat rocheux. D'après les observations de terrain, les joints ouverts dans un contexte extensif orienté E-W sont les structures qui enregistrent le stress le plus récent. Ces joints, parfois remplis avec de la calcite, forment des veines qui ont été échantillonnées afin de mieux comprendre le réservoir source de ces fluides et contraindre leurs âges de cristallisation. La géochimie des éléments traces et les isotopes stables (δ18O et δ13C) indiquent que les veines de calcite ont la même composition que la roche encaissante. Ces fluides ont été libérés de l'espace poreux des roches encaissante lors de la déformation qui ont par la suite cristallisé des veines de calcite. La géochronologie U-Pb, par les méthodes LA-ICP-MS, révèle un âge modèle de 101 ± 6 Ma (MSWD: 2.3). Cet âge est en accord avec la mise en place du champ de contrainte moderne

en Amérique du Nord, liée à un événement global durant le Crétacé qui a modifiés le mouvement relatif de toutes les plaques tectoniques. Cette étude démontre que les veines de calcite peuvent servir d’outils pour dater la déformation cassante dans le calcaire. Ceci peut avoir des applications dans l'exploration des hydrocarbures, la paléohydrologie, et la considération de sites souterraine pour l’entreposage de déchets dangereux.

Table of Contents

Geochronology and geochemistry of calcite-filled fractures, southern Ontario: Insight into Cretaceous deformation ..... **i**

Acknowledgements ..... **v**

Abstract ..... **vi**

1. Introduction **1**

2. Structural architecture **2**

3. Stratigraphic architecture **6**

4. Paleo-stress in eastern North America **7**

5. Previous work: brittle tectonics **8**

6. Previous work: geochronology and thermochronology **11**

7. New field observations **15**

7.1 Structural observations **19**

7.2 Calcite mineralization and sample collection **23**

8. Petrographic analysis **24**

8.1 Vein structure **25**

8.2 Microtectonics **27**

9. Trace element geochemistry **29**

9.1 Results: mineral separate analysis **31**

9.2 Results: in situ analysis **33**

10. Stable isotope geochemistry **40**

10.1 Results **41**

11. U-Pb geochronology **45**

11.1 Results **47**

12. Discussion **49**

12.1 Structures **49**

12.2 Geochemistry **53**

12.3 Brittle deformation and mineralization at c. 100 Ma **56**

12.4 Cretaceous global plate reorganization event **60**

13. Conclusions **62**

14. Recommendations for future work **62**

15. References **64**

16. Appendix **73**

Acknowledgements

I would like to thank my thesis supervisor Dr. David A. Schneider for his continued guidance, and endless patience throughout years. Dave allowed this paper to be my own work, while steering me in the right the direction when needed, which allowed me to become a confident geoscientist. Second, I thank Dr. Julie Brown from the Canadian Nuclear Safety Commission for proposing this project, insight as well as funding. I am fortunate for opportunities to collaborate with several researchers during this project, of these I would like to thank Drs. Don Davis and Chelsea Sutcliffe (University of Toronto) aiding with data reduction for U-Pb geochronology; Drs. Cécile Gautheron and Rosella Pinna for inviting me to use their facilities to conduct (U-Th)/He analysis (l'Université de Paris Sud); Drs. Duane C. Petts and Samuel Morfin (University of Ottawa) for their assistance on the LA-ICP-MS and discussions regarding implications of trace element geochemistry; Glenn Poirier for providing assistance to the use of SEM and the CL-microscope; the G.G. Hatch stable isotope laboratory; the workers in limestone quarries throughout Prince Edward County for allowing site access; my field assistant Cassy Powell, and finally, IKEA for providing limitless amounts of coffee and an ideal work environment for writing this (entire) thesis. I believe it is important to strike a balance with life outside the dark depths of the lab and for my own sanity I cannot stress enough the importance of weekly gatherings with friends to "hool-nation" and "da pump," and most importantly my parents for their unconditional love and support.

Abstract

Eastern North America preserves brittle deformation associated to tectonism since the assembly of the Canadian Shield in the Mesoproterozoic. In southern Ontario, middle Ordovician limestone overlies the Mesoproterozoic Canadian shield. Both the basement and cover rock are transected by NE-SW trending fault zones, including the Salmon River and Picton faults. Resolving the absolute timing of brittle deformation is a challenge since the classical chronometers required for analyses are often absent in limestone. Based on terminating joint relationships, the youngest stress recorded in the bedrock are vertical joints with a broad E-W orientation that hosts 1-7 mm thick calcite veins. In this study, we couple LA-ICP-MS U-Pb dating of calcite veins, with geochemical and microstructural analysis to tackle this dilemma and constrain the most recent deformation event. Some calcite veins preserve sub-horizontal slickensides and μm- to mm-scale offset. Calcite $\delta^{18}O$ and $\delta^{13}C$ values are analogous to the bulk composition of Middle to Late Ordovician limestones, suggesting vein material originates from connate fluids. Trace element geochemistry is highly variable, and REE profiles generally follow the moderately negative slope similar to the continental crust. LA-ICP-MS U-Pb dating on calcite yield model ages of 110.7 ± 6.8 Ma (MSWD: 0.53; n: 16) to 81.4 ± 8.3 Ma (MSWD: 2.6; n: 17). All veins are interpreted to have formed from the same event and have been regressed together, yielding an age of 101 ± 6 Ma (MSWD: 2.3). These veins are ~200 km to the west, and slightly younger than, the c. 140-120 Ma alkaline igneous rocks which mark the surface trace of the Great Meteor Hotspot and do not reflect this event. Instead, the ages are consistent with the timing of the most recent reorientation of North America's compressive stress field, which is attributed to a change in spreading direction along the Northern Mid Atlantic ridge and is linked to a global plate reorganization event from 105-100 Ma. These results suggest that the most recent redistribution of lateral stress was not a passive event, and generated brittle deformation and fluid flow ~500 km inland of North Americas Atlantic passive margin. LA-ICP-MS U-Pb dating of vein calcite was successful, and coupled with other geochemical information, can yield primary information about the timing and source of fluid flow through joints and fractures, which has direct applications to reducing risk associated with characterizing hydrocarbon reservoirs and deep geological repositories for nuclear waste.

1. Introduction

Since the amalgamation of the Canadian Shield in the Mesoproterozoic, eastern North America has witnessed the assembly and break up of two supercontinents, and this tectonism has generated regional, brittle deformation patterns (e.g. Kumarapeli, 1985; Hanmer and McEachern, 1992; Daneshfar and Benn, 2002). Previous investigations have focussed on linking brittle structures to known tectonic events, and identifying structures that are susceptible to reactivation under the current stress field as a part of seismic hazard assessments (e.g. Wallach et al., 1998; Mitchell, 2007). The current stress field in eastern North America is dominated by ENE-WSW directed ridge push associated with the expansion of the Atlantic basin, and was acquired during the Cretaceous due to a change in spreading direction along the northern Mid-Atlantic, causing North America to undergo a clockwise rotation (Lo, 1978; Adams and Bell, 1991). Far field tectonic stresses such as ridge push and changes in plate motion are difficult to resolve from brittle structures in continental settings.

In the St. Lawrence Lowlands of southeastern Canada, Paleozoic sedimentary strata unconformably overlays the Precambrian crystalline rocks of the southern Canadian Shield. NE-SW trending faults are structurally aligned with ancient deformation zones in the basement and can be linked though a bathymetric high across Lake Ontario to seismically active fault systems in the Central Lowlands and Appalachian Plateau of the US (Anderson and Lewis, 1975; McFall and Allam, 1990). In the St. Lawrence Lowlands, seismicity is sometimes hosted along NE-SW trending basement structures, however it is more commonly hosted along basement structures of the Ottawa-Bonnechere graben (OBG) with various orientations, or distant to any mapped structures. It remains ambiguous how lateral stress is distributed, and how NE-SW trending structures are effected.

Terminating joints and cross-cutting relationships indicate that joint populations with a broad E-W trend are the youngest structures, likely having propagated under the current stress regime and can be traced as far west as the midcontinent (Engelder, 1982). The bedrock along northern Lake Ontario preserves several systematic populations of joints that are locally filled and sealed with secondary calcite mineralization. The calcite mineralization indicate that fluid flow occurred syn- to post-deformation and the veins possess information on the source of fluid, as well as the timing of fluid flow which may reveal a better understanding of the deformation event. Aside from basement-rooted faults and joint sets, the sedimentary strata remain relatively undeformed, slightly

tilted to the south due to residence along the northern margin of the of the Appalachian Basin (Liberty, 1960).

The purpose of this investigation is to understand regional brittle deformation in an intra-cratonic setting, which is classically interpreted as tectonically stable, where calcite veins were used as a tool to constrain the absolute timing of deformation in the shallow crust. Integrating these results with structural observations, stable isotope analysis and trace element geochemistry can reveal the magnitude of this deformation event. The rocks of interest for this investigation include exposures along the northern shore of Lake Ontario consisting of Middle Ordovician limestone that unconformably resides on the Mesoproterozoic Grenville Province. The St. Lawrence Lowlands is an ideal location since the stratigraphy is relatively undeformed and the underlying basement structures provide the crustal pre-conditioning for tectonic reactivation and the opportunity to correlate joint propagation to underlying structures.

2. Structural architecture

The southeastern Canadian Shield consists of an Archean craton as well as a few major terranes that successively accreted to Laurentia in the Mesoproterozoic (**Figure 1**; Piper, 1975; Hoffman, 1991). Collectively, these collisions define the Grenville orogeny, and lead to the assembly of the supercontinent Rodinia. Orogeny began as an ancient Andean-style margin, composed of reworked Archean crust and juvenile material that has undergone crustal thickening and intense shortening (Carr et al., 2000). Two major NE-SW trending shear zones delineate these ancient terrane boundaries: the Central Metasedimentary Belt boundary tectonic zone (CMBbtz) and the Robinson Lake mylonite zone (RLmz; **Figure 1**). The CMBtz is composed of highly strained mylonitic gneisses that have undergone upper amphibolite facies metamorphism (Hanmer and Ciesielski, 1984; Carr et al., 2000). The RLmz is composed predominantly of greenschist facies marble and felsic to mafic mylonites, overprinted by breccias and ultra-cataclasites (Busch and van der Pluijm, 1996; Easton 1998; Carr et al., 2000). Locally, the RLmz forms an escarpment in the modern landscape that reaches heights of 30-60 m.

Major faults within these shear zones project southward into the Paleozoic sedimentary strata of the St. Lawrence Lowlands, that also coincide with magnetic and gravity lineaments, suggesting that they are probably basement-rooted structures that were inherited during fault reactivation (Ontario Geological Survey, 1991b; Wallach et al., 1998; Boyce and Morris, 2002).

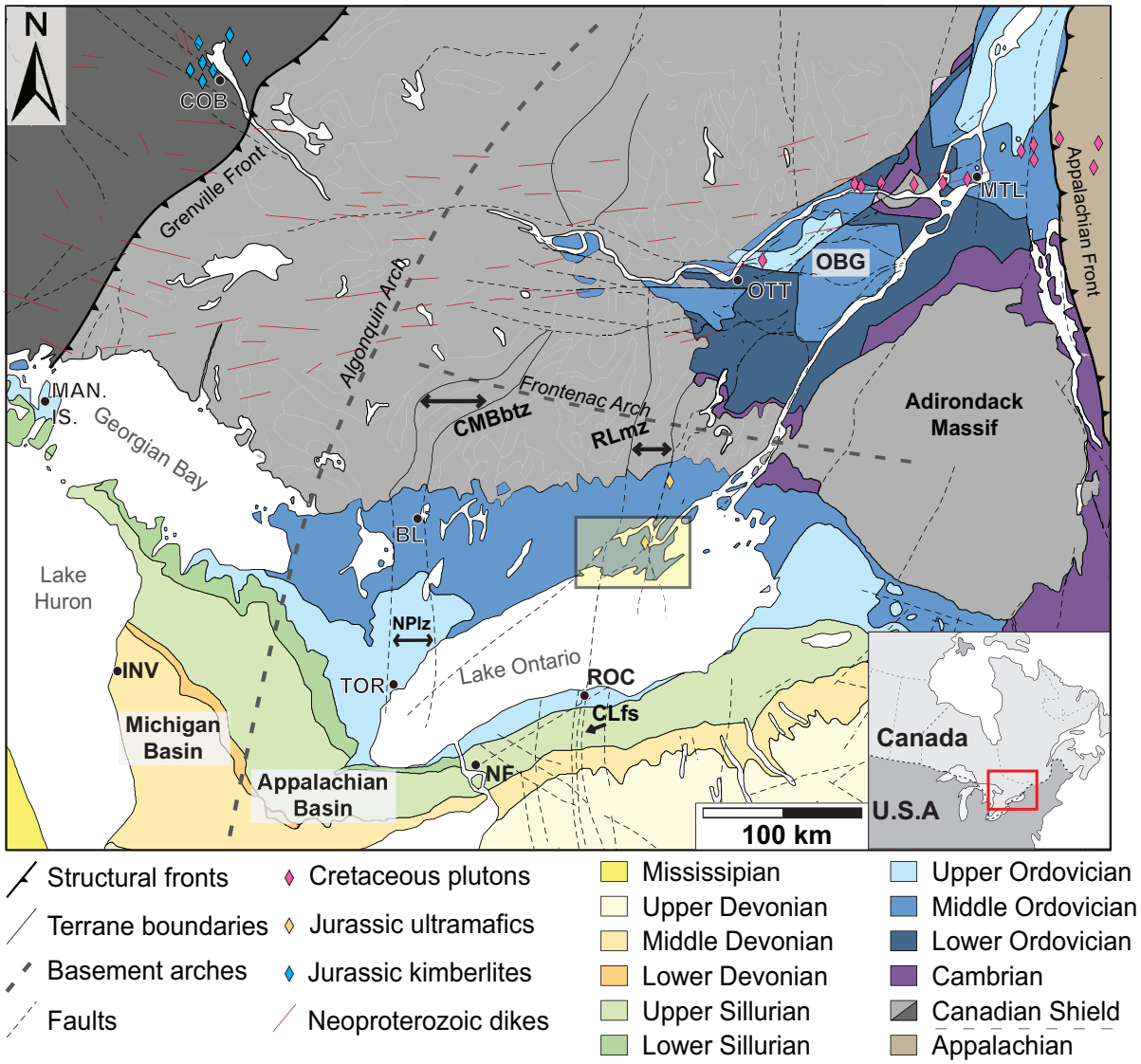


Figure 1 | Simplified geological map and structural framework of the Eastern Great Lakes region. The Central Metasedimentary Belt boundary tectonic zone (CMBbtz) and the Robinson Lake mylonite zone (RLmz) are northeast-southwest trending shear zones that represent Grenvillian terrane boundaries in the Canadian Shield. Fault traces are projected in the overlaying Paleozoic cover rock and are structurally aligned with the Clarendon Linden fault system (CLfs) in New-York. Paleozoic strata in southern Ontario was deposited in the Appalachian Basin (east) and Michigan Basins (west), with respect to the Algonquin arch, and in the Ottawa Bonnechere Graben (OBG), north of the Frontenac arch. Field area in Prince Edward County is highlighted by the yellow box. Locations referred to in this text reporting brittle deformation are projected as black dots: BL: Balsam Lake; INV: Inverhuron; COB: Cobalt; MAN. IS: Manitoulin island; MTL: Montreal; NF: Niagara Falls; OTT: Ottawa; ROC: Rochester; TOR: Toronto. Geological units, major structural features and intrusive bodies (Garrity and Soller, 2009); Ontario faults (OGS, 1991a); New York faults (Jacobi, 2002).

The CMBtz continues as N-S trending faults of the Niagara-Pickering lineament zone (NPlz) that transect the greater Toronto area (**Figure 1**). Notably, the projected trace of the RLmz in the overlying Paleozoic sedimentary strata transects our field area in Prince Edward County (Ontario) as the Salmon River Fault in the west and the Picton Fault in the east (McFall, 1993; **Figure 2**). The exact location of the faults is determined through aeromagnetic lineaments and supported by stratigraphic offset (McFall, 1993), and previous studies report the fault trace are partially exposed in small valleys that are filled with glacio-fluvial sediments that obscure fault surfaces (e.g. Cuddy, 1969; McFall, 1993). The Salmon River Fault splays into the Hamilton-Presqu'île Lineament, preserving 40 m of displacement. To the east, the Picton Fault splays into the Salmon Point Fault, and the Wellington Fault, which is projected to intersect the Salmon River Fault under Lake Ontario. The Wellington Fault is identified as an aeromagnetic lineament that coincides with a bedrock ridge, but the amount of displacement across the fault is unknown (**Figure 1**; McFall and Allam, 1991).

Exposed along the shoreline of the great lake, the Picton, Salmon Point and Salmon River faults align with structures forming a ~20 m bathymetric high in Lake Ontario, known as the Scotch Bonnet Rise (Anderson and Lewis, 1975). Further south, the rise is aligned with the Clarenden Linden Fault system (CLFS) within Devonian sedimentary strata in northern New York state (**Figure 1**). The Picton and Salmon River faults in southern Ontario as well as the CLFS record ~30 m of accumulative offset, with the southeastern blocks down-dropped, and have hosted modern seismicity (M_n <5; Liberty, 1960; Earthquakes Canada, 2017). The similarities of these structures suggest that they are a continuous feature.

Several continental arches form structural highs within the region (**Figure 1**), which have partitioned sedimentation as well as deformation over time. The NE-SW Algonquin Arch is the historical division between the Michigan and Appalachian basins, and is parallel to the dominant trend of the structures in the crystalline basement (Sanford, 1993). The E-W Frontenach Arch is the divide between the Appalachian Basin and the failed rift sequences of the OBG (Sanford, 1993; Rimando and Benn, 2005). Directly to the east, the Adirondack Highlands form a structural dome that exposes Grenville Province rocks, reaching a maximum elevation of 1600 m.

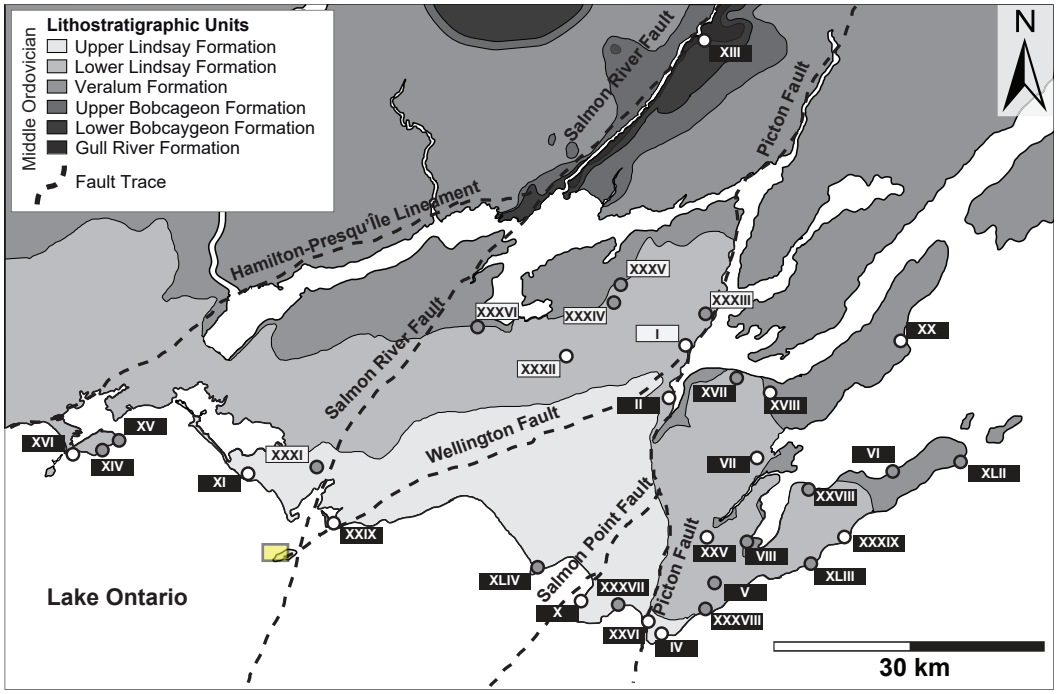


Figure 2 | Simplified geological map of Prince Edward County, Southern Ontario. Outcrop distribution of 32 visited stations represented by roman numerals. White dots are stations where samples were collected, grey dots are stations where exclusively structural measurements were taken. Numerals with a white backdrop are limestone quarries. Shaded yellow box represents the location of Figure 3 (Geological map of the Paleozoic strata of Prince Edward County was created from a compilation of preliminary maps P2411, P2412 and P2375 from the Ontario Geological Survey; D.M Carson, 1980; 1981, fault trace positions from McFall, 1993).

3. Stratigraphic architecture

Paleozoic rocks in this portion of the Appalachian Basin are relatively flat lying, shallowly dipping (<7°) to the south, and are 200-300 m thick (Carson, 1981; McFall, 1993). The oldest Paleozoic sedimentary unit is Cambrian sandstone, is only locally preserved in the St. Lawrence Lowlands, and is not present in the area of study. The Middle Ordovician strata are sub-divided based on their biostratigraphy (Liberty, 1960). The oldest formation exposed is the Gull River Formation, southeast of the Salmon River Fault (**Figure 2**). It consists of massive, grey to brown crystalline limestone with local colonial corals and massive cephalopods and has a total thickness of ~20 m. Overlying it is the Bobcaygeon Formation, a brown to medium grey, 13 m thick limestone unit that has been subdivided based on bed thickness: the lower formation has 20 cm thick beds, whereas the upper formation is interbedded with thin (<1 cm) shale beds (Liberty, 1960). Both the Gull River and Bobcaygeon formations are on the southwest side of the Salmon River Fault (**Figure 2**). The Veralum Formation is stratigraphically younger, which is exposed through Prince Edward County along the shore line of the eastern arm of the peninsula as well as within the walls of many limestone quarries (**Figure 2**). The boundary between the Upper Bobcaygeon and the Veralum formations is marked by the appearance of continuous shale beds of sub-equal thickness to the limestone beds (Liberty, 1960). The Veralum Formation consists of interbedded grey-brown shale beds with bioclastic limestone, most commonly possessing brachiopods and bryozoans. Bed thicknesses vary from 3 to 15 cm, and the total thickness of the formation is estimated to be ~90 m (Liberty, 1960). The youngest biostratigraphic unit is the Lindsay Formation, which is identified by the rock's blue-grey color. A gradational contact marks the transition from the Veralum to Lindsay and the contact is defined as the last appearance of bioclastic limestone (Liberty, 1960). The Lindsay Formation is exposed along much of Prince Edward County's shore line, and extends up to 30 km inland (**Figure 2**). Bed thicknesses varies from 3-10 cm, often separated by thin beds of shale giving the rock a nodular texture. The Lindsay Formation is also sub-divided by its fossil content. The Lower Lindsay has beds of crystalline limestone and a total thickness of ~30 m. The Upper Lindsay consists of interbedded crystalline and fossiliferous beds, the most common fossils are brachiopods, gastropods, bryozoa and tribolites (Liberty, 1960). The Upper Lindsay is the youngest rock formation in the study area, so a minimum thickness is estimated to be 60 m.

4. Paleo-stress in eastern North America

Initial estimates of the modern stress field in eastern North America were not resolved until the mid-20th century. Engineers near Niagara Falls reported mechanical difficulties with quarry machinery, where pit walls were collapsing inwards, bending beams and creating buckles on quarry floors (Winder, 1955). These observations lead to the identification of a compressive stress field in the shallow crust, which was later measured through borehole breakouts in the 1970's (Palmer and Lo, 1976). Similar magnitudes of stress originating from the ENE-WSW were measured throughout eastern North America. Lo (1978) suggested the horizontal stresses in the shallow crust are related to the modern motion of continental plates, and that along the eastern continent the current stress field originates from far field stresses on its eastern plate boundary associated to ridge push from the expansion of the Atlantic basin. The discovery of a contemporary stress field in the shallow crust not only provided valuable information on ongoing seismicity and deformation, but also encouraged geologists to theorize on the evolution of the paleo-stress on the geological time scale: a compressive stress field (σ_1) can be inferred on ancient structures that can then be related to major tectonic events. Associating brittle structures to past events can be difficult, particularly since multiple tectonic events have generated similar stress fields.

A number of brittle deformation episodes have been recorded and identified in eastern North America. Brittle structures for the purposes herein are planes of weakness that formed in the shallow crust and are susceptible to reactivation during later tectonic events. Mesoproterozoic tectonism has pre-conditioned discrete regions of the crust (i.e. shear zones) to be susceptible to subsequent reactivation. During the Neoproterozoic-early Paleozoic, continental extension (σ_1: ESE-WSW) initiated with the break-up of Rodinia and the opening of the Iapetus Ocean (Kumrapeli, 1985). Rifting was accommodated by normal faulting and crustal thinning, which formed the OBG and generated dike swarms that parallel the structural framework of the graben (Kumrapeli, 1985; **Figure 1**). Subsequently, the Appalachians formed an ensemble of terranes and island arcs that accreted to North America during three successive periods of orogeny, each with their respective direction of paleo-stress: Taconic Orogeny (σ_1: NW-SE to WNW-ESE), Acadian Orogeny (σ_1: WNW-ESE), and Alleghanian Orogeny (σ_1: NNW-SSE; Faure et al., 2004; **Figure 1**).

The end of Appalachian collisions marks the assembly of the Pangea supercontinent (Faure et al. 2004). Continental rifting was initiated in the Triassic, leading to the opening of the Atlantic

Ocean in the Jurassic (σ_1: WNW-ESE; Sanford, 1993; Rimando and Benn, 2005). This extension reactivated structures in the OBG and generated mantle melts in the St. Lawrence Lowlands. The major faults in the Paleozoic strata served as pathways for deep-seated magmas, intruding as ultramafic dikes (**Figure 1**; Barnett et al., 1983). In the Late Cretaceous (c. 100 Ma), North America underwent a clockwise rotation which re-oriented the stress field (σ_1: ENE-WSW; Adams and Bell, 1991) and was accompanied by an increased spreading rate along the Northern-Mid Atlantic ridge until c. 80 Ma (Adams and Bell, 1991; Matthews et al., 2011). This change in the direction and rate of spreading along the Northern-Mid Atlantic ridge has been linked by previous authors to a global plate reorganization event from 105-100 Ma (Matthews et al., 2011).

In the Pleistocene, the stress field was temporarily reoriented to the NNW-SSE due to ice sheet unloading (Adams, 1989). Except for glacial unloading in the Pleistocene, the horizontal stress field in southeastern Canada has been dominated by a ENE-WSW signature since the Cretaceous, and originates from ridge push at distal plate boundaries. It remains ambiguous how stress is distributed around pre-existing basement-rooted structures. Dynamic models that integrate the crustal geometry with stress measurements suggest that major basement-rooted structures (within the CMBbtz, RLmz, and the OBG) can locally affect the compressive stress field to align itself with these structures (Baird and McKinnon, 2007). In Prince Edward County, this would imply that the stress field locally rotates clockwise to align itself with NE-SW trending structures of the Salmon River fault, and the Picton fault (Baird and McKinnon, 2007).

Epicenters from modern seismic events have been linked to the trace of basement-rooted faults in the Eastern Great Lakes region, as well as younger faults with various orientations suggesting that pre-existing basement-rooted structures are susceptible to reactivation under the modern stress field (Sanford, 1993; Carr et al., 2000; Earthquakes Canada, 2017).

5. Previous work: brittle tectonics

Identifying ancient fault zones, as well as constraining their geometries, and geographic extent, reveals information that is relevant during seismic hazard assessments. Major faults within the CMBbtz and the RLmz have strong gravimetric and magnetic lineaments. Through the St. Lawrence Lowlands, the Paleozoic sedimentary strata obscure this signature, and the region was classically interpreted as magnetically "flat." Boyce and Morris (2002) used micro-levelling and image enhancement to improve the resolution on magnetic and gravimetric maps in southern

Ontario, which resulted in the identification of new NE-SW magnetic and gravimetric lineaments that transect the Paleozoic strata of the region. These lineaments correspond to mapped faults that align (to the north) with lineaments from the RLmz in the Canadian Shield (**Figure 1**). The continuity of NE-SW oriented structures in the Canadian Shield through the overlying Paleozoic sedimentary cover rocks supports a "structural inheritance model," whereby basement faults were reactivated and propagated upwards into the overlying Paleozoic sedimentary strata (Boyce and Morris, 2002). At depth, the faults generally have listric shapes that merge on a decollement at the basement-cover contact (Fakundiny and Pomeroy, 2002). Stratigraphic offsets along the lower sections of Paleozoic sedimentary strata suggest there has been successive periods of fault reactivation from the Phanerozoic to the middle Ordovician during Appalachian orogenies. Similarly, faults within the Paleozoic cover rock overlying the OBG are also interpreted to have been inherited from underlying basement structures during subsequent tectonism (Kay, 1942; Kumrapeli, 1985).

Previous authors have suggested that the intersections of major structural features are more susceptible to reactivation (e.g. Hildenbrand, 1985; Barosh, 1986). For example, in Eastern Canada the intersection of the E-W trending Frontenach arch with the NE-SW trending CMBbtz and RLmz (**Figure 1**) are at higher risk of fault reactivation, whereas in Prince Edward County, the intersections of the NE-SW trending Picton and Salmon River faults with the E-W trending Hamilton-Presqu'île, Salmon Point and Wellington faults (**Figure 2**) should be at higher risk of fault reactivation (Hildenbrand, 1985; McFall, 1993).

Statistical approaches have been used to correlate natural seismicity to fault populations. The findings suggest that under the current stress field (ENE-WSW), NW-SE oriented faults (at a high angle to the maximum compressive stress) are most susceptible to fault reactivation, and NE-SW oriented faults are the least susceptible to fault reactivation (Daneshfar and Benn, 2002). This agrees with modern seismicity clustering around structures within the OBG (Earthquakes Canada, 2017). Increments of NE-SW trending faults (e.g. RLmz, Picton fault, CLfs) that have experienced reactivation (M_n <5) could represent localized deflections of the compressive stress field to align itself with basement-rooted structures (McFall, 1993; Baird and McKinnon, 2007).

Often the surface expression of these deep-seated deformation zones are joints. A joint is a continuous fracture within a rock that does not have discernible offset. Isolated joints may form however, they often form systematically at regular spatial intervals. A group of joints with a

common orientation may be identified as a joint population. Where multiple joint populations are present, the relative timing of joint propagation can be resolved through terminating relationships, as the terminating joint is younger since it cannot propagate across a free surface (Hancock, 1985). Joints can open in two main fashions, forming extensional joints and conjugate joints. Extensional joints open and propagate parallel to the principal axis of compressive stress (σ_1), whereas conjugate joints form in pairs and the principal axis of compressive stress (σ_1) is oriented along the acute angle (2θ) between the two joints (Dunne and Hancock, 1994). There may be a minor shearing component associated to the propagation of conjugate joints (Hancock, 1985).

Like other brittle structures, the timing of joint propagation can be resolved by inferring a paleo-stress field and associating it to a known tectonic event. Joint patterns were first reported in the Devonian shales of the Central Lowlands (Rochester, NY) in 1886, which fostered further studies (Niagara Falls, NY) where similar patterns were observed (Gilbert, 1886; Wilson, 1902). Since then, systematic joint patterns have been mapped in detail throughout eastern North America (**Figure 1**). Initial mapping pre-dates the understanding of plate tectonics, and most brittle structures were misinterpreted to record glacial unloading in the Pleistocene.

Systematic sub-vertical ENE-WSW oriented joints are reported around the Great Lakes, including Manitoulin Island and as far west as Wisconsin (**Figure 1**; Parker, 1942; Powell, 1976; Holst and Foote, 1981). Engelder (1982) proposed that ENE-WSW joints propagated under the modern stress regime, and they are extensional joints. Occasionally the stress field is locally deflected and joint orientations deviate accordingly, such that there are regions that preserve NNE-SSW joints (e.g. Appalachian Plateau; Sbar, 1977; Haimson, 1981; Engelder, 1982). In the eastern Great Lakes, field investigations report multiple joint sets. In Inverhuron of the Bruce Peninsula of Georgian bay along the eastern shores of Lake Huron, three joint sets have been mapped: NNW-SSE, ENE-WSW and a less pervasive NE-SW population (**Figure 1**; Cruden, 2011). The joints in Bruce Peninsula are interpreted to have propagated under conditions of elevated pore fluid pressure and in the presence of carbonate-rich brines that were driven by lateral flow from the east during Acadian or Alleghanian tectonism (Cruden, 2011; Davis, 2016). Rutty and Cruden (1993) report similar joint sets (NW-SE, E-W, and NE-SW) near Balsam Lake, north of Toronto, which is located directly over the trace on the CMBbtz (**Figure 1**). Notably, the E-W joint population is interpreted to have propagated under the current stress field (Rutty and Cruden, 1993).

Within the Paleozoic cover rock adjacent to the RLmz, ENE-WSW trending joints follow the regional trend of extensional joints that are interpreted to have propagated under the modern stress field (Engelder, 1982; Mitchell, 2007). Within the Paleozoic sedimentary strata directly overlying the RLmz, joint patterns deviate and have a different pattern: two sets of conjugate joints are reported (NW-SE / WNW-ESE and NNE-SSW / NE-SW), as well as WNW-trending normal faults and ESE-trending dextral faults. Faulting is interpreted to have initiated during the Acadian orogeny and initial rifting in the opening of the Atlantic (Mitchell, 2007). In contrast, McFall (1993) interprets the NW-SE joints to have propagated during the Acadian orogeny. Notably, no structures within the Paleozoic cover rock directly overlying the RLmz are interpreted to have propagated under the current stress field (Mitchell, 2007).

To summarize, NE-SW trending faults transecting the St. Lawrence Lowlands align with magnetic and gravimetric anomalies associated to ancient faults within the CMBbtz and the RLmz. The faults within the Paleozoic sedimentary cover rock are interpreted as structures that were inherited during the reactivation of basement-rooted structures. Moreover, systematic ENE-WSW extensional joints have been reported throughout eastern North America. These joints are compatible with the current tectonic stress regime, and are interpreted as the youngest joint population in eastern North America (Engelder, 1982). Through geologic history, multiple tectonic events have generated similar compressive stress fields (σ_1), and it remains elusive how basement-rooted structures (e.g. RLmz) deviate the compressive stress field in the shallow crust. Therefore, without terminating joint relationships, it is difficult to resolve the tectonism associated to jointing.

Joints that are locally filled and sealed with secondary calcite mineralization exhibit various orientations and are reported throughout the region (e.g. McFall, 1993; Mitchell, 2007). Aside from faults and joints, the St. Lawrence Lowland is structurally featureless with flat lying stratigraphy possessing a shallow dip (Liberty, 1960). Notably, none of the joint patterns that have been mapped are indicative of continental swelling, which suggests that the region was not structurally affected by the passage of the Cretaceous hot spot (e.g. McFall, 1993; Rutty and Cruden, 1993).

6. Previous work: geochronology and thermochronology

The timing of joint formation based on field observations can be equivocal, since different tectonic events can generate similar stress fields and stresses can be deflected in anisotropic crust.

Presuming fluid flow is synchronous with jointing, the crystallization ages on secondary mineral precipitates collected from joints may provide some resolution to the timing of jointing. At Inverhuron on Bruce Peninsula (**Figure 1**), Davis (2013, 2016) conducted U-Pb geochronology on calcite veins collected from Devonian strata at the surface, as well as Upper Silurian rocks collected from drill cores. Seven samples collected from calcite veins from the surface and the upper 35 m of core yield crystallization ages varying between 110-80 Ma, and smaller populations at c. 60 and c. 40 Ma. The U-Pb dates are dispersed, likely recording several events with the younger ages potentially representing a mixture of a 100 Ma event with (a) younger event(s). At a depth of ~200 m, vertical joints are essentially non-existent within these drill cores, and thin veins are present but do not have the same morphology as veins at the surface. Calcite veins collected from core at a depth of ~350 m (Silurian host rock) do not record a 100 Ma event, but yield crystallization ages of 318 ± 10 Ma, and those collected at depths of ~680 m and ~780 m (Upper Ordovician host rock) yield ages of 451 ± 38 Ma and 468 ± 25 Ma, respectively, which is close to the age of deposition (Davis, 2016).

The Great Meteor Hotspot (GMHS) was long lived and has generated magmatism from the Jurassic period through the Tertiary (Duncan and Clague, 1985; Heaman and Kjarsgaard, 2000). Presuming the location of the Great Meteor hotspot remains static, geochronology on surface and near surface alkaline volcanic rocks can be used to track the rate of divergence between the North American and African plates as well as absolute plate motions. Through central Canada, dispersed kimberlite fields can be linked along a broad, 200 km long NW-SE path. U-Pb ages on perovskite record crystallization ages of c. 148 Ma near Cobalt, Ontario (Heaman and Kjarsgaard, 2000). Apatite fission track (AFT), Ar-Ar and Rb-Sr yield ages of c. 127-124 Ma within alkaline plutons of the Monteregian Hills of southern Quebec (**Figure 1**; Eby, 1984). Within the central OBG, ~110 km to the west of the Monteregian Hills intrusive units, narrow carbonatite dikes cross cut the middle Ordovician sedimentary strata with AFT ages of c. 118-103 Ma (Hogarth and Rushforth, 1988). Similarities in mineral assemblages and geochemistry of carbonatite dikes and the alkaline plutons may indicate that they originated from the same magmatic suite (e.g. Hogarth and Rushforth, 1988). The youngest continental expression of the GMHS is in the White Mountains of New Hampshire, where K-Ar biotite ages of c. 115 Ma have been reported (Foland and Faul, 1977). The New England Seamounts are the continued expression of the GMHS in the western Atlantic basin. The seamounts consist of over 30 submarine volcanoes, and several whole rock

samples have been dated via K-Ar and $^{40}Ar/^{39}Ar$ methods giving ages from 103 Ma to 82 Ma that young to the southeast (Duncan, 1984). The linear trend of the New England seamounts is obstructed by a kink or bend in its trace, which reflects a clockwise rotation of the North American plate. Crystallization ages from seamounts that neighbor the bend constrain this event to ca. 100 Ma (Duncan, 1984).

There are some additional data from the region that documents Atlantic rifting. Phlogopite K-Ar geochronology was conducted on lamprophyre dikes collected along the Picton Fault in Prince Edward County (**Figure 1**), yielding ages of 173 Ma (Barnett, 1983). The timing of emplacement is consistent with the opening of the Atlantic, and the dikes are interpreted as decompressional mantle melts resulting from this extension, and deep-seated faults served as pathways for the magmas infiltration (Barnett, 1983; McFall, 1993).

In addition to geochronology, thermochronology can be useful to establish the timing of tectonic episodes such as uplift, exhumation, and low-temperature heating events. In eastern North America, it has served as a tool in understanding its unusual landscape, such as the relief of the Grenville rocks in the Adirondacks, the elevated Atlantic rift margin, as well as identify regional heating associated with migration over the GMHS. Within the sedimentary strata of the OBG and St. Lawrence Lowlands, accelerated low-temperature (<150°C) cooling at c. 100 Ma is documented through (U-Th)/He thermochronology (Emberley and Schneider, 2017; Hardie et al., 2017). In the Adirondacks, AFT dates range from Middle Jurassic to Late Cretaceous (Miller and Lakatos, 1983; Roden-Tice et al., 2000; Taylor and Fitzgerald, 2011). Roden-Tice et al. (2000) demonstrated a gradational pattern of AFT ages: the highlands record cooling ages of 168-135 Ma, whereas the oldest ages in the lowlands in the northwest and southwest Adirondacks record slightly younger ages of 146-114 Ma. This gradational trend of cooling ages correlating with topography is consistent with continental swelling from regional heating, however these cooling ages predate the passage of the GMHS (e.g. Crough, 1981; Roden-Tice et al., 2009).

Slightly younger cooling ages are documented through the Adirondack massif adjacent to major NE-SW trending fault traces: within the highlands of the east-central Adirondacks, cooling ages 101-93 Ma are recorded on Prospect Mountain via AFT dating, and similar ages of 112-83 Ma were recorded within the lowlands via (U-Th)/He and fission track dating on apatite (Roden-Tice et al., 2000; Tayor and Fitzgerald, 2011). Middle Cretaceous cooling ages adjacent to major fault traces post-date the passage of the GMHS, and disrupt the age versus elevation profile trend

that could be explained by continental swelling. Instead, these age discrepancies likely record fault reactivation which could best be explained by tectonic processes. In addition, comparable age discrepancies along major NE-SW trending faults in eastern North America also record Cretaceous fault reactivation. Along the Ammonoosuc Fault zone that transects the New England Appalachians, the youngest AFT cooling ages are 88-70 Ma in western New Hampshire and New York, 106-89 Ma in Massachusetts, and 124-107 in Connecticut (Roden-Tice and Tice, 2005). Along the Norumbega Fault in Maine, AFT ages from the southeast side of the fault record cooling ages of 150-149 Ma, whereas the northwest side records younger ages of 113-89 Ma (West and Roden-Tice, 2003). Passive margins have classically been interpreted to undergo uplift (recorded as cooling) following initial rifting, however some modern models instead suggest post-rift subsidence followed by uplift thus reoccurring Cretaceous cooling ages adjacent to North America's Atlantic margin could reflect margin rejuvenation (Japsen et al., 2012a; Amidon et al., 2016). Notably, Cretaceous cooling ages measured through Eastern North America coincide to the timing of the most recent reorientation of paleo-stress (Adams and Bell, 1991).

In summary, crystallization ages from magmatism associated to the GMHS are a useful tool to track North America's plate motion through the Jurassic-Cretaceous (Heaman and Kjarsgaard, 2000). During the Cretaceous, the GMHS was in the Atlantic basin off the coast of Maine. A kink in the New England Seamounts is constrained to ~100 Ma, suggesting the North American plate underwent a clockwise rotation at this time (Duncan, 1984). Consequently, the modern stress field was acquired (σ_1: ENE-WSW; Adams and Bell, 1991; Duncan, 1984; Rimando, 2005). Age discrepancies of ~100 Ma are measured across major faults through the Adirondacks of New York, Maine, New-Hampshire, Connecticut, and Quebec record Cretaceous fault reactivation (e.g. Roden-Tice and Tice, 2005; Tayor and Fitzgerald 2011; Emberley and Schneider 2017; Hardie et al., 2017). Regional fault reactivation is potentially associated to a re-orientation of the compressive stress field in the Cretaceous. Crystallization ages of ~100 Ma are also recorded in calcite veins in Bruce Peninsula (Davis, 2013, 2016). If these ages record the same event, this would imply that a Cretaceous tectonic event also initiated fluid flow within the shallow crust extending to the mid continent.

7. New field observations

The purpose of field work was two-fold: 1) map and collect structural data on brittle structures preserved in the bedrock in the St. Lawrence Lowlands, and 2) sample secondary mineral precipitates within these structures for geochemical and geochronological analyses. Structural measurements such as joint orientations are useful in identifying joint populations, whereas the relationships between different joint populations reveals the relative timing of joint propagation. Collecting calcite veins was for laboratory analysis with the purpose of resolving the source and timing of fluid flow. Field strategy was based on 1) geological maps of the Paleozoic geology of southern Ontario (Carson 1980, 1981), 2) coordinates in published literature that report brittle structures (e.g. Barnett, 1984; McFall, 1991, 1993; Mitchell 2007), and 3) satellite imagery, particularly useful for quarries and coastal exposures. Station locations were selected to cover a broad geographic distribution, both proximal and distal to fault traces to identify structures that record evidence of displacement or reactivation (e.g. slicken-slides, offset). A total of 32 stations preserving brittle deformation were identified. Station locations are labelled with Roman numerals, shown on the map in **Figure 2** and UTM coordinates listed in **Table 1**. Stations include seven limestone quarries, nine roadside outcrops and sixteen coastal outcrops along the northern shore of Lake Ontario. A total of ~1600 joint measurements were taken, and projected on Rose diagrams in **Figure DR-1**. Based on terminating joint relationships, joints with a broad E-W often adapt a ENE-WSW orientation, and are the youngest joint population observed during field work, which is consistent with previous reports. Calcite veins sealing joints with a broad E-W orientation were targeted during sampling to help understand the most recent deformation event. A total of 38 calcite samples were collected from fifteen stations, which are listed in **Table 1**.

Locating suitable outcrop was difficult due the relatively subdued topography and dense vegetation. Limestone quarries were ideal for vertical exposures, revealing up to 40 m of rock section. Within the eastern county, vertical rock exposure was locally preserved in roadside outcrops, which allowed nine stations. The best rock exposure was along the northern shore of Lake Ontario where ~50 m of lateral rock is exposed when water levels are low, with some small beach outcrops exposing ~1 m of vertical rock exposure. Sample collection was problematic: horizontal exposures offered few options to remove intact samples and vertical outcrops preferentially erode along joint surfaces exposing calcite mineralization, making it difficult to

Table 1: List of station locations, samples collected and summary of all analysis conducted

Station	UTM *	Rock Formation*	Comment	Sample number	Vein orientation	Vein thickness*/ comment	Stable Isotope		Thin Section	Trace elements		Geochronology
							δ13C V-PDB (‰)	δ18O V-SMOW (‰)		Mineral separates	In-Situ	
I	328992.51W 4880483.13N	Veralum	Quarry: *ESSROC Italcamenti*	PEC-15-12B	085/86	Exp.	0.75	20.57	✓	✓	-	-
				PEC-15-13	035/86	Exp.	0.49	19.65	-	✓	-	-
				PEC-15-14I	-	<1 mm	-	-	✓	✓	-	-
				PEC-15-14II		1 mm; fibrous/ tabular	-0.92	21.85		✓	-	-
II	328912.29W 4877573.52N	Lower Lindsay	Behind Picton Harbor	PEC-15-25A	065/74	1.5 mm	5.68	23.65	-	✓	-	✓
				PEC-15-25B	052/78	1.3 mm	0.18	21.14	-	✓	-	-
				PEC-15-25C	190/07	5 cm	0.92	22.69	✓	✓	-	-
				PEC-15-25DI	-	3.3 mm	0.60	20.99	✓	✓	-	-
				PEC-15-25DII	-	3 mm	0.71	20.59	✓	✓	-	-
IV	327140.55W 4856320.58N	Upper Lindsay	Lake Ontario Shoreline: Point Petre	PEC-15-29	229	1.5 mm	-0.02	21.21	✓	✓	-	-
V	331722.60W 4860580.36N	Lower Lindsay	Forested area									
VI	344898.78W 4865785.72N	Veralum	Peninsula shoreline									
VII	335812.83W 4870075.04N	Lower Lindsay	Roadside outcrop: County road 16	PEC-15-2A	250/78	Exp.	5.57	22.57	✓	✓	✓	✓
				PEC-15-2C	310	1.5 mm	2.88	22.70	✓	✓	-	✓
				PEC-15-9	276/80	1 mm	0.03	23.25	-	✓	-	-
				PEC-15-27	285	~5mm (p. exp.)	5.83	22.90	✓	✓	-	-
				PEC-16-3	285	Exp.	2.78	22.76	-	-	-	-
VIII	335256.84W 4864727.56N	Veralum/ Lower Lindsay	Roadside outcrop									
X	320265.22W 4859287.37N	Upper Lindsay	Lake Ontario Shoreline: Salmon Point	PEC-15-4	280/76	7 - 9 mm	0.28	22.99	✓	✓	-	-
				PEC-15-31A	274	2.1 cm	0.12	23.03	✓	✓	✓	✓
				PEC-15-31BI	271	>6mm	0.62	22.74	✓	✓	-	-
				PEC-15-31BIII		vug-filled crystals	6.30	22.39		✓	-	-
				PEC-15-31C	272	4mm	1.68	22.34	✓	✓	-	-

Station	UTM *	Rock Formation*	Comment	Sample number	Vein orientation	Vein thickness*/ comment	Stable Isotope		Thin Section	Trace elements		Geochronology
							δ13C V-PDB (‰)	δ18O V-SMOW (‰)		Mineral separates	In-Situ	
XI	294264.44W 4872085.79N	Upper Lindsay	Lake Ontario Shoreline	PEC-15-5A	025/57	Exp.	-0.28	19.52	✓	✓	✓	✓
				PEC-15-5B	255	Exp.	-0.16	19.52	✓	✓	-	-
XIII	333646.11W 4906239.71N	Gull	Roadside outcrop: Desronto Rd	PEC-15-6	225/73	1.5 mm	-0.67	20.86	✓	✓	-	-
				PEC-15-7	015/86	2.5 mm	0.99	22.73	-	✓	-	-
XIV	283259.61W 4874018.94N	Lower Lindsay	Lake Ontario Shoreline: Presqu'ile National Park									
XV	283584.86W 4874190.66N	Lower Lindsay										
XVI	281163.06W 4874613.40N	Lower Lindsay		PEC-15-8	215	1 mm	1.00	24.04	✓	✓	✓	✓
XVII	335118.01W 4878231.5N	Lower Lindsay	Forested area									
XVIII	337816.43W 4877172.87N	Veralum/Lower Lindsay	Roadside outcrop: Mosquito Ln	PEC-15-10	232/86	Exp.	-0.07	23.97	-	✓	-	-
				PEC-15-28	312	Exp.	-0.08	21.57	-	✓	-	-
XX	347366.29W 4878058.74N	Veralum	Peninsula shoreline: County road 8	PEC-15-11	090/85	Exp.	-0.09	23.72	-	✓	-	-
XXV	332759.10W 4865859.34N	Lower Lindsay	Roadside outcrop: County road 10	PEC-15-26	256	1.5 mm	-0.05	23.37	-	✓	-	-
XXVI	326329.12W 4857319.74N	Upper Lindsay	Lake Ontario Shoreline	PEC-15-30	242	1.5 mm	-0.13	23.67	✓	✓	✓	✓
				PEC-16-1	267	8 mm	2.54	22.55	✓	-	-	-
				PEC-16-2	250	4 mm	0.07	23.34	✓	-	-	-
XXVIII	330108W 4872085.79N	Veralum/Lower Lindsay	Peninsula shoreline: Little Bluff									
XXIX	299833.03W 4866725.94N	Upper Lindsay	Lake Ontario Shoreline: Huick's point	PEC-15-32A	273	1.5 mm	0.03	23.01	-	✓	-	-
				PEC-15-32B	273	1.5 mm	-0.01	22.89	✓	✓	-	-
XXXI	298893.34W 4872686.98N	Upper Lindsay	Quarry: *Concecon (Lafarge)*									
XXXII	319786.21W 4876486.72N	Lower Lindsay	Quarry: *Foster Rock*	PEC-16-4A	087/80	3 mm	4.93	24.85	✓	-	-	-
				PEC-16-4B	268/72	2.5 mm	3.39	24.26	✓	-	-	-

Station	UTM *	Rock Formation*	Comment	Sample number	Vein orientation	Vein thickness*/ comment	Stable Isotope		Thin Section	Trace elements		Geochronology
							δ13C V-PDB (‰)	δ18O V-SMOW (‰)		Mineral separates	In-Situ	
XXXIII	330646.18W 4881687.21N	Lower Lindsay	Quarry: *Miller Paving Limited*									
XXXIV	323918.07W 4885387.07N	Lower Lindsay	Quarry: *Power Concrete Products*									
XXXV	324630.32W 4886760.11N	Lower Lindsay	Quarry: Abandoned									
XXXVI	311508.73W 4883147.18N	Lower Lindsay	Quarry: *Mountain view*									
XXXVII	324399.95W 4859643.20N	Upper Lindsay	Lake Ontario Shoreline									
XXXVIII	330108.13W 4858226.50N	Lower Lindsay	Lake Ontario Shoreline									
XXXIX	341398.74W 4862767.08N	Lower Lindsay	Lake Ontario Shoreline: Ostrander Rd.	PEC-16-5	281	4 mm	-0.12	22.98	✓	-	-	-
XLII	349826.88W 4865640.24N	Veralum	Lake Ontario shoreline; Structures measured via satellite imagery									
XLIII	338986.34W 4861710.02N	Lower Lindsay										
XLIV	316919.99W 4862357.77N	Upper Lindsay										

* All UTM coordinance are in zone 18T
* Rock formations are all middle-Ordovician
* Vein thickness: Exp. = Calcite exposed along the vein-hostrock interface

collect calcite that is attached to the host rock. Sampling was often not permitted along excavation walls in quarries.

Structural measurements in the field were taken with a Brunton compass, using the right-hand rule. In addition, prominent joints along the coast were measured via satellite imagery. The orientation of measurements taken via satellite imagery agree with structures measured in the field. Measurements from each station are projected on Rose plots for each station using a Python script. The number of bins and bin sizes varies on the number of structural measurements taken. At stations where less than eight measurements were taken, the number of bins is equal to the number of measurements. At stations where more than eight structural measurements were taken, the number of bins follows the following formula:

$$bins = 5\sqrt{n + 10}$$

where n: number of joint measurements. From trial and error, we found this formula to best represent our structural data.

7.1 Structural observations

Coastal outcrops expose the Upper and Lower Lindsay formations and the Veralum formation in the eastern arms of the peninsula. Within the mainland of Prince Edward County, mapped faults often occupy narrow valleys filled with glacio-fluvial sediments and along the shorelines and fault traces are inaccessible due to steep cliffs, however displaced blocks were observed. Interestingly, measurable fault displacement is also observed in stations that are distant to mapped fault traces (e.g. Station XXXII; **Figure 2**). Aside from minor offsets, no major (>1 m) fault displacement was observed during field work.

Joints are the most pervasive structural feature preserved in the bedrock of Prince Edward County. Structural measurements of sub-vertical joints from each station are projected on Rose diagrams in **Figure DR-1**. Joints are most easily observed at coastal outcrops, due to vast horizontal rock exposure. Joints paralleling the shoreline can be followed for >1 km, and can be seen through satellite imagery (**Figure 3**). In cross section, such as roadside outcrops and quarries, rocks preferentially erode along joint surfaces, sometimes preserving a thin veneer of calcite mineralization (**Figure 4**). On average, joints are spaced every 5-20 m, however, in intense joint zones that are 20-100 meters wide, joint densities can increase to every 0.5 m (**Figure 3**; **Figure 4**). Notably, zones with intense jointing may also be distal to mapped faults (e.g. Station XLIII;



Figure 3 | Satellite image of the bedrock of Prince Edward County on Nicholson island, refer to Figure 2 for relative location. Pervasive joints trending broadly E-W spaced every 5 to 10 meters in beach outcrops that project into Lake Ontario (Image acquired from Google Earth).

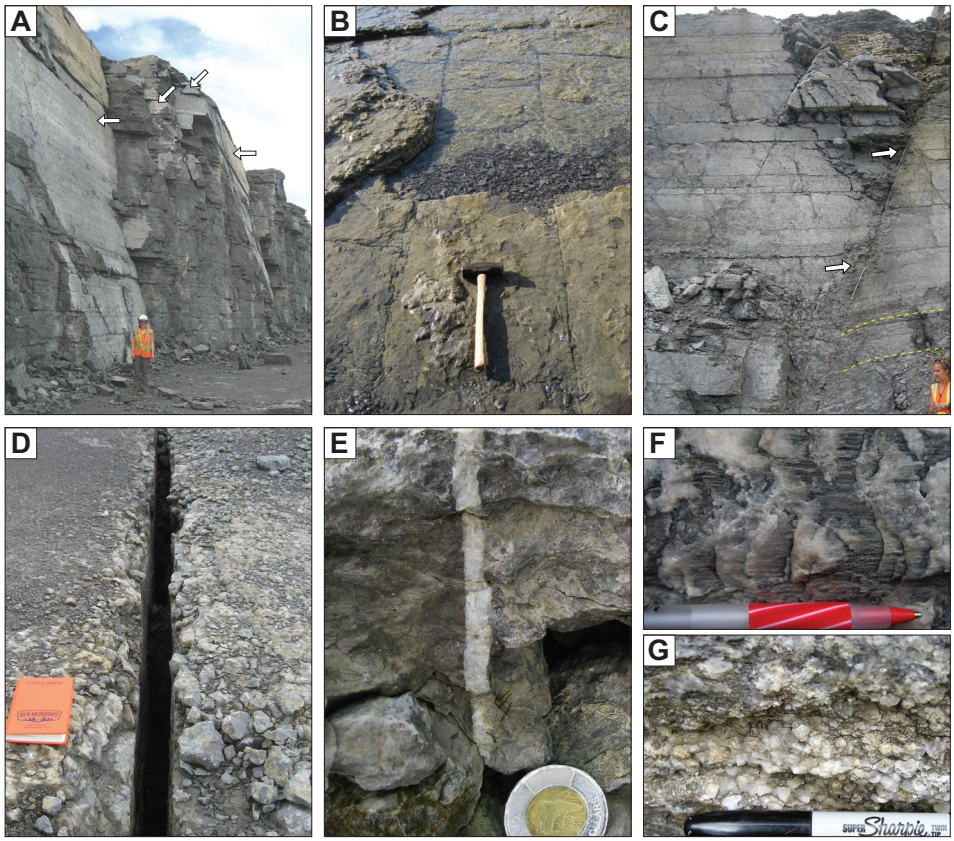


Figure 4 | Field photos of brittle structure: A) Limestone preferentially fractured along vein host rock interface during blasting, exposing over 50 meters of calcite mineralization trending 300°/ 85°, and smaller surfaces oriented at 268° (white arrows), photo facing northwest, Station I; B) Joints oriented at 261°, photo facing west, Station XXIX; C) Excavation surface oriented at 215° with two parallel joints oriented at 135°/74°. Joint on the right hosts calcite mineralization (white arrows, sample PEC-16-4B) with dragged offset at the base of the excavation (yellow dashed line), photo facing northwest, Station XXXII; D) Dilated joint oriented at 268° at the top of 50-meter-high excavation of limestone quarry, photo facing west, Station XXXV; E) Calcite vein with a uniform thickness of 7 mm oriented at 274° (Sample PEC-15-31A) crossing a small beach outcrop, photo facing east, Station X; F) Slicken-slide fabric oriented 07°- 290° within a sub-vertical calcite vein, photo facing south, Station I; G) Host rock preferentially fractured along vein-host rock interface oriented 285°, exposing calcite vein with euhedral crystals up to 5 mm wide, photo facing north, Station VII.

Figure 2). Joints are often partially filled or sealed with secondary calcite mineralization, forming calcite veins. At any station, the orientation of the joint set within a population varies <15°. Two prominent joint populations were observed: 1) NW-SE trending and 2) broadly E-W trending. The relationship of these joint populations varies: forming conjugate sets, and E-W trending joints terminating upon intersecting joints of the NW-SE population. Generally, both joint relationships can be observed at a single station. The opening of joints as conjugate sets is supported by sub-horizontal slicken-fabrics along the host rock (**Figure 4**). Joints from the E-W population often have euhedral calcite overgrowth that sometimes overgrows directly on sub-horizontal slicken-fabrics. This is observed at stations located on fault traces (e.g. station I: 18°-085°), and distal to mapped faults (e.g. station VII: 10°-285°). Terminating E-W trending joints upon intersecting NW-SE joints, and euhedral calcite overgrowth suggests the E-W trending joints have undergone dilation that post-dates the formation of conjugate joints sets (**Figure 4**).

A third (less prominent) joint population trending broadly NE-SW is sometimes present. At the northern extend of the field area (~50 km north of Lake Ontario), station XIII is located on the southeast side (footwall) of the Salmon River Fault trace, which exposes a portion of the Gull River Formation (**Figure 2**). Here, NNE-SSW and NE-SW joints form conjugate sets. Along the western continuation of the Salmon River Fault on the trace of the Hamilton Presqu'île lineament (station XVI), the most prominent joint populations are NE-SW and NW-SE, although neighboring stations (XIV and XV) have almost exclusively E-W trending joints (**Figure 2**; **Figure DR-1**). Near the intersection of the Salmon River Fault and the Wellington Fault near Lake Ontario (station XXIX), N-S trending joints terminate upon intersecting much more prominent E-W trending joints and neighboring stations (e.g. station XXXI) have the same joint pattern (**Figure 2**; **Figure DR-1**).

The northernmost station along the Picton Fault (station I) is within a limestone quarry (**Figure 2**). Notably, this is the only station located along a mapped fault where offset was observed (~15 cm of normal-sense displacement). The third joint population is not present and only NW-SE and E-W trending joints occur. Within the excavation area, a ~15 m-wide fracture zone has NW-SE trending joints spaced about every meter. Sub-horizontal slicken-slide fabrics with euhedral calcite overgrowth were also observed within the fracture zones (**Figure 4**). In addition, a 4-8 cm wide Jurassic ultramafic dike within a region of densely spaced, E-W oriented joints is reported in previous studies (Barnett, 1983). Since this is an active quarry, in situ collection of the

dike was not possible, however within blasted rock debris a piece of the ultramafic rock was collected from the quarry floor. In this sample, the ultramafic dike is about 4 cm wide and remains intact within the limestone host rock and the dike is perpendicularly cross-cut by calcite veins. Along the trace of the Picton Fault where it splays to the Salmon Point Fault (station X), NE-SW trending joints terminate upon intersecting E-W trending joints, although the E-W joint population is much more pervasive. The less prominent NE-SW joint population is sometimes present distal to mapped faults, for example, at station XLII which is more that 15 km to the east of the Picton Fault (**Figure DR-1**).

To summarize, the most pervasive joint set populations are NW-SE and broadly E-W. The relationship between these joint populations varies from forming conjugate sets, and E-W trending joints terminate upon intersecting NW-SE trending joints. Sub-horizontal slicken-slide fabrics evinces some joints opening as conjugate sets. Euhedral calcite overgrowth along joints from the E-W population suggest post-shearing dilation along these joint surfaces. Variably oriented and intense joint sets, a third (less pervasive) NE-SW joint population, and measurable displacement is generally observed at stations that overlay fault traces, but are also present at stations that are distant to mapped faults.

7.2 Calcite mineralization and sample collection

To resolve the most recent brittle deformation event recorded in the rocks, calcite veins with a broad E-W orientation were targeted during sample collection as their terminating relationships suggest that they are the youngest joint population. A total of 38 calcite veins were sampled from fifteen stations (**Figure 2**; **Table 1**). Calcite veins exceeding a width of 3 mm were found almost exclusively along the shore of Lake Ontario, and often trend ENE-SWS. Hairline veins are also present at these locations. The size of calcite crystals is generally proportional to vein thickness, and all veins were monomineralic calcite veins. Calcite mineralization along dilated joints are often eroded, leaving a thin veneer of mineralization along joint surfaces (**Figure 4**). Therefore, it is possible that some joints with no obvious filling material did contain calcite that has been eroded away.

Two calcite veins had multiple crystal morphologies along a continuous vein, that were manually separated during sample collection to form separate samples to conduct independent analysis (PEC-15-14I and -14II; PEC-15-31BI and -31BIII). At station X, a calcite vein oriented

at 271° with cavities along the side of the vein hosts calcite with larger crystals than the main portion of the vein: the vein itself (PEC-15-31BI), where the sample is intact within the host rock, and the "cavity"-filled calcite (PEC-15-31BIII) that is characterized by larger euhedral crystals, up to 7 mm wide. At station I in (the Intalcamenti quarry) calcite veins cross-cutting the ultramafic dike varies in crystal morphology: "normal" equant crystals (PEC-15-14I) and locally a more tabular crystal morphology with a slicken-fabric (PEC-15-14II). At station VII, euhedral calcite crystals form overgrowth on a slicken-fabric 10°-285° (**Figure 4**). The slicken-slide fabric formed a thin layer of mineralization intact to the host rock, that we were unable to sample, however, calcite overgrowth was collected (PEC-15-27). In addition, at station II, sample PEC-15-25DI and PEC-15-25DII are from rock fragments that were not in place, however they were found in rock debris beside a cliff face and it is assumed the blocks eroded from this cliff. All other samples collected are sub-vertical, except for sample PEC-15-25C which is sub-horizontal (190°/07°).

8. Petrographic analysis

Petrographic analysis was conducted for several purposes: 1) describe crystal morphologies and gain insight on the crystallization processes, and 2) identify microstructures that are indicative of post-crystallization deformation such as sutured grain boundaries and mechanical twinning, which may suggest the structures have been potentially reactivated. A total of 25 polished thin sections (30 μm thick) were prepared. We were not able to make thin sections of all 38 veins because thin section preparation was problematic for veins preserving <1 mm of material where only one side of the host rock was preserved. Analysis was conducted via Olympus BX41 binocular polarizing microscopes and images were acquired using Image-Pro software package. Larger structures requiring a magnification <5x (i.e. photos of entire veins) were analyzed with a polarizing WILD Makroscope. Both microscopes are equipped for transmitted and reflected light capabilities. In addition, cathodoluminescence (CL) microscopy was performed on representative thin sections. The CL microscopy was done on a CITL Mk5 Optical Microscope Stage. General operating conditions include a beam energy (accelerating voltage) of 78-27 kV, beam current of 460-600 mA, and operating vacuum of 0.03-0.05 torr. Scanning electron microscopy (SEM) images were taken with a JEOL 6610LV Scanning Electron Microscope (University of Ottawa) using secondary electron imaging in a high vacuum with a 1.7 kV beam.

8.1 Vein structure

Most calcite veins have large equant crystals (~300 μm) in the center of the vein with a reduction of crystal size (<100 μm) at the vein-wall rock interface (**Figure 9**). The relationship of these crystal morphologies is characteristic of syntaxial-biaxial vein growth, where nucleation initiates on both sides of the host rock, forming small crystals with their long-axis oriented perpendicular to the host rock (**Figure 5**). These crystal boundaries are more easily distinguished under CL. Luminescence under CL provides a qualitative perspective on chemical variations that rely primarily on the presence of Mn and lack of Fe (Hemming et al., 1989). Under CL, the internal structure of these crystals often forms compositional zonation shown by alternating rims of illuminated and quenched material (**Figure 5**). The centers of these concentric rims are located along the host rock, suggesting that nucleation initiated along the host rock during the first stage of vein filling (**Figure 5**). After this first stage of crystal growth, subsequent crystallization is slower, forming equant crystals that fill the center of the vein. Crystal growth initiated from both sides of the vein at similar rates leads to "competition growth," where the internal crystals of the vein are equidimensional (Fisher and Brantley, 1992; Bons and Jessell, 1997). In the center of veins, the presence and intensity of luminescence under CL is variable (**Figure 5**). During syntaxial-biaxial growth a median line is generally preserved in the center indicating the last stage of crystal growth, however this line was not observed in this study. Large crystals in the center of the vein suggest there was a lack of growth competition, and suggests that the veins have not undergone episodic reactivation, but rather the vein crystallized from a single event (Bons and Jessell, 1997).

One sample preserved elongated, fibrous crystals (PEC-15-14). This crystal morphology is typical in veins that have opened through a crack and seal mechanism, suggesting that they have been episodically reactivated through re-opening of the vein (cracking), and a later pulse of fluid which "sealed" the vein. The fibrous crystals in this one sample are truncated, indicating an abrupt change in opening direction. This one sample is the only vein suggesting episodic reactivation.

Larger veins (>3 mm) are sometimes cross-cut by smaller veinlets. The veinlets are <1 mm wide, and have similar crystal morphologies as the other veins: equant crystals with a reduction of crystal size at vein-wall-rock interface. Veinlets are generally deflected along large crystal boundaries of the main vein (**Figure 5**). Cross-cutting relationships of the veinlets with larger veins suggests that fractures were opened to accommodate a later pulse of fluid that post-dates the main

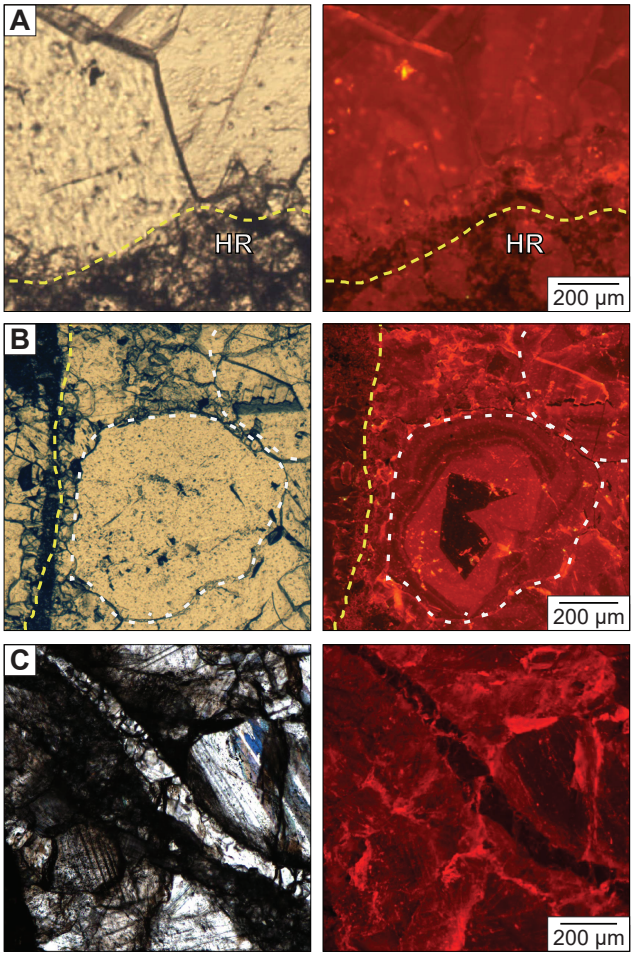


Figure 5 | Photomicrographs of calcite veins in plane light (PL; left) and cathodoluminescence (CL; right): A) Tabular calcite crystals growing perpendicular to the host rock (HR) are zoned under CL with concentric rims converging at the host rock, Sample PEC-15-2C; B) Crystals vary in luminescence under CL: crystal on the left of yellow dashed line is quenched and the crystal on the right is ignite with compositional zonation (contoured by white dashed lines), Sample PEC-15-31BI; C) Photomicrograph within a calcite vein that is cross-cut by a smaller veinlet that is extinct in CL, Sample PEC-16-1.

crystallization event, however this subsequent fluid pulse did not fully re-open the veins. These cross-cutting relationships of smaller veinlets through a main vein suggests a single reactivation event rather than episodic reactivation that would create a crack and seal texture.

Representative samples were imaged under CL to gain a qualitative perspective on the chemical variation in different crystals and cross-cutting veinlets. Some veinlets have similar luminescence under CL to the main vein, whereas other veinlets are quenched relative to the main vein (**Figure 5**). Trace element geochemistry was conducted to quantify chemical variations in the calcite crystals and across the veins.

8.2 Microtectonics

Microscopy is necessary to identify evidence of deformation that is not observable on the outcrop scale, such as minor offsets along veins and intra-crystalline deformation resulting in mechanical twinning and undulous extinction. Under a macroscopic observation (<5x), sample PEC-15-32B evinces displacements of fossil fragments (<350 μm; **Figure 6**). Notably, this sample was collected along the projected trace of the Wellington Fault (station XXIX; **Figure 2**).

Mechanical twinning is the dominant crystal-plastic deformation mechanism in calcite and provide valuable information regarding the magnitude of strain the rock has undergone after crystallization. Mechanical twins follow a spectrum (type I to IV) that correlate to increasing strain and deformation temperatures (Burkhard, 1993). Type I twins develop under low strain (<170°C), and appear as thin (<10 μm) black lines. With increasing strain (~200°C), type II twins develop, which have color fringes with measurable widths, also referred to as lamellar twins (Turner and Ch'ih, 1953). The thickness of calcite twins is inversely proportionate with twin density (twin/mm): at lower temperature, closely spaced type I twins dominate calcite crystals, whereas at higher temperatures, dispersed thick lamellar twins develop (Ferrill, 1991). With increasing strain (>200°C), type III twins develop, which are a continued growth of lamellar twins. Twinned material migrates into untwinned sections of the crystal forming curved and lensoid shapes, and eventually sweeping the entire crystal (Vernon, 1981). Finally, type IV twins develop (>250°C) when twins become tapered and discontinuous. Type IV twins are the first step of recovery during dynamic recrystallization. Crystals that are in the process of recovery also preserve sub-grain growth development. Under the last stage of recovery, when calcite has been completely

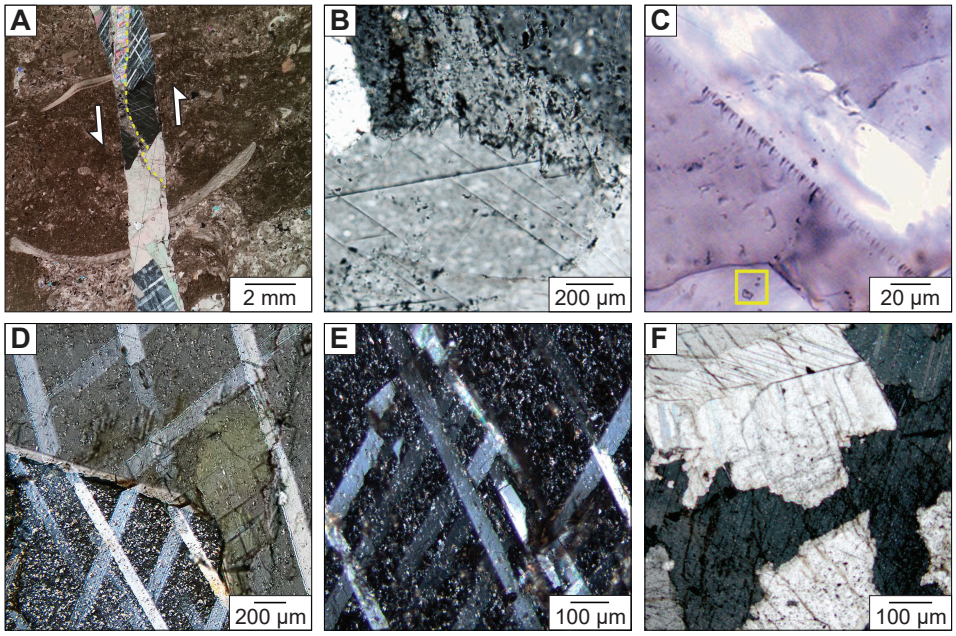


Figure 6 | A) Calcite vein displacing fossil fragments (white arrows). Calcite vein is cross-cut by a veinlet with higher birefringence (white dashed line). Intra-crystalline deformation varies in different crystals through the vein, photo in XPL, Sample PEC-15-32B; B) Pressure solution at grain boundaries, photo in PL, Sample PEC-15-5A; C) Trail of elongated secondary fluid inclusions contouring a type II twin (~45 µm thick) with long axis perpendicular to calcite twin. Cluster of fluid inclusions containing solid precipitates contoured by yellow box, photo in PL, Sample PEC-15-5A; D) Lamellar twins developed at grain boundaries. Crystal developed through sub grain growth at the center of the photomicrograph lacks twinning, photo in XPL, Sample PEC-15-31C; E) Lamellar twins that are kinked and offset, photo in XPL, Sample PEC-15-25DII; F) Photo within calcite vein. Calcite crystals have bulging grain boundaries and undulous extinction, photo in XPL, Sample PEC-15-25C.

recrystallized, calcite crystals have "jig-saw-like" grain boundaries, pervasive undulous extinction, and pre-existing twins are erased (Groshong, 1988; Burkhard, 1993).

Type I and II twins can also form during crystal growth, although twin types III and IV form exclusively during deformation. In this study, type II twins often develop at crystal boundaries (**Figure 6**). The highest differential stress during deformation focusses at grain boundaries, therefore type II twins at crystal boundaries suggest that they developed during deformation (**Figure 6**). In addition, type II twins are locally kinked, broken and offset, suggesting that calcite experience low temperature post-twinning, brittle deformation (**Figure 6**). No veins contain crystals with uniform twinning (types, thicknesses and densities). For example, in sample PEC-15-31C crystals were identified with exclusively type I twins with an average twin thickness of ~8 μm in width, and a density of 11 twins/mm, whereas other crystals have pervasive type II twins with an average thickness of ~65 μm width and a density of 3 twins/mm (**Figure 6**). Similarly, in sample PEC-15-31A a calcite crystal with extensive lamellar twins cross-cuts a recrystallized calcite crystal with no twins. All calcite veins preserve both type I and type II twining, whereas type III and type IV twins are less common. Secondary fluid inclusions are also indicative of deformation as inclusion trails form along healed fracture planes that cross-cut crystals (Goldstein, 2003). Trails of secondary fluid inclusions in our samples are observed under high magnification (50x). Often, several trails of secondary fluid inclusions parallel each other. Elongated fluid inclusions are also found perpendicular to type II twins, and locally contain solid inclusions (**Figure 6**).

Only one sample is composed exclusively of calcite that is completely recrystallized (PEC-15-25C). Crystal boundaries are irregular, and calcite crystals have undulous extinction, however faint type II twins can be observed (**Figure 6**). Notably, this is the only calcite vein that was parallel to bedding. Also, sutured grain boundaries from pressure solution is only observed in one vein (PEC-15-5A, station XI; **Figure 6**). Notably, this sample was collected distal to major fault traces (**Figure 2**).

9. Trace element geochemistry

Calcite crystals were manually separated from the veins. The crystal size varied from <200 μm to ~3 mm. From samples with smaller crystals, we targeted the largest crystals with defined crystal habit. Crystals larger that 1.5 mm were crushed and sieved, and we targeted crystals without

obvious inclusions or discoloration. Five to eleven crystals were selected from each sample, mounted in epoxy, and polished to expose their interior surfaces. Every crystal was analyzed, and one crystal from each sample was analyzed twice.

Trace element geochemistry was done at the University of Ottawa using the Photon Machines Analyte Excite 193 nm Excimer laser coupled with an Agilent 7700x ICP-MS. The laser beam diameter for was 90 μm with a repetition rate of 10 Hz and a fluence of 7 J/cm^2. Each point analysis consisted of 30 s of background measurement, 50 s of ablation followed by 30 s of flushing the system. Each analysis measured Mg, Si, Mn, Fe, Sr, Y, Ba, La, Ce, Pr, Nd, Sm, Eu, Gd, Tb, Dy, Ho, Er, Tm, Yb, Lu, ^{204}Pb, ^{207}Pb, ^{208}Pb, ^{232}Th and ^{238}U. The analyses were calibrated to the internal standard NIST-612, which was analyzed after every five unknowns. MACS-3 was used as an external standard. Calcium values were measured adjacent to each point analysis using a using a JEOL JXA-8230 Superprobe at the University of Ottawa, which were input to *Glitter* software to convert our measurements from counts/second to ppm values. *Glitter* was also used to isolate an appropriate signal for each measurement. Only elements three times above the detection limit were quantified. To avoid biases from instrumentation, all values below the limit of quantification were rejected and attributed a zero value during data reduction.

In addition, trace elements were measured in situ on 100 μm thick sections from five vein samples. A series of traverses across the width of calcite veins were conducted using 90 μm beam size with a repetition rate of 15 Hz and a fluence of 7 J/cm^2. Traverses consist of one continuous measurement during the ablation of the traverse. The signal acquired from the traverse can be used to show relative variations and distribution of trace elements across calcite veins by aligning photomicrographs to the ablated traverse with the raw signal. The absolute values of the signal acquired are equivocal. To resolve this problem and calibrate the acquired signal, in situ point analyses were done adjacent to the traverse profiles. The analytical conditions and data reduction for in situ point analysis are the same as the point analysis done on mineral separates, except Zr was measured and ^{204}Pb was not. The absolute values acquired from the point analysis were added to the traverse signal aligned to photomicrographs. The raw signal was vertically adjusted to fit point analyses that are representative of the composition along the ablated traverse (i.e. within the same crystal). From each point analysis, the sum of all REE's was calculated ($\sum$REE = La + Ce + Pr…+ Lu), and Eu anomalies (Eu/Eu*) were quantified. Eu* is calculated by comparing the measured Eu value with the expected value using the following formula (Brookins 1989):

$$Eu/Eu^* = {Eu}/{\sqrt{Sm \times Gd}}$$

where Eu, Sm, and Gd are measured values. A negative Eu anomaly is defined by values between 0 and 1. The negative anomaly increases when values approach zero.

9.1 Results: mineral separate analysis

The main purpose of conducting trace element geochemistry was to identify samples with the highest ^{238}U content, as these samples are the best candidates for U-Pb geochronology. We also measured major elements and REE to identify different vein populations based on their geochemistry, and to gain insight on the source of fluids. Trace element geochemistry was done on mineral separates from 31 samples from 29 calcite veins, including two veins that were separated into two samples based on crystal morphologies to evaluate if there is a correlation between crystal habit and crystal chemistry. Trace element geochemistry was conducted via LA-ICP-MS, where up to six measurements were taken on each sample, with at least one crystal selected for two-point analysis. Data are available in **Table DR-1**.

Within a sample, the abundance of Mg and Mn varies on a similar order of magnitude whereas other elements (Si, Fe, Sr, etc.) appear to be homogenous within samples. Similar variability is observed in crystals with multiple point analysis. These observations suggest that elements are not distributed homogenously across calcite veins, or even throughout a single crystal. With the variability in elemental concentrations, the data do not follow a normal distribution, therefore median values are more representative of overall results (Mood et al., 1974). The median values of some of the elements are as follows: Mg: 975 ppm; Si: 295 ppm; Mn: 881 ppm; Fe: 2002 ppm; Sr: 129 ppm. A common problem during data collection via LA-ICP-MS analysis is spectroscopic interferences from atoms and ions that have the same mass to charge as the measured analyte (Reed et al., 1994). Instrumental software is used to correct interferences from overlapping isotopes, but not for polyatomic interferences. For calcite, Si and Fe are subject to polyatomic interferences and the reported concentrations may be false (Reed et al., 1994). Of all elements analyzed, Sr values are most homogeneous within samples, and can loosely be used to group samples into three main categories: a depleted Sr population (<120 ppm; n: 14), a normal Sr population (120-190 ppm; n: 11), and a population that is enriched in Sr (>190 ppm; n: 6).

The incorporation of lanthanides into calcite can reveal information on the crystallization conditions. REE values were normalized to chondritic composition to create spider plots (Sun and

McDonough, 1989). A plot was created for each station and different symbols are used to distinguish each sample, and profiles are plotted against the composition of the upper continental crust (**Figure DR-2**). Most calcite separates have similar REE profiles that exhibit a negative slope from LREE to HREE with a negative Eu anomaly (Eu/Eu*). Eu anomalies (Eu/Eu*) and the sum of REE's (∑REE) are also available in **Table DR-1**. Median Eu/Eu* values from all samples is 0.22. At any station, the relative abundance of REE's varies in different samples, and within any sample REEs fractionate from one to three orders of magnitude. Not all samples contained concentrations of lanthanides that were over detection limit of the instrument. In addition, considerable amounts of Y were only measured in three samples.

Three samples have anomalous profiles. The first sample is PEC-15-8, which was collected along a NE-SW trending joint, is relatively enriched in all REEs relative to the upper continental crust (∑REE = 175 ppm) exhibiting a flat REE profile with a strong negative Eu anomaly (Eu*: 0.11; **Figure DR-2**). This sample is relatively enriched in Mn with a median value of 9228 ppm, and is one of the three samples with measurable amounts of Y (median of 165 ppm).

Sample PEC-15-14I and sample PEC-14II were collected from calcite veins that cuts a Jurassic ultramafic dike in the Intalcamenti quarry (Station I). These samples were collected from the same vein but were segregated based on crystal morphologies as PEC-15-14II has distinct fibrous crystal habit. The purpose of dividing the mineral separates from this sample was to evaluate if there is any correlation between crystal morphology and crystal chemistry. The results from the analysis indicate that these two samples have identical geochemistry, it is, however, distinct from other samples in the study. These samples are relatively enriched is LREE compared to the upper continental crust, and have steep REE profiles, a strong negative Eu anomaly (Eu*: 0.13) and ∑REE of 293 ppm (**Figure DR-3**). These samples are also the most enriched in Si (2052 ppm), Mg (3650 ppm), and Sr (572 ppm). Elevated Si measurements could be the inaccurate due to interferences in the LA-ICP-MS (Reed et al., 1994).

The third sample with noticeably different profiles is PEC-15-31B, which was the other calcite vein that was manually separated based on crystal morphologies: the main vein (PEC-15-31BI) and large crystals filling irregular cavities along vein margins (PEC-15-31III). In these samples, some correlations can be made between crystal morphologies and crystal chemistry. The median values of cavity-filling crystals are relatively depleted in most elements, for example: Mn: 929 ppm; Mg: 396 ppm; ∑REE: 1 ppm and U: 0 ppb, whereas the main vein was relatively enriched

in these elements: Mn: 1902 ppm; Mg: 507 ppm, ∑REE: 101 ppm and U: 74 ppb. In addition, the REE profiles from the main vein (PEC-15-31BI) is relatively enriched by two orders of magnitude compared to cavity-filling crystals (**Figure DR-2**).

As aforementioned, only three samples had measurable quantities of Y, their respective median values are: PEC-15-8 with Y: 165 ppm; PEC-15-5A with Y: 5 ppm; and PEC-15-5B with Y: 8 ppm. Notably, sample PEC-15-8 was collected from station XVI, which is the westernmost station of the field area, and is potentially transected by the Hamilton-Presqu'île Fault. The neighboring station to the east is station XI, where both samples PEC-15-5A and -5B were collected (**Figure 2**). Being that no other samples consistently measure Y, it is possible that there is a correlation between Y and proximity to the Hamilton-Presqu'île Fault. No other correlations have been made between trace element geochemistry and geographic distribution of samples, nor the biostratigraphic unit from which samples were collected.

With respect to finding samples suitable for U-Pb geochronology, measurable amounts of U were not present in most samples. Only four samples consistently measured ^{238}U above the ICP-MS's limit of detection; these samples and their respective median values of ^{238}U in ppb are: PEC-15-2A: 39 ppb, PEC-15-2C: 56 ppb, PEC-15-8: 75 ppb, and PEC-15-31A: 70 ppb. In addition, sample PEC-15-30 contained variable amounts of ^{238}U from 0-510 ppb. A single point analysis of 510 ppb ^{238}U also yielded a Si content of 6557 ppm, which is 22x higher than the median of all samples, suggesting that the analysis could be an inclusion, although the high Si value could falsely be caused by interferences (Reed et al., 1994). Two-point analysis from the same crystal in sample PEC-15-30 measured similar values (320 ppb and 318 ppb), suggesting the distribution of ^{238}U varies from crystal to crystal within the calcite vein. Based on our preliminary geochemical work, these five aforementioned samples were prioritized for U-Pb geochronology. Two additional samples were later selected for U-Pb geochronology that were selected based on their stable isotope signature in an attempt to target samples from different populations, which is discussed below. These samples are: PEC-15-5A with ^{238}U values varying from 0-92 ppb and a median of 4 ppb, and PEC-15-25A with ^{238}U values varying from 0-17 ppb and a median of 6 ppb.

9.2 Results: in situ analysis

Imaging under CL gives a qualitative perspective on the distribution of Mn and Fe, since these elements are known to control luminescence, however CL does not provide information on

the distribution of all other trace elements (Hemming et al., 1989). From geochemical analysis on mineral separates it is evident that crystal chemistries are highly variable throughout veins, as well as single crystals. Geochemical analysis on mineral separates provides no spatial context on the location of calcite crystals within the vein. An in situ analysis was conducted with the purpose of mapping the distribution of trace elements across the width of calcite veins, and purposely targeting cross-cutting veins, crystals with different morphologies, as well as crystals that are zoned under CL. The in situ analyses were also conducted via LA-ICP-MS, and the beam was rastered across the width of the calcite veins, and corrected by adjacent point analysis. Point measurements from the in situ analysis are in agreement with measurements taken on mineral separates for their respective samples and were used adjust the raw signal acquired from the traverse. Aligning photomicrographs of the ablated traverses provides a qualitative comparison on chemical variations that correlate to crystal boundaries, inclusions and distinguish the composition of the cores and rims of zoned crystals. This method also provides a unique opportunity to correlate variable luminescence to other trace elements. The analysis was conducted on five samples that were selected for U-Pb geochronology. Traverses of ^{238}U, Sr and ∑REE are presented in **Figure 7, Figure 8, Figure 9, Figure 10,** and **Figure 11**), and absolute values from point analysis are available in **Table DR-1**.

From the traverses, the most evident observation is a correlation between sharply elevated concentrations in Sr, ^{238}U, and ∑REE that align with opaque material observed in polarized petrography (e.g. **Figure 7**; **Figure 11**) as well as with crystal boundaries (e.g. **Figure 8**; **Figure 9**). Also, an antithetic relationship between ∑REE's and Sr is often present (e.g. **Figure 9**; **Figure 11**). Variability in crystal chemistries across calcite veins is different in all samples. For example, traverses from samples PEC-15-5A and PEC-15-31A analyzed over a dozen crystals however, in PEC-15-31A, the Sr and ∑REE signals are highly variable in each crystal suggesting that crystal chemistry is highly variable, whereas in PEC-15-5A, the Sr and ∑REE signal is relatively flat suggesting the crystal chemistry is uniform across the vein (**Figure 8**; **Figure 11**). In veins that show evidence of syntaxial-biaxial growth (e.g. PEC-15-8), there is a correlation between crystal size and chemistry: smaller crystals residing at the vein-wall rock interface are relatively enriched in Sr (~60 ppm), and equant crystals filling the center of the vein are relatively depleted in Sr (<40 ppm; **Figure 9**). In the same sample, there is compositional zonation of ∑REEs in the equant crystal filling the center of the vein (~400 μm wide), with ~100 ppm in its core and ~40 ppm at

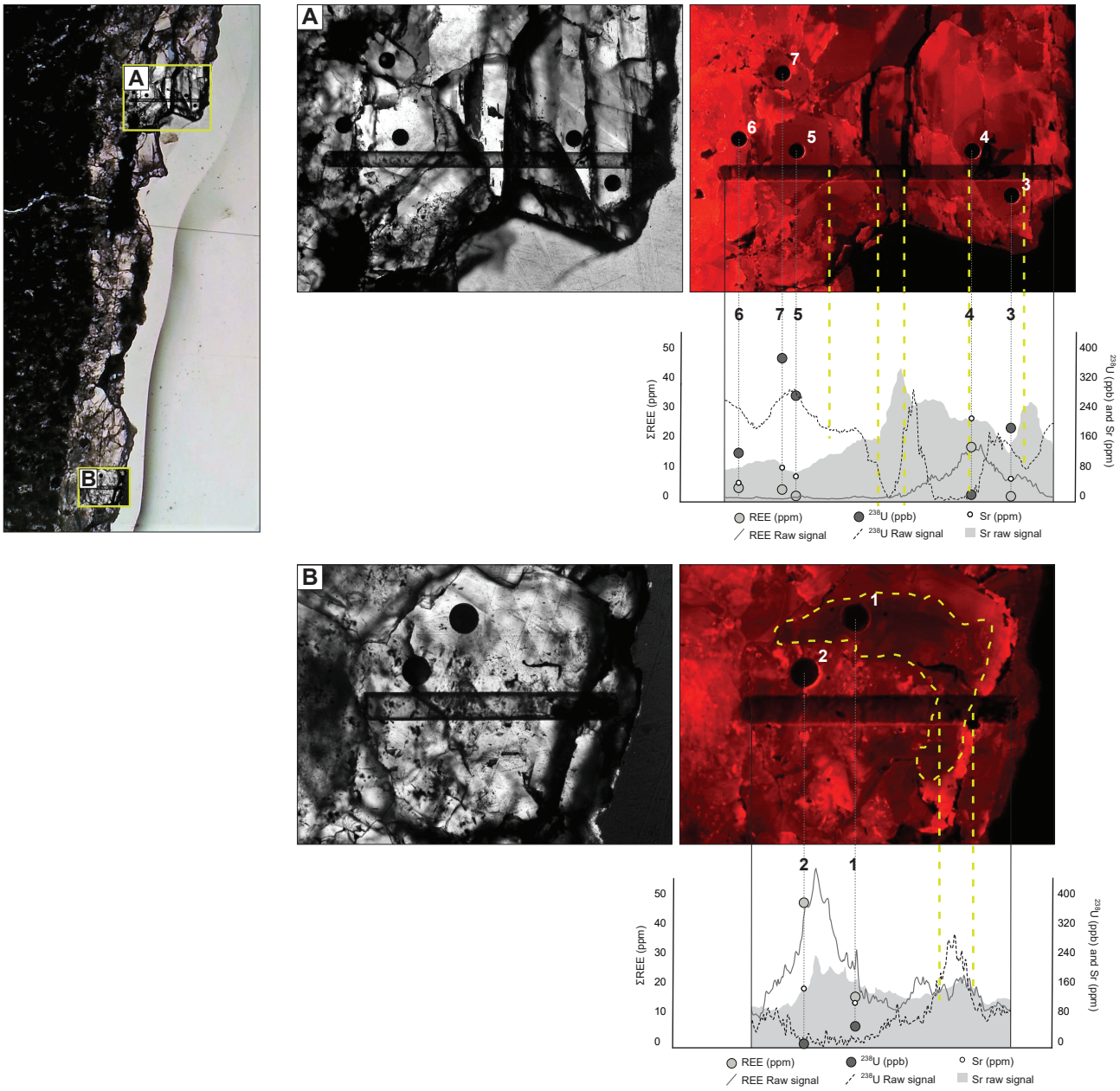


Figure 7 | LA-ICP-MS traverse profiles and point analysis for REE's, 238U and Sr for sample PEC-15-2A. Relative position of traverses A and B are highlighted by yellow boxes in thick-section photo (left). Photomicrographs of the ablated traverses in CL are aligned with the raw signal acquired, projected in the diagrams below: Black vertical lines mark the start/end of the traverse and vertical yellow-dashed lines mark crystal boundaries. Measurements from point-analysis are projected as points in the diagram: REEs are measured in ppm, corresponding to the vertical axis on the left, 238U is measured in ppb and Sr is measured in ppm corresponding to the vertical axis on the right. Calcite crystals vary in composition. Traverse A shows 238U residing at crystal boundaries and the relative abundance of REEs varying in different crystals. Traverse B shows REEs residing in crystal domains with abundant fluid inclusions (refer to photomicrograph in PL), and 238U residing at crystal boundaries as well as in crystal domains that are quenched under CL (white dashed line). REE and 238U distribution seem to be inversely correlated. The numbered points are the names of the spot analysis listed in Table DR-1 where geochemical values are available. Ablation pits from point analysis are 100 μm in diameter for scale.

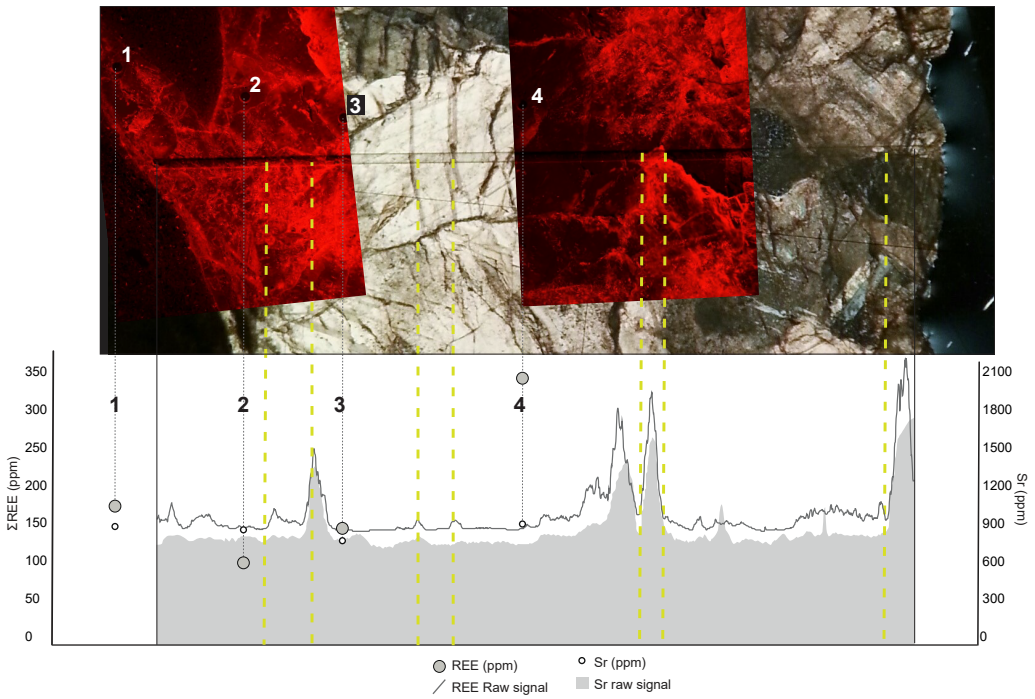


Figure 8 | LA-ICP-MS traverse profile and point analysis for REEs and Sr for sample PEC-15-5A. The 238U signal from the traverse is flat, and excluded from this figure. A compilation of photomicrograph of the ablated traverses in CL and XPL are aligned with the raw signal acquired, projected in the diagram below: Black vertical lines mark the start/end of the traverse and vertical yellow-dashed lines mark crystal boundaries. Measurements from point-analysis are projected as points in the diagram. REEs and Sr are measured in ppm, REE values correspond to the vertical axis on the left, and Sr values correspond to vertical axis on the right. Calcite crystal appear to be relatively homogenous in composition, and are enriched in Sr (>600 ppm). Peaks in the REE signal align with crystal boundaries that are ignite under CL, and fractures in calcite crystals. The numbered points are the names of the spot analysis listed in Table DR-1 where geochemical values are available. Ablation pits from point analysis are 100 μm in diameter for scale.

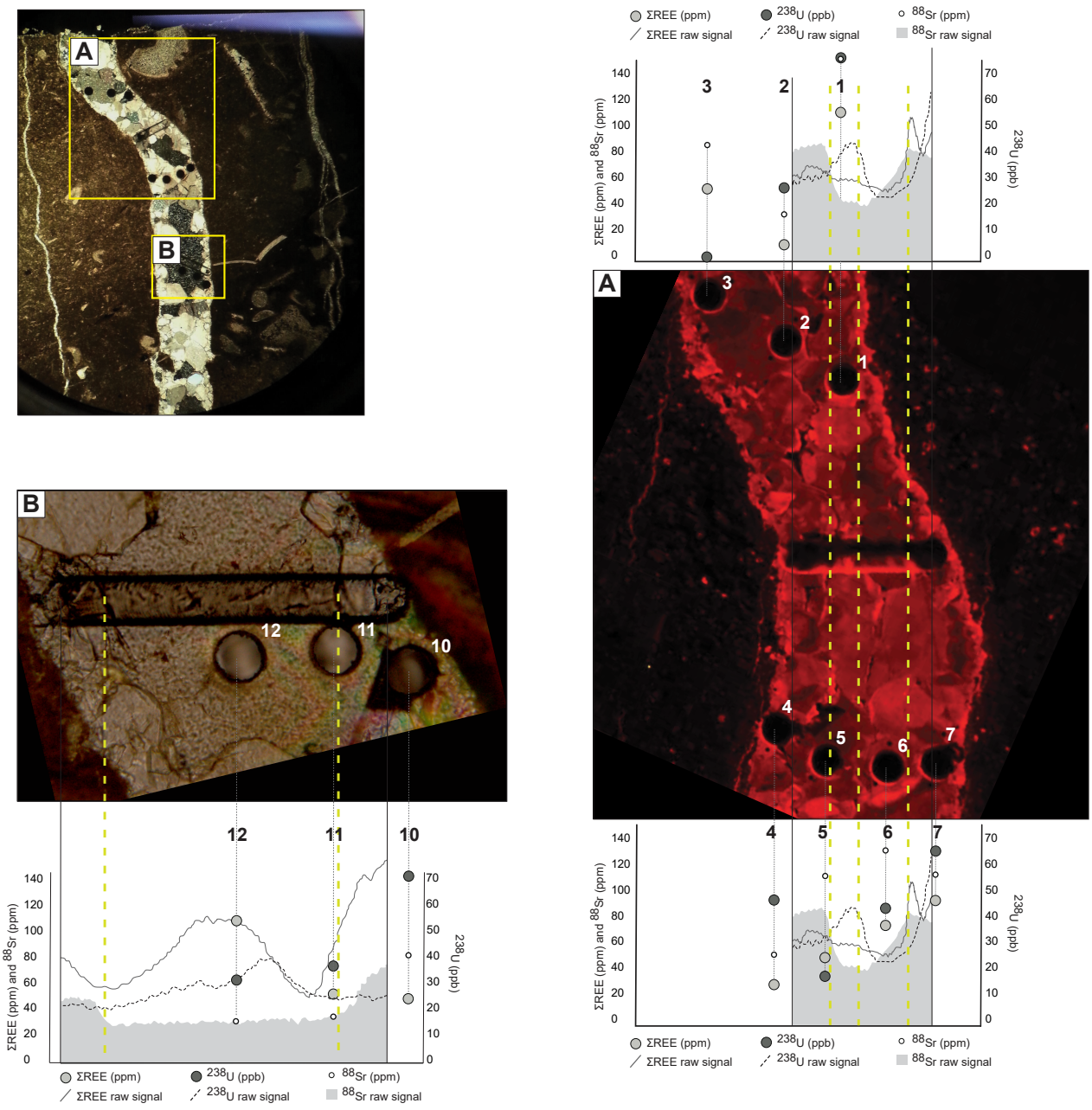


Figure 9 | LA-ICP-MS traverse profiles and point analysis for REEs, 238U and Sr for sample PEC-15-8. Relative position of traverses A and B are highlighted by yellow boxes in thick-section photo. Photomicrographs of the ablated traverses in XPL/CL aligned with the raw signal acquired, projected on their respective diagrams. Black vertical lines mark the start/end of the traverse and yellow-dashed lines mark crystal boundaries. Measurements from point-analysis are projected as points in the diagram: REEs and Sr are measured in ppm, and correspond to the vertical axis on the left. 238U is measured in ppb and corresponds to the vertical axis on the right. Calcite crystal vary in composition. All traverse signals suggest an enrichment in Sr in small crystals residing at the vein-wall-rock interface. The large equant crystal in the center of traverse B is zoned in 238U and REE's. In traverse B, 238U and REEs are concentrated at crystal boundaries. The numbered points are the names of the spot analysis listed in Table DR-1 where geochemical values are available. Ablation pits from point analysis are 100 μm in diameter for scale.

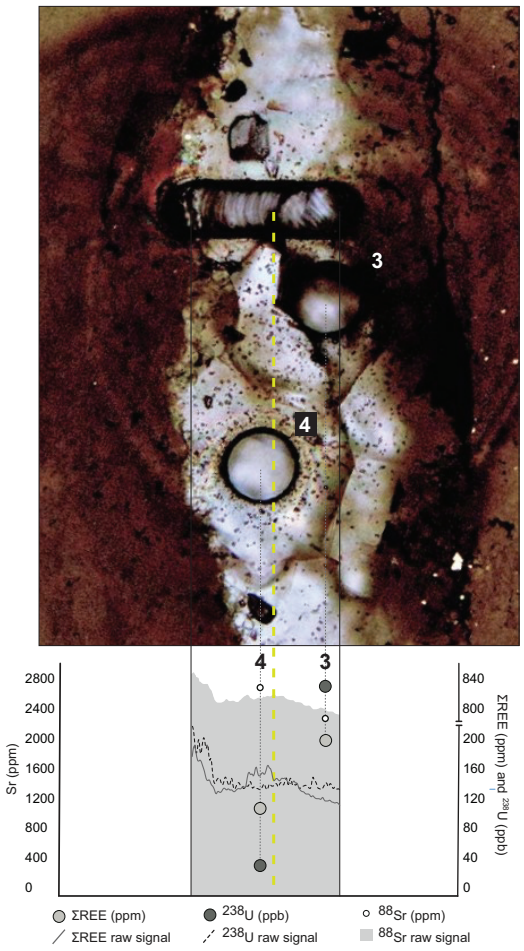


Figure 10 | LA-ICP-MS traverse profiles and point analysis for REEs, 238U and Sr for sample PEC-15-30. Photomicrograph of the ablated traverses in XPL is aligned with the raw signal acquired, projected in the diagrams below: Black vertical lines mark the start/end of the traverse and vertical yellow-dashed line mark crystal boundaries. Measurements from point-analysis are projected as points in the diagram: Sr is measured in ppm, corresponding to the vertical axis on the left, 238U is measured in ppb and Sr is measured in ppm corresponding to the vertical axis on the right. Calcite vein is relatively enriched in Sr (>1600 ppm). Calcite crystals have fluid inclusions. Point 3 is located at a crystal boundary and is enriched in 238U and REE's. The numbered points are the names of the spot analysis listed in Table DR-1 where geochemical values are available. Ablation pits from point analysis are 100 μm in diameter for scale.

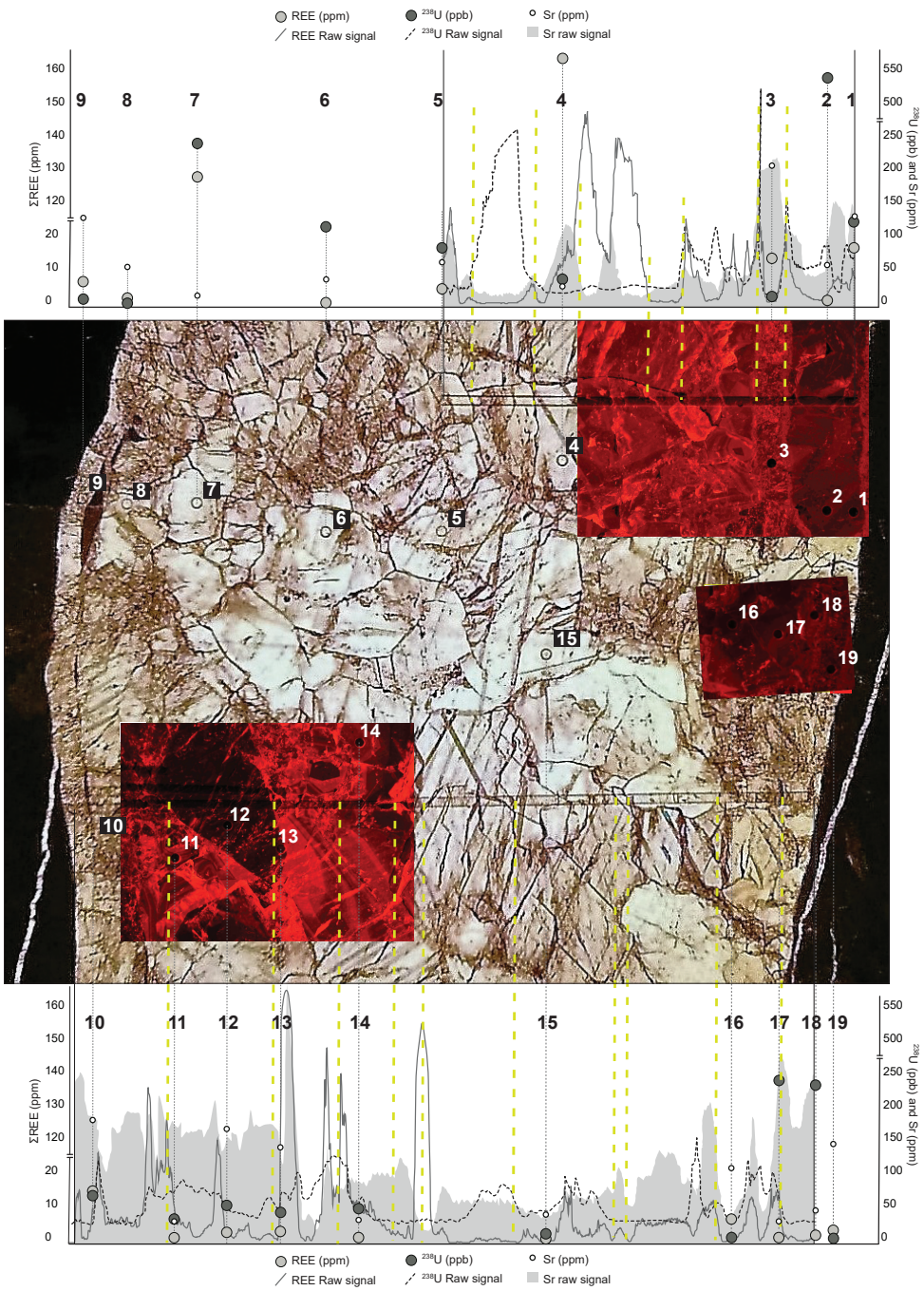


Figure 11 | LA-ICP-MS traverse profiles and point analysis for REEs, 238U and Sr for sample PEC-15-31A. Photomicrographs of the ablated traverses in CL are aligned with the raw signal acquired, projected in the diagrams above and below: Black vertical lines mark the start/end of the traverse and vertical yellow-dashed lines mark crystal boundaries. Measurements from point-analysis are projected as points in the diagram: REEs are measured in ppm, corresponding to the vertical axis on the left, 238U is measured in ppb and Sr is measured in ppm corresponding to the vertical axis on the right. Calcite crystals vary in composition. Sr concentrations vary in different crystals. 238U and REE peaks allign with opaque material residing at recrystalized grain boundary. The numbered points are the names of the spot analysis listed in Table DR-1 where geochemical values are available. Ablation pits from point analysis are 100 µm in diameter for scale.

the crystals rim, however no zonation was observed in CL for this crystal. In other samples, there are correlations between luminescence and trace elements (**Figure 9**). For example, in PEC-15-2A, sector zones that are quenched under CL are relatively enriched in ^{238}U (~150 ppb) compared to the rest of the vein (<50 ppb; **Figure 7**). In the same sample, ∑REEs reside in crystal domains with abundant fluid inclusions.

Cross cutting veinlets are observed in the traverses of sample PEC-15-31A. A cross cutting veinlet has 201 ppm of Sr, whereas adjacent crystals have values have Sr values of ~50 ppm. In the same sample crystals that are uniformly quenched under CL are relatively enriched in Sr (~150 ppm) compared to parts of the vein that are illuminated (<50 ppm). Overall, the Sr concentration is variable across the width of calcite vein with marked variations aligning with crystal boundaries. The chemical signature of the cross cutting vein is very minor, and similar variations are present in zoned crystals, and between neighboring crystals, thus variability in trace elements between neighboring crystals can be larger than cross cutting veinlets.

10. Stable isotope geochemistry

Stable isotopes fractionate in different proportions during geologic and chemical processes (Faure and Mensing, 2005). Major fluid reservoirs have known isotopic fingerprints that can be used to compare values measured from unknown samples to gain information on the source of fluids. Stable isotope values are measured by comparing the ratio of heavy to light isotopes. The isotope's mass affects the strength of their covalent bonds, and dictates how they fractionate. In this study, calcite samples were measured for $\delta^{18}O$ and $\delta^{13}C$. $\delta^{18}O$ is the ratio of $^{18}O/^{16}O$, where ^{18}O is 12.5% heavier than ^{16}O and accounts for 0.2% of oxygen (Faure and Mensing, 2005). $\delta^{18}O$ values are normalized to the *Vienna Standard Mean Ocean Water* (V-SMOW; Coplen et al., 2002). $\delta^{13}C$ is the ratio of $^{13}C/^{12}C$, where ^{13}C is 8.4% heavier and accounts for 1.1% of carbon. $\delta^{13}C$ values are normalized to a marine carbonate standard of *Vienna Pee-Dee Belemnite* (V-PDB; Coplen et al., 2002).

Calcite was separated from the veins, crushed into a fine powder, and weighed into exetainers with 0.1 mL of H_3PO_4 (S.G. 1.91). The exetainers are capped and He-flushed while horizontal. Reaction at 25°C for 24 hrs is followed by extraction in continuous flow. The measurements are performed on a Thermo Finnigan Delta XP and a Gas Bench II at the University of Ottawa. See Application Flash Report G31 from Thermo Finnigan for instrument details.

Analytical precision (2 sigma) is ±0.1‰. Oxygen data was normalized using international standards NBS-18 and NBS-19, and carbon data was normalized using international standards NBS-18, NBS-19, and LSVEC. $\delta^{13}C$ and $\delta^{18}O$ values were measured relative to V-PDB. δ18O V-PDB values were converted to $\delta^{18}O$ VSMOW values by using the following formula by Coplen et al. (2002):

$$\delta^{18}O \text{ V-SMOW} = 1.0309\ \delta^{18}O \text{ V-PDB} + 30.92$$

10.1 Results

All calcite veins were analyzed for $\delta^{13}C$ and $\delta^{18}O$ except for one sample that did not provide sufficient material (PEC-15-14II) yielding a total of 36 samples for analysis, reported in **Table DR-1**. $\delta^{13}C$ values vary between -0.9‰ and 6.2‰ and $\delta^{18}O$ values between 19.5‰ and 24.8‰ (**Figure 12**). To determine the source of fluids from the calcite veins in this study, measured $\delta^{18}O$ of $\delta^{13}C$ values were compared to theoretical values associated to various fluid reservoirs. Notably, the most relevant comparable isotopic values to our study were that of Middle Ordovician marine carbonate ($\delta^{13}C$: 0-4.5‰ V-PDB and $\delta^{18}O$: 22-25‰ V-SMOW; Coniglio et al., 1994). Values from other fluid reservoirs such as meteoric fluids, mantle source, or magmatic fluids do not overlap any measured values in this study (e.g. Faure and Mensing, 2005). The theoretical values of Middle Ordovician marine carbonate were used as a constraint to identify samples with identical compositions (Coniglio et al., 1994; **Figure 12**). A total of fifteen samples plot within Middle Ordovician marine carbonate material, and another five plot directly below the lower $\delta^{13}C$ constraint between -0.01‰ to -0.13‰. By including these five samples, most (n: 20) samples fall within the constraint of Middle Ordovician marine carbonate material. Numerous factors effect isotope fractionation for example, higher $\delta^{18}O$ and $\delta^{13}C$ values can be attributed to a slow rate of crystal growth, higher pH of fluid, or lower temperatures during crystallization (e.g. Faure and Mensing, 2005; Gabitov and Watson, 2005). In addition, dispersed values can also be attributed to increased fluid-rock interaction (Gabitov and Watson, 2005). It is difficult if not impossible within the scope of our study to attribute isotope fractionation to a specific parameter with the numerous unknown variables in a natural environment.

Four groups were created based on similar stable isotope signatures relative to the composition of Middle Ordovician marine carbonate material. This was done to identify similarities between samples of a specific group (e.g. crystal morphology or crystal chemistry) that

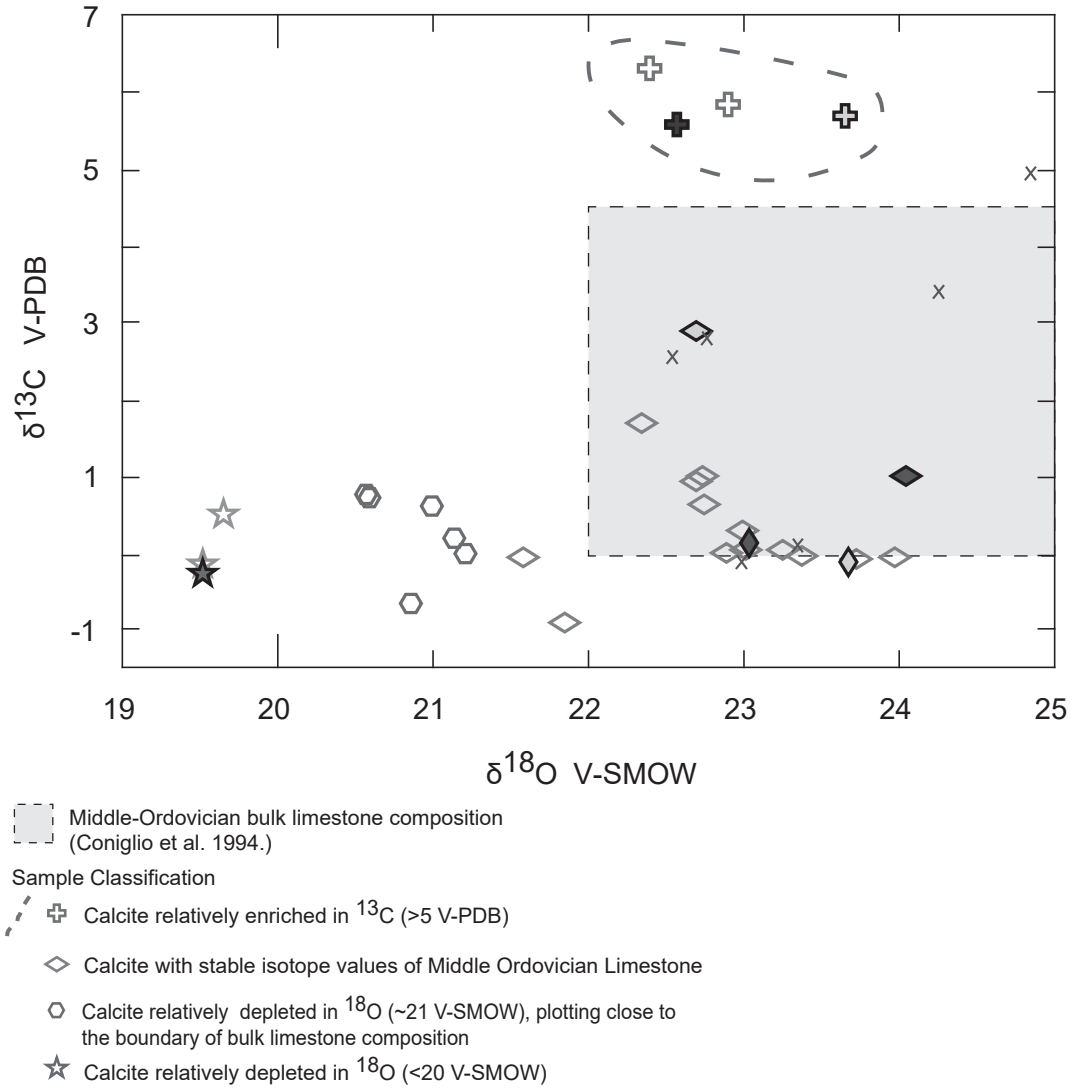


Figure 12 | Carbon vs. oxygen isotopic composition of 36 calcite veins. Samples are grouped based on their isotopic signature. Samples with an enriched δ13C signature are contoured by a dashed line and are also distinguished by dashed lines in their respective spider plots in Figure DR-2. Samples measured via U-Pb are distinguished by distinct symbols: PEC-15-2A:✚; PEC-15-2C:◇; PEC-15-5A:★; PEC-15-8:◆; PEC-15-25A:✜; PEC-15-30:◊; PEC-15-31A:⧫. Samples without trace element geochemistry are represented by an "x" symbol.

could potentially reveal information on some of the parameters that control fractionation during crystallization. The first group consists of samples with the same composition as Middle Ordovician marine carbonate material (n: 20). The second group is relatively enriched in $\delta^{13}C$ with respect to group 1 ($\delta^{13}C$ >4.5‰; n: 5). The other two groups have normal $\delta^{13}C$ values, but are relatively depleted in $\delta^{18}O$ with respect to group 1; the third group is slightly depleted in $\delta^{18}O$ ($\delta^{18}O$: 20-22‰; n: 8), and the fourth group is more depleted in $\delta^{18}O$ ($\delta^{18}O$ <20‰; n: 3). Different groups are unique symbols in **Figure 12**.

The five samples enriched in $\delta^{13}C$ values are PEC-15-25A (station II), PEC-15-31BIII (station X), PEC-16-4A (station XXXII), and PEC-15-2A as well as PEC-15-27 (station VII). At station VII, both PEC-15-2A and PEC-15-27 are composed of crystals with a distinctly larger crystal habit (~1 mm; **Figure 12**) and the internal structure of the vein is exposed along the face of the fracture since the adjoining host rock as eroded away. Sample PEC-15-27 is a euhedral overgrowth on a slicken-slide fabric, indicating that it is secondary overgrowth. Other samples collected from station VII (PEC-15-2C; PEC-15-9; PEC-16-3) have smaller crystal habits, and have the same stable isotope signature as Middle Ordovician marine carbonate material reference.

Sample PEC-15-31BIII also has distinctly large crystal habit. The sample is cavity-filling crystals along the vein margin of sample PEC-15-31BI. Notably, these cavity-filling crystals have an enriched $\delta^{13}C$ signature (6.3‰) relative to the main vein ($\delta^{13}C$: 0.64‰), which has the same signature of Middle Ordovician marine carbonate reference. All other samples collected from station X (PEC-15-4; PEC-15-31A; PEC-15-31C) also have the same stable isotope signature as Middle Ordovician marine carbonate material.

Sample PEC-16-4B was collected along at the base of an excavation wall of the Foster Rock limestone quarry (station XXXII) within a fault plane preserving cm-scale offset (**Figure 4**). This sample has an anomalous stable isotope signature that is elevated $\delta^{13}C$ signature (4.9‰) but does not cluster with other samples due to its high $\delta^{18}O$ value (24.9‰), which is the highest $\delta^{18}O$ value measured in this study (**Figure 7**). Similar to other samples from with an elevated $\delta^{13}C$ signature, this sample also has a large crystal habits (>2 mm).

The last sample with an elevated $\delta^{13}C$ signature is PEC-15-25A ($\delta^{13}C$: 5.7‰) from station II. Comparatively, this sample is a 1.5 mm wide vein with a considerably smaller crystal habit (<100 μm) then the other samples with high $\delta^{13}C$. Other samples collected from station II have different stable isotope signatures: PEC-15-25C has the same isotopic signature as Middle

Ordovician marine carbonate reference, and PEC-15-25B, PEC-15-25DI and PEC-15-25DII are part of the group that is slightly depleted in $\delta^{18}O$ ($\delta^{18}O$: 20-22‰). Interestingly, PEC-15-25B is also a mm-wide vein, whereas PEC-15-25DI and PEC-15-25DII are larger veins (>3 mm wide) with larger crystal habit. Also, PEC-15-25C is the only sub-horizontal vein in this study, however it is the only vein that has the same isotopic signature as Middle Ordovician marine carbonate material from this station. Notably, station II is located directly on the trace of the Picton Fault (**Figure 2**).

Five other samples are part of the group that is slightly depleted in $\delta^{18}O$ are: PEC-15-6 (station XIII), PEC-15-28 (station XVIII), PEC-15-29 (station IV), and PEC-15-12B as well as PEC-15-14II (station I). Of the stations where multiple samples were collected, different samples often plot in different stable isotope population. For example, samples PEC-15-7 and PEC-15-10 were collected from stations XIII and station XVIII, respectably and have the isotopic composition of Middle Ordovician limestone. These four samples are all mm-wide, and have a similar geochemistry so there is no obvious correlation to attribute to their variable isotopic signatures. At station I, PEC-15-14II ($\delta^{18}O$: 21.9‰) is a mm-wide calcite vein hosted in a Jurassic ultramafic dike, and PEC-15-12 ($\delta^{18}O$: 20.6‰) is a calcite vein hosted in limestone within the excavation wall with a much larger crystal habit and both samples have a stable isotope signature that is slightly depleted in $\delta^{18}O$. Sample PEC-15-13 is also from station I, and resembled sample PEC-15-12 in the field, however PEC-15-13 is anomalous and has the lowest $\delta^{18}O$ values in this study (19.7‰; **Figure 12**). It is surprising that the stable isotope signature of the calcite vein collected from the ultramafic dike was not affected by its host rock, and there is no obvious explanation for the low $\delta^{18}O$ signature of sample PEC-15-13. The other two samples that are most depleted in $\delta^{18}O$ are PEC-15-5A and PEC-15-5B, both collected from station XI (**Figure 2**). The station is not located on the trace of any mapped faults, however there is petrographic evidence of subtle deformation through pressure solution is at crystal boundaries (**Figure 6**; **Figure 12**).

To summarize, the stable isotope signature of all samples measured in this study are the same, or at least comparable to the Middle Ordovician marine carbonate reference. Various factors such as the temperature and pH of the fluid during crystallization, fluid wall rock interaction, and the rate of crystal growth can affect $\delta^{18}O$ and $\delta^{13}C$ values (e.g. Faure and Mensing, 2005; Gabitov and Watson, 2005). Samples were grouped into four different populations based on stable isotope signature with the purpose of identifying other similarities between veins of a given group and can

potentially reveal information on the parameters responsible for isotope fractionation. Samples with an elevated $\delta^{13}C$ signature have large euhedral crystals (>2 mm), and sometimes secondary growth (e.g. PEC-15-27 and PEC-15-31BIII), although sample PEC-15-25A is an exception and has a smaller crystal habit. Samples collected along the northern extent of the Picton Fault (stations I and II) are depleted in $\delta^{18}O$ relative to Middle Ordovician marine carbonate material (n: 7). No other correlations were made between stable isotope signature and geographic distribution since the majority of stations where multiple samples were collected often possess samples with stable isotope signatures from more than one of the populations that we defined. Finally, there are no obvious correlations between trace elements and stable isotope signature. For example, the three samples that have distinct high Y values, and enriched in REEs (PEC-15-5A, PEC-15-5B, PEC-15-8) do not share the same stable isotopic signature: PEC-15-5A and PEC-15-5B are depleted in $\delta^{18}O$, and PEC-15-8 has the same signature as Middle Ordovician marine carbonate material. Also, the calcite vein collected from the Jurassic dike with a distinct REE profile (PEC-15-14II) is only slightly depleted in $\delta^{18}O$ whereas neighboring veins hosted in limestone are more depleted in $\delta^{18}O$ (PEC-15-13).

11. U-Pb geochronology

Seven samples of secondary calcite were selected for U-Pb geochronology, which was conducted on the same polished mineral mount analyzed for trace element geochemistry. After imaging, samples were ablated and analyzed using a New Wave UP-193 laser ablation system with a 193 nm beam coupled to an Agilent 7900 Inductively Coupled Mass Spectrometer (ICP-MS) housed at the University of Toronto (UT). The laser beam diameter for calcite unknowns and calcite reference material was 150 μm, at 10 Hz, and with a fluence of ~5 J/cm2. Frequency and beam size were reduced for NIST 612 and NIST 610 glass reference materials (50 μm, 5 Hz), which possess U concentrations of 37 ppm and 462 ppm, respectively. In order to determine relative Pb/U ablation fractionation of these glass standards versus calcite material, a calcite sample of known age was used. NIST 610 was used for the Pb-Pb calibration and the 254 ± 6 Ma Walnut Creek calcite (WC-1; Roberts et al., 2017) was used for U-Pb calibration. The fractionation correction was zero as no detectable fractionation was measured upon analysis of WC-1 normalized to NIST610. During the experiment, four unknowns were analyzed between each reference material analysis. Spots were pre-ablated by rastering the beam over an area larger than

the beam diameter to clean the surface. Following a 10 s period of baseline accumulation the laser was turned on and data were collected for 25 s followed by a washout period. Measurements of ^{206}Pb (40 ms), ^{207}Pb (40 ms) and ^{238}U (20 ms) yield age information, ^{88}Sr and ^{43}Ca (10 ms) assess efficiency of ablation, and ^{232}Th (10 ms) evaluates detrital material or secondary mineralization. The analytical set-up for calcite dating outlined here have resulted in reproducible data that have been verified via isotope-dilution thermal ionization mass spectrometry (ID-TIMS) U-Pb geochronology in an independent study (Davis, 2013, 2016).

Data reduction used in-house VBA software written by D. Davis (UT). Data acquisition involves collecting hundreds of cycles of ^{207}Pb, ^{206}Pb and ^{238}U measurements (~150 ms/cycle) as the beam penetrates deeper into the sample and displays the ratios in a time-resolved profile. The traditional approach to data reduction is to define an acceptable window within the data profile and average the ratios. Calcite typically has low (<1 ppm) U concentrations and the most useful samples for dating are those with very low initial common Pb concentrations so that a significant proportion of the Pb is radiogenic. Relatively young (<100 Ma) radiogenic samples will have much lower Pb concentrations compared to U. One problem with averaging ratios is that when the signal approaches baseline values, the ratios become highly variable since a near-zero measured value in the denominator will cause the apparent ratio to increase without limit so the average tends to skew toward higher values. We attempted to prevent this problem by establishing the average ratio on the sum of total counts in the numerator and denominator peaks. A discussion of the statistical theory is available in Ogliore et al. (2011). A limitation of this approach is that the calculation of standard deviations cannot be based on the scatter of individual measurements as with ratio averaging. Instead, we calculated a standard deviation for the ratio based on the root-mean-square of $1/\sqrt{N}$ where N is the number of counts in each measurement. This is a minimum estimate of the true standard deviation. The total standard deviations (σ) for Concordia coordinates and their cross correlations (ρ) are determined by increasing each input parameter (measured sample and standard ratios) by 1σ, calculating the results, and then taking the root-mean-square values of the deviations of these results from the means to produce variances and covariance for the mean Concordia coordinate values.

Another problem with data collected from calcite is that there are often numerous signal surges (i.e., spikes), particularly on the Pb isotopes, due to the explosive nature of the ablation process. Therefore, some data sets may have to be heavily edited. In the ratio averaging approach,

anomalously high or low $^{207}Pb/^{206}Pb$ and $^{206}Pb/^{238}U$ ratios can be edited independently. In the peak summing approach that we applied, peaks rather than ratios are edited and the rejection of one peak requires removal of all other peaks in the cycle. In most cases anomalous spikes are much higher than surrounding signals so the choice of editing is obvious, but this is not always the case thus there is the danger of over-editing, which could bias data. The current software version has an 'auto edit' feature that allows peaks to be edited to a chosen multiple of a standard deviation ($1/\sqrt{N}$).

Time-resolved profiles of ratios for zoned calcite often show varying $^{207}Pb/^{206}Pb$ and $^{206}Pb/^{238}U$ values, which may be due either to variable age or to variations in the ratio of U to initial common Pb. A feature of the software is that it presents a time-resolved profile of model ages. Where data are sufficiently precise, resolving and averaging of specific age zones is meaningful and results in more consistent and statistically robust ages. Meaningful age information can be extracted even when Pb signals are only a few counts in each cycle.

For LA-ICPMS data, ^{204}Pb cannot be measured accurately so measurements of total Pb/U isotopes are plotted. The presence of significant common Pb has the effect of shifting data to the right and upward towards an age of ca. 5000 Ma. Hence, multiple data with a similar age but different levels of common Pb will form a linear array on the Concordia plot with the lower Concordia intercept giving the age of the radiogenic component. Model ages are calculated for each LA-ICPMS datum by projecting along a radiogenic-common Pb mixing line to Concordia, assuming a $^{207}Pb/^{206}Pb$ ratio of 0.83 for the common Pb based on the Stacey and Kramers (1975) growth curve. Reduced data are plotted and averaged using Isoplot (Ludwig, 2003). Ages and error ellipses are given at 2σ unless otherwise noted.

11.1 Results

Seven samples were strategically selected for U-Pb geochronology to obtain crystallization ages of calcite veins (**Figure 13, Table DR-2**). Samples were collected over a broad geographic extent, both proximal and distal to major fault traces: samples PEC-15-5A (station XI), PEC-15-2A and PEC-15-2C (station VII) were collected distal to major faults, sample PEC-15-25A (station II) and PEC-15-30 (station XXVI) are collected on the trace of the Picton Fault, sample PEC-15-8 (station XVI) was collected near the Hamilton Presqu'île lineament and sample PEC-15-31A (station X) was collected along the trace of the Salmon Point Fault.

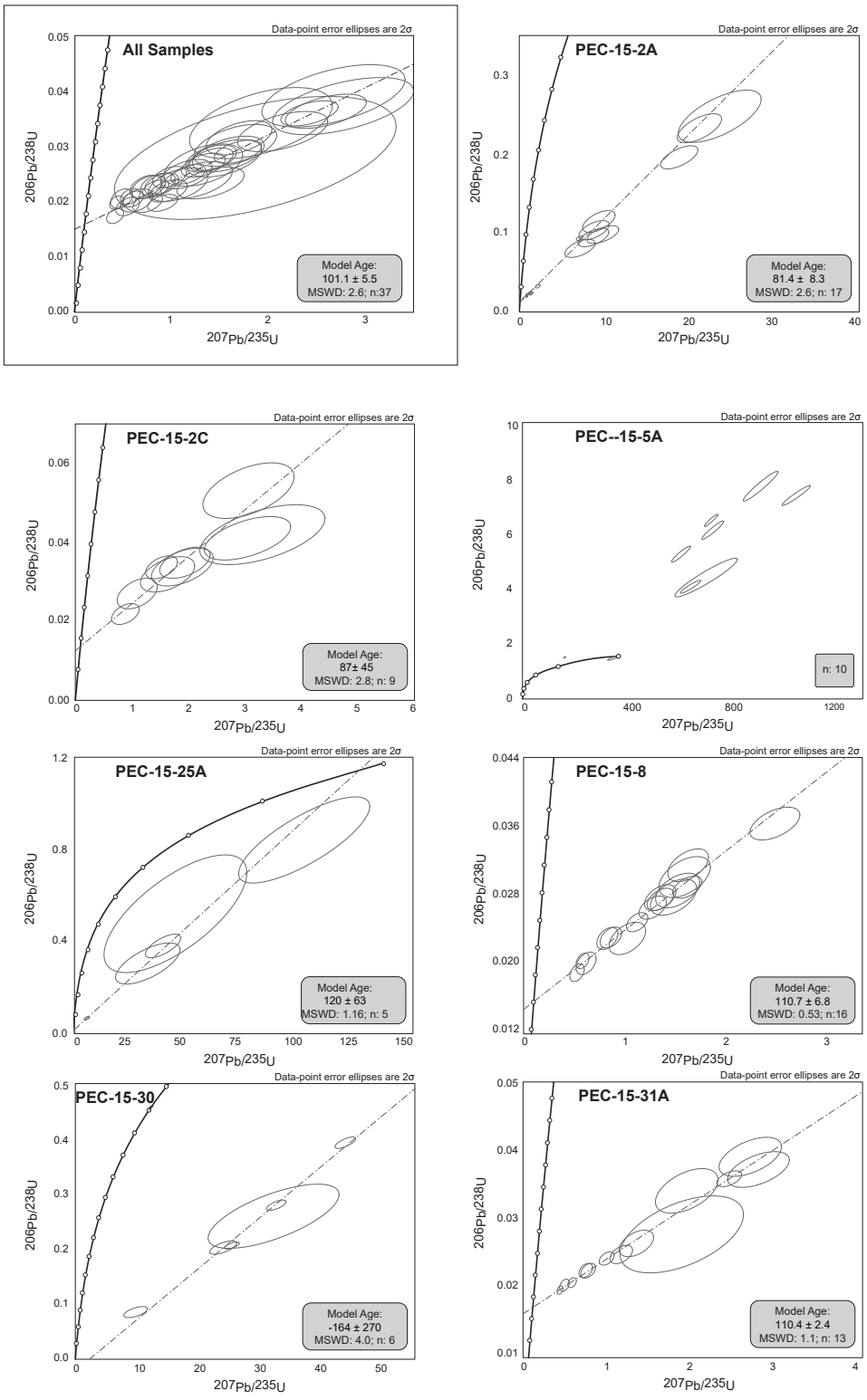


Figure 13 | U-Pb Concordia diagrams from LA-ICP-MS data yielding model ages of calcite mineralizing. Diagrams of seven samples that were dated, as well as a compilation of all measurements regressed on a single concordia diagram (n: number of measurements).

Three of the four samples that consistently measured ^{238}U above detection limit during trace element geochemistry provided the most reliable model ages: sample PEC-15-2A yielded the youngest model age of 81.4 ± 8.3 (MSWD: 2.6, n: 17), sample PEC-15-31A with a model age of 110.4 ± 2.4 (MSWD: 2.4, n: 13) and sample PEC-15-8 with a model age of 110.7 ± 6.8 (MSWD: 0.53, n: 16). Notably, sample PEC-15-31A is cross cut by a smaller veinlet and yields a reliable age. These three samples provide robust model ages and because of their similar ages and similar structural orientation were regressed on a single Concordia diagram to yield a model age of 101.1 ± 5.5 (MSDW: 2.6; n: 37; **Figure 13**). Sample PEC-15-2C yielded a model age with larger uncertainty at 87 ± 45 (MSWD: 2.8, n: 9). Sample PEC-15-30 was also chosen due to its high ^{238}U content assessed during trace element geochemical analysis, despite a few point analyses with ^{238}U values below detection limits. This analysis generated a meaningless model age of -164 ± 270 (MSWD: 6). Notably, these five samples are all relatively depleted in Sr (<120 ppm), and have stable isotope values indicative of Middle Ordovician limestone, except for sample PEC-15-2A that is somewhat enriched (>5‰) in $\delta^{13}C$. For the remaining two samples selected for U-Pb geochronology, we targeted samples that were defined by different stable isotope signatures and Sr values than the other samples. From the three samples that are relatively depleted in $\delta^{18}O$ (<20‰), PEC-15-5A is the only sample that also enriched in Sr (>190 ppm) and was selected for radiometric dating. From 10-point analysis, the sample yielded a discordant age, and no model age was calculated. Sample PEC-15-25A was chosen because it possesses moderate Sr concentration (120-190 ppm) and is enriched in $\delta^{13}C$ (>5‰). Sample PEC-15-25A yielded a model age of 120 ± 63 (MSWD: 1.16; n: 5).

12. Discussion

12.1 Joint orientations and vein structure

Since the birth of plate tectonic theory, an interest among geologists is to genetically relate brittle structures to specific tectonic events, and identify structures that are susceptible to reactivation as part of seismic hazard assessments. Brittle structures preserved in the Precambrian basement and Paleozoic sedimentary strata throughout the St. Lawrence Lowlands are recognized to have formed during discrete tectonic events (e.g. Rimando, 2005; Daneshfar and Benn, 2002; Mitchell, 2007). Since deposition of the Paleozoic sediments, the compressive stress field has rotated in a clockwise manner, highlighted by three major tectonic events: 1) the closing of Iapetus

ocean and the onset of Appalachian orogenesis (σ_1: varying from NNW-SSE to WNW-ESE) during the Ordovician-Permian, 2) the opening of the Atlantic (σ_1: WNW-ESE) during the Triassic, and 3) the current stress field (σ_1: ENE-WSW) (Adams and Bell, 1991; Faure et al. 2004; Rimando and Benn, 2005; Mitchell, 2007). The latter was established during the Cretaceous due to a change in spreading direction along the Northern Mid-Atlantic and consequently changed North America's direction of absolute plate motion. A geodynamic change in plate motion is a relatively passive event in comparison to continental collision and rifting, and is often overlooked for more spectacular tectonic events.

Transecting the Middle Ordovician limestones of Prince Edward County in the St. Lawrence Lowlands of southern Canada, the Picton Fault and the Salmon River Fault are spatially aligned with, and structurally linked to, crustal-scale shear zones of the RLmz of the underlying Grenville Province (Daneshfar and Benn, 2002; Mitchell, 2007). Previous investigations and new observations herein provide field evidence that these faults are inherited structures from the underlying crystalline basement, and possess joints and lineaments that are continuous across the Mesoproterozoic-Paleozoic unconformity (Sanford, 1993). Field investigations suggest that these basement-rooted faults have been episodically reactivated through their geologic history in response to North America's evolving stress field (Sanford, 1993). Statistical approaches suggest that NE-SW Grenvillian faults are at low-risk of hosting seismicity such that their orientation is not compatible with the current stress field (Daneshfar and Benn, 2002). In the St. Lawrence Lowlands, seismic epicenters sometimes project on the traces of mapped faults, however in Prince Edward County they more commonly project away from these faults, where no apparent structural feature is identified (Daneshfar and Benn, 2002; Earthquakes Canada, 2017). The exact location of the mapped faults are largely based on magnetic and gravity anomalies from basement-rooted structures and their exact location is not well constrained (Ontario Geological Survey, 1991; Wallach et al., 1998). In this study, field observation support faulting was observed at stations that are distal to published mapped faults (e.g. stations XXVIII, XXXII; **Figure 2**).

Throughout the peninsula, the most pervasive joint populations preserved are oriented NW-SE and broadly E-W (**Figure DR-1**). The relationship between these two joint populations vary: 1) conjugate sets, where a shearing component is preserved as slicken-fabrics of calcite along the host rock (**Figure 4**), and 2) joints with a broad E-W orientation terminating upon intersecting NW-SE oriented joints. Less commonly, a third joint population trending broadly NE-SW is

present. Generally, the less pervasive (NE-SW) joint population are at stations along fault traces (e.g. station XXIX), which could be the result of basement-rooted structures deflecting the compressive stress field, and modifying the direction of joint propagation. Some stations that are distant to mapped faults (e.g. station XXXII) also preserve NE-SW trending joints (**Figure 2**; **Figure DR-1**). Notably, these stations generally preserve 20-100 m-wide intense joint zones, where joint densities increase to ~1 joint/meter, and minor faulting. Stations that are distant to fault traces and have joints that deviate from the dominant orientations, combined with intense joint zones and minor faulting, could indicate underlying structural features of the RLmz fault network may not have been yet identified.

Pervasive conjugate joint sets oriented NW-SE and broadly E-W corresponds to a compressive stress field originating from WNW-ESE, which is most compatible with the stress field during the Taconic orogeny (σ_1: NW-SE to WNW-ESE; **Figure 14**; Faure et al., 2004; Rimando, 2005). The same joint pattern is preserved in Balsam Lake region, structurally overlying the Central Metasedimentary Belt boundary tectonic zone to the west, with a similar interpretation (e.g. McFall, 1993; Rutty and Cruden, 1993).

During joint propagation, younger joints terminate upon intersecting preexisting joints since a new fracture cannot propagate across a free surface. From terminating joint relationships, joints with a broad E-W orientation are interpreted as the youngest joint population. This joint orientation fits a regional trend of extensional joints that is recognized to extend to the midcontinent, and are compatible with modern stress field (σ_1: ENE-WSW) with an extensional mode of opening (**Figure 14**; Engelder, 1982). ENE-WSW extensional joints adapting a broad E-W orientation in the St. Lawrence Lowlands can also be attributed to deflecting stress along basement rooted structures. In addition, E-W oriented joints forming conjugate sets with NW-SE joints often have slicken fabrics with overgrowth of large euhedral crystals. This implies the joint surface opened as conjugate joints which is supported by sub-horizontal slicken fabrics, and E-W oriented joints were selectively reactivated with an extensional mode of opening to accommodate euhedral overgrowth (**Figure 14**).

Joints are often partially filled or sealed with calcite mineralization to form calcite veins. Calcite mineralization sealing joints indicates that fluid flow in the shallow crust occurred syn- to post-joint propagation, and joints served as pathways to accommodate fluid flow. Microscopy was not possible with veins possessing slicken-fibres since sampling was difficult, thus petrography

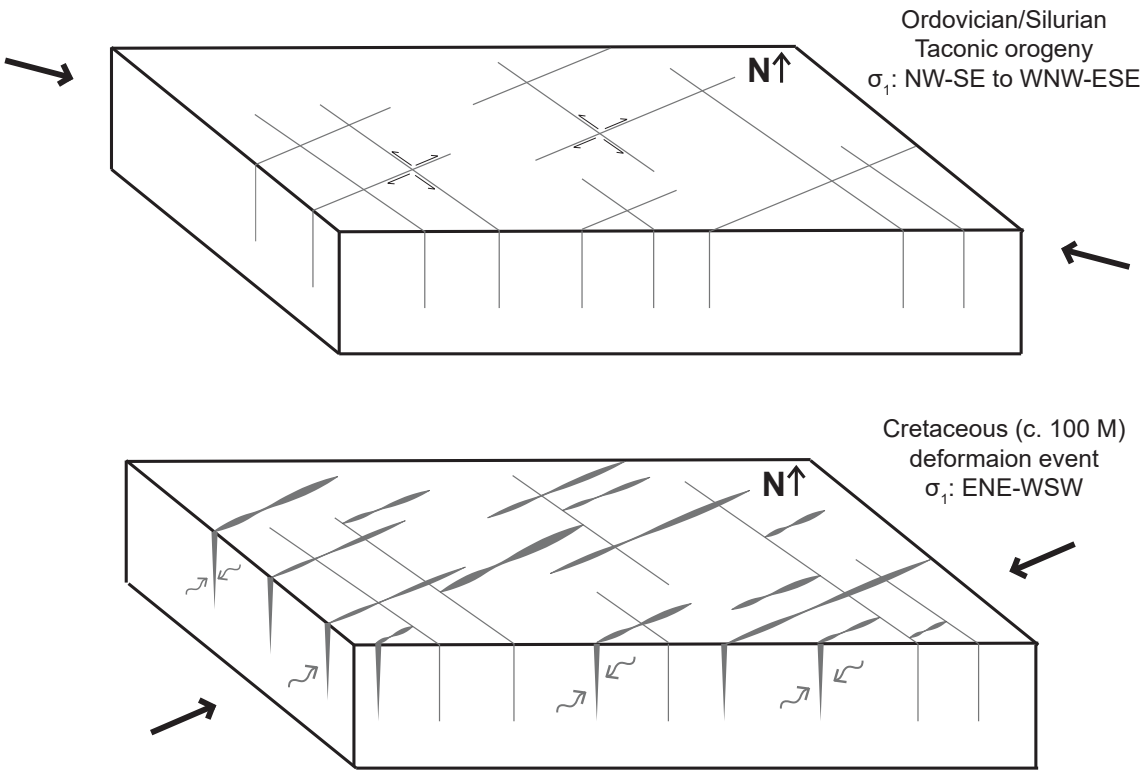


Figure 14 | Summary of the formation brittle structures preserved in the bedrock of Prince Edward County from the (A) Taconic orogeny and (B) a Cretaceous deformation event. Direction of maximum compressive stress (σ_1) of the respective events are projected as black arrows. A) Propagation of conjugate joints trending NW-SE and broadly E-W. Sub-horizontal slicken-fabrics on the host rock suggests a minor shearing component during joint propagation. B) Pre-existing E-W trending joints are selective reactivated and new E-W trending extensional joints propagate, both with an extensional mode of opening. Increase of lateral stress during deformation dewaters the host rock and connate fluids migrate along dilated E-W trending joints to crystallize as calcite veins. Joints dissipate at a depth of ~50 meters suggesting that elevated lithostatic pressure impedes jointing at depth, and deformation is confined to the upper section of the continental crust.

was only conducted on joints with an extensional mode of opening. Petrography reveals that calcite crystals are small along the vein-host rock contact with larger equidimensional crystals in the center (**Figure 9**). The initial stage of crystallization is evident in CL through alternating compositional zones of illuminated and quenched material that converge at the host rock interface (**Figure 5**). This pattern is indicative of syntaxial-biaxial growth where nucleation is initiated on the wall rock and large equant crystals fill the vein during the final stage of crystallization. Veins with crystal morphologies indicative of syntaxial-biaxial growth reveal that the veins crystallized during a single event, and likely not episodic reactivation that would preserve a crack-and-seal texture. Some veins are cross cut by smaller veinlets, which also preserve evidence of syntaxial-biaxial growth, suggesting the veins were partially reactivated without completely reopening the vein (**Figure 5**). Cross cutting veinlets could indicate that the deformation event that initiated fluid flow outlasted the crystallization rate of the main vein.

12.2 Geochemistry

Information regarding the fluid reservoir from which the vein material originates is concealed within the stable isotope signature and trace element geochemistry of the calcite crystals. All calcite veins in this study have the same, or a similar, $\delta^{13}C$ and $\delta^{18}O$ fingerprint to Middle Ordovician marine carbonate reference material (**Figure 12**). Constraints from other fluid reservoirs (e.g. meteoric fluids, mantle source, or magmatic fluids) do not obviously overlap with the new values, although it is possible that samples with low $\delta^{18}O$ values (<20‰) could reflect some mixing with meteoric fluids (Bowen, 2002; Faure and Mensing, 2005; **Figure 11**). In addition, the REE profiles of calcite crystals normalized to chondrite follow the same pattern as theoretical values of the upper continental crust: A slight negative slope from LREE to HREE and a negative Eu anomaly (**Figure DR-2**). The REE profiles and stable isotope signature of calcite veins resemble the host rock, suggesting that the fluids involved in the mineralization process were derived from connate water.

Three samples collected proximal to the trace of the Hamilton Presqu'île lineament are the only samples with measurable amounts of Y. Notably, these samples are also relatively enriched in other REE's, and Mn. It is possible that the structures of the underlying Hamilton Presqu'île lineament tapped a slightly different reservoir, prescribing the samples with a specific geochemical fingerprint. No other correlations were made between sample distribution and calcite

geochemistry. Stations where multiple samples were collected often have samples belonging to slightly different populations of stable isotope groups and have minor geochemical variations.

Minor variations in trace element geochemistry and $\delta^{13}C$ and $\delta^{18}O$ values potentially reflect the crystallization conditions such as the fluid interaction with the host rock, the temperature and pH of the fluid and the calcite's rate of crystallization (Paquette and Reeder, 1995). The incorporation of trace elements into calcite is via the substitution of the trace element with the Ca^{2+} site. Cations with the same charge, and similar ionic radius are usual candidates for substitution such as: Mg^{2+}, Mn^{2+}, Fe^{2+}, Mn^{2+}, and to a lesser extent Sr^{2+} and Ba^{2+} (Mucci and Morse, 1990). In addition, LREE are more easily incorporated into calcite than HREE due to their larger ionic radius (Brookins, 1989). By integrating petrographic observations with trace element geochemistry, the incorporation of trace elements into calcite was quantified through traverses with the LA-ICP-MS. In veins that show evidence of syntaxial-biaxial growth, crystals along the host rock are relatively enriched in Sr relative to large equant crystals at the center (**Figure 9**). Mucci and Morse (1990) demonstrate that Mg and Sr are preferentially incorporated into calcite at higher precipitation rates, and Fe and Mn are preferentially incorporated at lower precipitation rate. A relative enrichment of Sr in crystals along the vein-wall rock interface is interpreted to represent rapid crystallization during the first stage of vein filling (**Figure 9**). Crystals with field evidence of crystallizing during the final stage of vein growth (e.g. filling irregular cavities along vein margins, or euhedral overgrowth) have slightly variable crystal chemistries. For example, independent geochemical analysis of calcite crystals that fill irregular shaped cavities along vein margins (PEC-15-31BIII) with calcite from the main vein (PEC-15-31BI) reveal that most trace elements are preferentially incorporate into calcite during the initial stage of vein growth, since cavity-filled crystals are relatively depleted in most trace elements (e.g. Mg, Mn, REE's and ^{238}U), although cavity-filled crystals have a high $\delta^{13}C$ signature compared to the main vein (**Table DR-1**; **Figure 12**). Samples with high $\delta^{13}C$ signatures and depleted in most trace elements are interpreted to represent the final stage of vein filling and reflect the composition of a more evolved fluid. These samples generally have a large crystal morphology suggesting a lack of competition growth and allowing the development of equant crystals.

Previous work on synthetic calcite shows that the incorporation of trace elements is complex, and compositional zonation do not necessarily represent the bulk composition of the fluid. Under controlled, open system conditions, crystal sectors that are time equivalent can vary up to 1000

ppm in various trace elements, and compositional zonation is common (Paquette and Reeder, 1995). Multiple theories have been developed to explain this phenomenon. Watson (1996) proposed a growth entrapment model, where the incorporation of trace elements on the crystals surface represents the composition of the fluid that is in equilibrium with the crystal. The fluid at the surface of the crystal creates a buffering effect between the fluid reservoir and crystal, and they are not in equilibrium. Meanwhile, trace elements at the surface diffuse from the crystal to regain equilibrium with the fluid. Compositional zoning occurs when the rate of crystallization exceeds the diffusion rate of trace element of the enriched layer. Essentially, enriched sectoral zones become "buried" or "trapped" during progressive crystallization, inhibiting the diffusion of trace elements from the crystal lattice. Sector zoning is an interplay on the diffusivity of trace elements and the rate of crystallization, and does not require variations of bulk-fluid geochemistry (Watson, 1996). Alternatively, Wang and Merino (1991) propose an alternative model, where H^+ builds up on the crystals surface that prevents other cations to attach to the growth site, causing sectoral zoning that is depleted in certain trace elements. The temperature and pH of the fluid, and the crystallization rate of calcite are proven to control the incorporation of trace elements in calcite. Geochemical traverses show that neighboring crystals that appear to be cogenetic often have distinct geochemistry, and vary luminescence under CL (e.g: **Figure 5**; **Figure 11**). With the numerous factors that can affect the incorporation of trace elements into calcite, it is difficult to draw conclusions on the conditions during across crystals that show no indication of reactivation and appear to be time equivalent. Variability in geochemistry is attributed to the complex system from which it has crystallized.

Where cross cutting veinlets are present, in situ traverses show that both the vein and cross cutting veinlet have similar chemical composition and variations are often larger in neighboring crystals that show no evidence of reactivation (**Figure 11**). This suggests that the cross cutting veinlet probably originates from the same fluid source, and supports the interpretation that these veins were only partially reactivated. One spurious calcite vein (PEC-15-14I) collected from a Jurassic ultramafic dike shows evidence of repeated reactivation through a crack and seal fabric, and a distinct geochemistry that is enriched in Si, Mg, Sr and REE and has an unusually steep REE profile due from its enrichment in LREE. The station is located along the Picton Fault trace (station I), and the Jurassic dike is interpreted to have used the basement-rooted fault as a pathway for magma infiltration. Episodic vein reactivation could represent episodic fault reactivation during

later tectonism, and its unusual geochemistry could be the product of fluids interacting with the ultramafic dike and leaching some trace elements.

To reiterate, calcite veins crystallize from a complex system and minor variations of the calcite trace element geochemistry and $\delta^{18}O$ and $\delta^{13}C$ values can be attributed to numerous variables at play, such as the temperature and pH of the fluid during crystallization, the rate of calcite crystallization and fluid-wall rock interaction. Regardless of minor variability, all calcite veins collected in this study are analogous to the bulk composition of Middle to Late Ordovician limestones that dominate the St. Lawrence Lowlands, and REE profiles follow similar trends as the upper continental crust. This implies that calcite veins have the same composition as its host rock, and vein material originates from connate fluids of the surrounding stratigraphy. The release of connate water from pore-space is most easily explained through a deformation mechanism, where an increase in stress squeezes connate water from pore-spaces and is channeled along dilated fractures and joints to crystallize as calcite veins (e.g. Dunne and Hancock, 1994; Bowers, 1995). A change in stress could be the product of 1) an increase of vertical stress during burial/subsidence of the Appalachian Basin, or 2) an increase in lateral stress from tectonism (Lohest, 1909; Dunne and Hancock, 1994). The second option is the preferred interpretation since the veins are hosted in dilated joints that are compatible with a regional joint trend that extends beyond the limit of the Appalachian Basin. This interpretation also suggest that fluid flow occurred synchronous to regional joint propagation (**Figure 13**).

12.3 Brittle deformation and mineralization at c. 100 Ma

Since the opening of the Atlantic, the maximum compressive stress field in Eastern North America is controlled by the rate and direction of spreading along the northern Mid-Atlantic Ridge which also controls the absolute motion of the North American plate. North America's plate motion through the Jurassic-Cretaceous can be reconstructed with the surface trace of volcanism associated to the Great Meteor Hot Spot. The youngest continental expression of the GMHS is at c. 115 Ma in the White Mountains (New Hampshire), which aligns with the New England seamounts in the western Atlantic Basin with crystallization ages of 103 Ma to 82 Ma (Foland and Faul, 1977; Duncan, 1984; **Figure 15**). A kink or bend in the seamounts has been constrained to c. 100 Ma by dating adjacent seamounts (Duncan, 1984; **Figure 15**). This kink reflects a clockwise rotation of the North American plate, attaining a new spreading direction along the northern Mid-

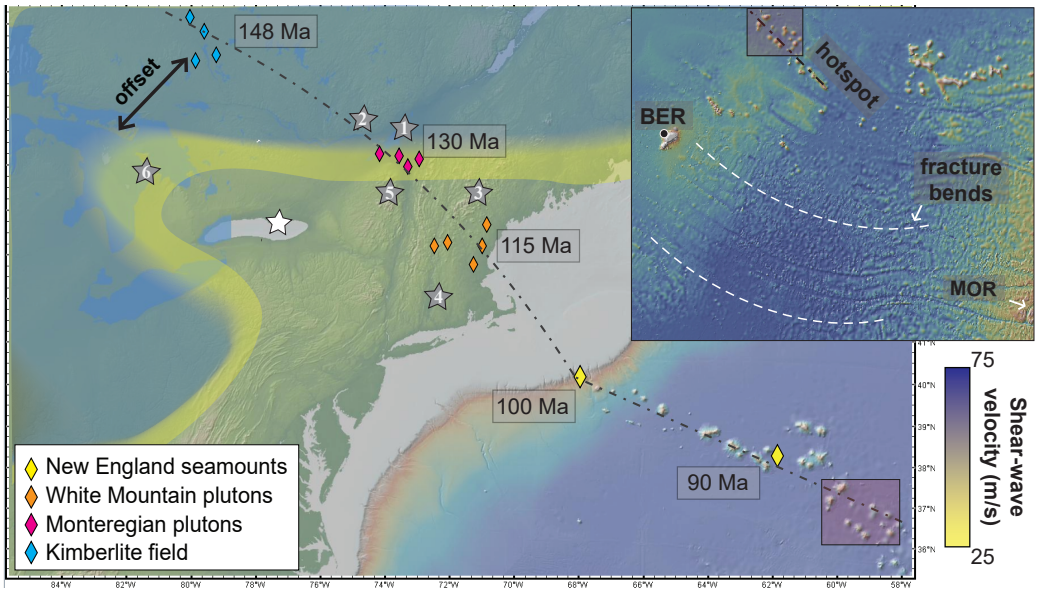


Figure 15 | Map of east Eastern North America overlaid with a gradational shear wave velocity perturbation map with velocities slower than 25 m/s at a depth of 200 km. Magmatism associated to the passage of the Great Meteor Hot Spot track is projected as colored diamond symbols with their respective crystallization ages in grey boxes and the hot spot track projected as a black dashed line. The slow shear wave velocity anomaly is associated to the hotspot track in the lithospheric mantle and is offset from its surface expression. Offset increases with age from 100 Ma, which marks a clockwise rotation of North America at this time. This study is projected as a white star. Grey stars represent previous studies reporting 100 Ma cooling ages: 1: (Emberley and Schneider, 2016); 2: (Hardie, Schneider and Garver, 2017); 3: (West and Roden-Tice, 2013); 4: (Roden-Tice and Tice, 2005); 5: (Taylor and Fitzgerald, 2011); and crystallization ages on calcite veins, 6: (Davis, 2016). Inset in the top right corner is the central Atlantic. The shaded red box in the map and the inset contour the same area. White dashed lines trace fracture bends in the mid-Atlantic that are associated to the same deformation event at ~100 Ma. Bermuda (BER) and the mid-ocean ridge (MOR) are indicated as geographic reference.

Atlantic Ridge (Duncan, 1984; Eaton and Frederiksen, 2007). Consequently, the far-field stress underwent a clockwise rotation from WNW-ESE to the ENE-WSW, and the modern compressive stress field in eastern North America was established at this time (Adams and Bell, 1991). In the mantle lithosphere, residual heat after the passage of a hotspot generates a slow shear wave anomaly. Eaton and Frederiksen (2007) mapped the anomaly associated to the GMHS at a depth of 200 km below the St. Lawrence Lowlands, and demonstrate that it is laterally offset from its surface expression. The offset increases with age, and is traced to the kink in the New England Seamounts at c. 100 Ma, which indicates that this event may have decoupled the continental crust from the mantle lithosphere (**Figure 15**; Eaton and Frederiksen, 2007). The change in plate motion can also be observed in the seafloor fabric of the Atlantic Basin through large fracture bends (**Figure 15**). In addition, seafloor roughness suggest that the rate of spreading accelerated for c. 20 m.y. following the change in plate motion in the mid-Cretaceous (Matthews et al., 2011). A change in tectonic plate motion is often not an event recorded in structures preserved in continental crust, however decoupling of the continental and mantle lithosphere and accelerated spreading rate for 20 m.y. suggest that this deformation may have been larger than previously envisioned.

In continental North America, ENE-WSW trending joints are reported to extend to the mid-continent, and are compatible with the current stress field with an extensional mode of opening (Engelder, 1982). Basement structures can locally deflect the stress field, causing joints to deviate from their normal trend (Baird and McKinnon, 2007). In the St. Lawrence Lowlands, joints adapting a broad E-W trend can be associated to deflections of stress from underlying structures of the RLmz and are interpreted to follow the same regional joint trend that extends to the mid-continent. In addition, pre-existing E-W joints forming conjugate sets with NW-SE joints from the Taconic orogeny were selectively reactivated under the modern stress field with an extensional mode of opening (**Figure 14**). In Prince Edward County, calcite veins were collected from joints trending broadly E-W and yield Cretaceous U-Pb ages. The three samples of calcite veins with some of the highest ^{238}U provide reliable U-Pb model ages between 81.4 ± 8.3 and 110.7 ± 6.8 Ma (**Figure 13**). Veins show syntaxial-biaxial growth, suggesting the veins crystalized from a single event. None of the veins that were dated show evidence of permanent reopening or episodic reactivation, suggesting they record a Cretaceous event rather than a mix of multiple ages. Since these veins were collected from the same joint population, it is reasonable to assume that they record the same event. These three ages were regressed on a single Concordia diagram to yield a

model age of 101.1 ± 5.5 Ma (MSDW: 2.6; n: 37; **Figure 13**). An additional four samples were also dated via U-Pb that yield a model age c. 100 Ma, however the analyses possess large uncertainties, attributed to low concentrations of ^{238}U (**Figure 13**). Nevertheless, it is quite encouraging that all vein dates broadly suggest a single, distinct event.

U-Pb ages agree with the time the modern stress field was established in Eastern North America during the Cretaceous. Fluid flow and vein crystallization is interpreted to have occurred synchronous to joint propagation when the modern stress field was established. As aforementioned, this Cretaceous event decoupled the mantle lithosphere with the continental lithosphere, and was accompanied with an increase in spreading rate. An increase in spreading rate could have temporarily increased the lateral stress in the rock, dewatering the host rock and forcing connate fluids to migrate along dilated joints and crystallize as calcite veins (**Figure 14**). A fluid reservoir originating from connate fluids is supported by the calcite's stable isotope signature resembling the composition of Middle Ordovician limestone, and REE profiles following the trend of the upper continental crust.

Notably, c. 100 Ma U-Pb ages were also measured calcite vein ages in Inverhuron (Lake Huron) from joints with similar orientations (Cruden, 2011; Davis, 2013). The Algonquin Arch forms a structural high between the Appalachian Basin (Prince Edward County) and the Michigan Basin (Inverhuron), and it is possible that the ages from these two locations do not record the same event despite recording similar ages. If, however the 100 Ma ages from Inverhuron and Prince Edward County record the same event, this would imply that the Cretaceous tectonism is recorded ~350 km further west than reported in this study, and joint propagation and fluid flow were not restricted by the basement high of the Algonquin Arch. In addition, this would suggest that regional deformation is confined to the surficial rocks due to confining lithostatic pressure that does not permit joint propagation at great depths (Hancock, 1985).

Thermochronology studies reporting cooling ages of c. 100 Ma through eastern North America are prevalent in the literature (e.g. West and Roden-Tice, 2003; Roden-Tice and Tice, 2005; Taylor and Fitzgerald, 2011; Amidon et al., 2016; Hardie et al., 2017; Emberley and Schneider, 2017). Occasionally, the 100 Ma cooling is documented along major faults, which may potentially record regional fault reactivation in the Cretaceous. It has been postulated these Late Cretaceous cooling ages through Eastern North America record the passage of the GMHS. This interpretation seems improbable for several reasons: 1) The St. Lawrence Lowlands shows no

evidence of uplift, which would be expected if the geothermal gradient was high enough to induce continental swelling; 2) thermochronology across the GMHS does not record Cretaceous heating event that can be unequivocally linked to the hot spot activity; 3) hotspot-related cooling ages should follow a spatial progression (e.g. younging to the southeast) rather than widespread occurrences of c. 100 Ma across a broad region, and; 4) At c. 100 Ma, the GMHS was erupting the New England seamounts off of the passive margin. Therefore the 100 Ma ages on continental North America does not fit the timeline of the GMHS (e.g. Crough, 1981; Duncan, 1984; Hardie et al., 2016; **Figure 14**). Instead, it seems more probable for regional brittle deformation to be induced by tectonic processes. Cooling ages of c. 100 Ma reflecting brittle tectonism is also compatible with the time the modern stress field in North America from a change in spreading direction and speed along the Northern Atlantic ridge. It is possible that Cretaceous cooling ages through Eastern North America record fault reactivation related to the same tectonism that generated jointing and fluid flow in this study.

12.4 Cretaceous global plate reorganization event

It is postulated that Atlantic passive margins have undergone post-rift subsidence, and were uplifted by a later event (e.g. Japsen et al., 2012). In eastern North America, Amidon et al. (2016) suggests that Cretaceous regional fault reactivation is associated to margin rejuvenation-related tectonism. Increased sedimentation rates into the major watersheds of the eastern US occurred just after the Cretaceous tectonism that has been documented with geochronology (Pazzaglia and Brandon, 1996). Interestingly, similar studies in Africa and South America report Cretaceous ages of Atlantic margin rejuvenation which is supported by increase sedimentation rates in the Atlantic Basin (Poag, 1989; Japsen et al., 2011; Cogne et al., 2012; Fairhead et al., 2013). Comparable cooling ages surrounding the Atlantic Basin suggest a common mechanism of margin rejuvenation associated to a change in spreading rate and direction along the Mid-Atlantic ridge. From this, a larger question emerges: What happened at 100 Ma to initiate a change in spreading direction along the Northern Mid-Atlantic Ridge?

Cretaceous tectonism is not confined to the Atlantic Basin, and similar trends are observed on all tectonic plates. Cretaceous-age fracture bends and sea floor roughness are preserved in most oceanic basins, for example: fracture zones in the Weddell Sea (between Antarctica and South America) record a clockwise rotation in spreading at 105 Ma; fracture bends in the Wharton Basin

(between Australia and India) record a clockwise rotation in spreading at 104 Ma; seafloor roughness in the Southern Atlantic records accelerated spreading from 102-96 Ma; and fracture bends in Bay of Bengal (between Antarctica and India) record a clockwise rotation in spreading at 98 Ma (Eagles, 2007; Matthews et al., 2011; Matthews et al., 2012; Gibbons et al., 2012). In addition, the Pacific plate records an absolute change in plate motion at 100 ± 8 Ma through a kink in hotspot related seamounts (Duncan and Clague, 1985). In addition, all major continental plates have Cretaceous unconformities which can be interpreted to represent a sudden change in global seawater levels or basin inversions, and potentially reflect tectonism at that time (Zorina et al., 2008).

Plate reorganization events are periods of change in plate motion, generally accompanied by an increase plate velocities. On geologic timescale, these events are relatively short and interrupt much longer periods of tectonic stability and uniform plate motion (Bercovici, 2003). Numerous authors have suggested that the timeframe of 105-100 Ma is period of global plate reorganization because of the reoccurring and discrete Cretaceous events on all major tectonic plates. Matthews et al. (2012) compiled all global tectonic and volcanic events that occurred between 110 Ma and 90 Ma to create a comprehensive model that constrains the timing the geographic extent of these events as well as its driving mechanism. The model proposes that the cessation of subduction along 7000 km of eastern Gondwanaland's trench triggered the Cretaceous plate reorganization event: Two closely spaced ridges resulted in young crust entering a subduction zone with insufficient negative buoyancy to drive subduction, causing the trench to transition to strike slip motion and this redistribution of lateral stress affected its neighboring plates (Matthews et al., 2012). In addition, the eruption of the Bouvet plume between the Africa - Antarctica - South America triple junction between 100-94 Ma could also have contributed to this event (Matthews et al., 2012). These events initiated a domino effect that modified lithospheric stress patterns in neighboring plates and ultimately lead to a global plate reorganization event.

To integrate the results of this study in a global context, the northern Mid-Atlantic ridge was effected by this global event by changing its spreading direction which induced a clockwise rotation of North America, and the compressive stress field was temporarily increased due to an increase in spreading rate. This event is interpreted to have initiated the propagation of ENE-WSW trending extensional joints that extend to the midcontinent, as well initiating fluid flow in the shallow crust by releasing connate fluids stored in pore space to migrate through dilated joints and

crystallized as calcite veins. It is interesting that about 500 kilometers inland of North America's Atlantic passive margin preserves a subtle fingerprint of Cretaceous tectonism.

13. Conclusions

1) Subvertical joints trending broadly E-W are the youngest brittle tectonic structures preserved in the St. Lawrence Lowlands and follow a regional trend of extensional joints that are compatible with the modern stress field.

2) Joints are locally filled and sealed with calcite mineralization that have the stable isotope fingerprint of Middle Ordovician limestone, consistent with the joint's host rock. REE patterns of the calcite veins have similar profiles as the upper continental crust reference. The geochemical signatures indicate that the vein material likely originates from connate fluids from adjacent host rock that was dewatered during a deformation period.

3) Crystal morphology of most calcite veins suggests crystallization from a single event through syntaxial-biaxial growth and locally large veins are cross-cut by very thin veinlets. Mechanical twinning and pressure solution developed after crystallization and potentially reflects the protracted nature of the shallow crustal stresses.

4) U-Pb geochronology on the calcite veins yields a model age of 101.1 ± 5.5 Ma. This is synchronous with North America's acquisition of its current plate-scale stress field, which suggests that far-field effects transmitted brittle deformation into the St. Lawrence Lowlands consequently fracturing the crust (joints) and remobilizing connate fluids (calcite veins).

5) This study suggests that a subtle fingerprint of brittle tectonism is preserved >3000 km from the active plate margin.

14. Recommendations for future work

1) Fluid inclusion work would provide additional information of this deformation event and temperature of the fluid.

2) The isotopic signature of Middle Ordovician limestone are theoretical values. Stable isotope analysis of the host rock where each calcite vein collected would provide a more accurate reference, and may also reveal information on how far the fluid migrated in relation to isotopic fingerprints of specific formations.

3) New questions arise from this work, such as: Did the rheology of limestone facilitate fluid flow? How does the crystalline rock (Canadian Shield) record this event?

4) From Bruce Peninsula, ~200 km to the west, drill cores show that jointing and veins disappear at a depth of 34 m. In Prince Edward County, the Paleozoic sedimentary strata are estimated to be ~280 m thick. Drill cores from Prince Edward County could better resolve the depth at which the joints and veins extend, and if they terminate along the basement-cover unconformity.

5) ENE-WSW are reported in the literature as being present through the midcontinent. Similar studies on vein filling material could determine the geographic extent of fluid flow in the interior of North America.

6) This study demonstrated that a subtle fingerprint of Cretaceous plate reorganization event can is preserved distal to the active plate boundary; does this extend to the other side of the Atlantic basin?

15. References

Adams, J., 1989, Postglacial faulting in eastern Canada: Nature, origin and seismic hazard implications: Tectonophysics, v. 163, p. 323–331.

Adams, J., and Bell, J.S., 1991, Crustal stresses in Canada: In Neotectonics of North America Edited by D.B. Slemmons, E.R. Enghdahl, M.D. Zoback and D.D. Blackwell. Geological Society of America, Decade Map Volume 1, Boulder, Colorado, p. 367–386.

Amidon, W. H., Roden-Tice, M., Anderson, A. J., McKeon, R., and Shuster, D., 2016, Late Cretaceous unroofing of the White Mountains, New Hampshire, USA: An episode of passive margin rejuvenation?: Geology, v. 44, p. 415–418.

Anderson, T.W., and Lewis, C.F.M., 1975, Acoustic profiling and sediment coring in Lake Ontario, Lake Erie, and Georgian Bay: Geological Survey of Canada, Paper 75-1, Part A, p. 373–376.

Barnett R.L., Arima M., Blackwell J.D., and Winder C.G., 1983, The Picton and Varty Lake ultramafic dikes: Jurassic magmatism in the St. Lawrence Platform near Belleville, Ontario: Canadian Journal of Earth Sciences, v. 21, p. 1460–1472.

Barosh, PJ., 1986, Neotectonic movement, earthquakes and stress state in the eastern United States: Tectonophysics, v. 132, p. 117–152.

Bercovici, D., 2003, The generation of plate tectonics from mantle convection: Earth and Planetary Science, v. 205, p. 107–121.

Bons, P.D., and Jessell, M.W., 1997, Experimental simulation of the formation of the formation of fibrous veins by localized dissolution-precipitation creep: Mineral Magazine, v. 61, p. 53–63.

Bowen, G., and Wilkinson, B., 2002, Spatial distribution of ^{18}O in meteoric precipitation: Geology, v. 30, p. 315–318.

Bowers, T. S., 1995, Pressure-Volume-Temperature Properties of H_2O-CO_2 Fluids, *in* Ahrens, T.J., eds., Rock Physics and Phase Relations, A Handbook of Physical Constants American Geological Union Reference Shelf 3, p. 45–72.

Boyce, J.I., and Morris, W.A., 2002, Basement-controlled faulting of Paleozoic strata in southern Ontario, Canada: new evidence from geophysical lineament mapping: Tectonophysics, v. 353, p. 151–171.

Brookins, D., 1989, Aqueous geochemistry of rare earth elements. In Geochemistry and mineralogy of rare earth elements, *in* Bruce, R.L and McKay, G., eds., Reviews in Mineralogy, v. 21, Mineralogical Society of America, p. 201–225.

Burkhard, M., 1993, Calcite twins, their geometry, appearance and significance as stress–strain

markers and indicators of tectonic regime: a review: Journal of Structural Geology, v. 15, p. 351–368.

Busch, J.P., and Van der Pluijm, B.A., 1996, Late orogenic, plastic to brittle extension along the Robertson Lake shear zone: Implications for the style of deep-crustal extension in the Grenville orogen, Canada: Precambrian Research, v. 77, p. 41–57.

Carr, S.D., Easton, R.M., Jamieson, R.A., and Culshaw, N.G., 2000, Geologic transect across the Grenville orogen of Ontario and New York: Canadian Journal of Earth Sciences, v. 37, p. 193–216.

Carson, D.M., 1980, Paleozoic geology of the Trenton-Concecon area, southern Ontario: Ontario Geological Survey, Preliminary Map P2375, scale 1:50 000.

Carson, D.M., 1981, Paleozoic geology of the Belleville-Wellington area, southern Ontario: Ontario Geological Survey, Preliminary Map P2412, scale 1:50 000.

Carson, D.M., 1981, Paleozoic geology of the Kaladar-Tweed area, southern Ontario: Ontario Geological Survey, Preliminary Map P2411, scale 1:50 000.

Cogne, N., Gallagher, K., Cobbold, P.R., Riccomini, C., and Gautheron, C., 2012, Post-breakup tectonics in southeast Brazil from thermochronological data and combined inverse-forward thermal history modeling: Journal of Geophysical Research, v. 117, p. 11–13.

Coniglio, M., R. Sherlock, Williams-Jones, A. E., Middleton, K., Frape, S. K., 1994. Burial and hydrothermal diagenesis of Ordovician carbonates from the Michigan Basin, Ontario, Canada *in* Purser, B., Tucker, M., Zenger, D., eds., Dolomites a volume in honour of Dolomieu: Special Publications of the International Association of Sedimentologists 21, p. 231–254.

Coplen, T.B., Böhlke, J.K., De Bièvre, P., Ding, T., Holden, N.E., Hopple, J. A., Krouse, H. R., Lamberty A., Peiser, H. S., Révész, K., Rieder, S. E., Rosman, K. J. R., Roth, E., Taylor, P. D. P., Vocke, Jr. R.D., and Xiao, Y. K., 2002, Isotope-abundance variations of selected elements: United States Geological Survey Water ressources investigations Open-File Report 01-4222, 30 p.,

Crough, S.T., 1981, Mesozoic hotspot epeirogeny in eastern North America: Geology, v. 9, p. 2–6.

Cruden, S., 2011, Outcrop fracture mapping: OPG's Deep Geologic Repository for Low & Intermediate Waste Open File-Report NWMO TR-2011-43, 54 p.,

Daneshfar, B., Benn, K., 2002, Seismic-reflection profiles of the central part of the Clarendon–Linden fault system of western New York in relation to regional seismicity: Tectonophysics, v. 353, p. 31–44.

Davis, D., 2013, Application of U-Pb geochronology methods to the absolute age of determination of secondary calcite: Nuclear Waste Management Organization Open File Report TR-2013-21, 31 p.,

Davis, D., 2016, Continued Application of U-Pb Geochronology Methods to the Absolute Age Determination of Secondary Calcite, 2014–2016: Nuclear Waste Management Organization Open File Report NWMO-TR-2016-07, 72p.,

Duncan, R.A., 1984, Age progressive volcanism in the New England sea mounts and the opening of the central Atlantic Ocean: Journal of geophysical research, v. 89, no. b12, p. 9980–9990.

Duncan, R.A., and Clague, D.A., 1985, Pacific plate motion recorded by linear volcanic chains. In: Nairn, A.E.M., Stehli, F.G., Uyeda, S. eds., The Ocean Basins and Margins. Plenum, New York, v. 7a, p. 89–121.

Dunne, W.M., and Hancock, P.L., 1994, Palaeostress analysis of small-scale brittle structures: Continental Deformation: Oxford Pergamon Press Ltd, Oxford, 421 p.,

Earthquakes Canada, 2017, Geological Society of Canada: Earthquake Search (On-line Bulletin). Available online at: http://earthquakesCanada.nrcan.gc.ca/stnsdata/nedb/bull_e.php

Easton, R.M., 1998, Geology and mineral potential of the Puzzle Lake area, Central Metasedimentary Belt, Grenville Province; in Summary of Fieldwork and Other Activities: Ontario Geological Survey, Miscellaneous Paper, v. 169, p. 209–215.

Eagles, G., 2007, New angles on South Atlantic opening: Geophysical Journal International, v. 168, p. 353–361.

Eaton D.W., and Frederiksen A., 2007, Seismic evidence for convection-driven motion of the North American plate: Nature Letters, v. 446, p.428–431.

Eby, G.N., 1984, Geochronology of the Monteregian Hills, alkaline igneous province, Quebec: Geology, v.12, p. 468–470.

Emberley, J., and Schneider, D.A., 2017, Tracking low temperature tectonism of the St. Lawrence Platform and Humber Zone, southern Quebec Appalachians through apatite and zircon (U-Th)/He thermochronology: Canadian Journal of Earth Sciences, v: 54, no. 8, p. 827–849.

Engelder, T., 1982, Is there a genetic relationship between selected regional joints and contemporary stress within the lithosphere of North America?: Tectonics, v. 1, p. 161–177.

Fairhead, J.D., Green, C.M., Masterton, S.M., and Guiraud, R., 2013, The role that plate tectonics, inferred stress changes and stratigraphic unconformities have on the evolution of the West and Central African rift system and the Atlantic continental margins: Tectonophysics, v. 594, p. 118–127.

Fakundiny, R.H., and Pomeroy, P.W., 2002, Seismic-reflection profiles of the central part of the

Clarendon–Linden fault system of western New York in relation to regional seismicity: Tectonophysics, v. 353, p.173–213.

Faure, G., and Mensing, T.M., 2005, Isotopes: Principles and Applications: John, v. 3, Wiley & Sons publishing, 928 p.

Faure, S., Tremblay, A., and Malo, M., 2004, Reconstruction of Taconian and Acadian paleo-stress regimes in the Quebec and northern New Brunswick Appalachians: Canadian Journal of Earth Sciences, v. 41, p. 619–634.

Ferrill, D.A., 1991, Calcite twin widths and intensities as metamorphic indicators in natural low temperature deformation of limestone: Journal of Structural Geology, v. 13, p. 667–675.

Fisher D.M., and Brantley S.L., 1992, Models of quartz overgrowth and vein formation: Deformation and episodic fluid flow in an ancient subduction zone: Journal of Geophysical Reasearch, v. 97, p. 20043–20061.

Foland, K. A., and Faul, H., 1977, Ages of the White Mountain intrusives —New Hampshire, Vermont, and Maine, U.S.A.: American Journal of Science, v. 277, p. 888–904.

Gabitov, R.I., Watson, E.B., 2005. Preliminary experimental results for 18O and 13C uptake in calcite and at 32°C and various precipitation rates: Geochimica et Cosmochimica, v. 69 (10), A777.

Garrity, C.P., and R. Soller, D.R., 2009, Database of the Geologic Map of North America—Adapted from the Map by J.C. Reed, Jr. and others: U.S. Geological Survey Data, Series 424, scale 1:5 000 000.

Groshong, R.H., 1988, Low-temperature deformation mechanisms and their interpretation: Geological Society of America Bulletin, v. 100, p. 1329–1360.

Gilbert, G.K., 1886, An account of some new geologic wrinkles: American Journal of Science, v. 3, p. 324–334.

Gibbons, A.D., Barckhausen, U., Vanden B.P., Hoernle, K., Werner, R., Whittaker, J.M., and Müller, R.D., 2012, Constraining the Jurassic extent of Greater India: Tectonic evolution of the West Australian margin: Geochemical Geophysical Geosystems, v.13, no. Q05W13.

Goldstein, R.H., 2003, Petrographic analysis of fluid inclusions. In I. Samson, A. Anderson, & D. Marshall, eds. Fluid Inclusions: Analysis and Interpretation. Mineral Association of Canada, Short Course Ser. 32, p. 9–53.

Haimson, B. C., 1981, Stress measurements down to 1.5 km in the Precambrian granite of northern Illinois: Eos Transactions, AGU, v.62, p. 388.

Hancock, P. L., 1985, Brittle micro-tectonics: principles and practice: Journal of Structural Geology, v. 7, p. 437–457.

Hanmer, S.K., and Ciesielski, A., 1984, A structural reconnaissance of the northwest boundary of the Central Metasedimentary Belt, Grenville Province, Ontario and Quebec, in Current Research, Part B: Geological Survey of Canada, v. 84-1B, p. 121–131.

Hanmer, S., and McEachern, S., 1992, Kinematical and rheological evolution of a crustal scale ductile thrust zone, Central Metasedimentary Belt, Grenville orogen, Ontario: Canadian Journal of Earth Sciences, v. 29, p. 1779–1790.

Heaman, L.M., and Kjarsgaard, B.A., 2000, Timing of eastern North American kimberlite magmatism: Continental extension of the Great Meteor hotspot track?: Earth and Planetary Science Letters, v. 178, p. 253–268.

Hemming, N.G, Meyers, W. J., and Grams J. C., 1989, Cathode luminescence in diagenetic calcites; the roles of Fe and Mn as deduced from electron probe and spectrophotometric measurements: Journal of Sedimentary Research, v. 59, no. 3, p. 404–411.

Hildenbrand, T.G., 1985, Rift structure of the northern Mississippi embayment from the analysis of gravity and magnetic data: Journal of Geophysical Research, v. 90, p. 607–622.

Hoffman, P.F. 1991, Did the breakout of Laurentia turn Gondwanaland inside-out?: Science, v. 252, p. 1409–1412.

Hogarth, D. D., and Rushforth, P., 1988, The Blackburn carbonatites, near Ottawa, Ontario: Dykes with fluidized emplacement: Canadian Mineralogist. v. 26, p. 377–390.

Holst, T. B., and Foote G. R., 1981, Joint orientation in Devonian rocks in the northern portion of the lower peninsula of Michigan: *Geological Society* of America *Bulletin*, v. 92, p. 85–93.

Jacobi, R.D., 2002, Selected and proposed geological faults, New York state: Tectonophysics 353, p. 75–113. Map on page 86, scale 1:250 000 digitized by Karen Edelstein (FracTracker Alliance).

Japsen, P., Chalmers, J.A., Green, P.F., and Bonow, J.M., 2012a, Elevated, passive continental margins: Not rift shoulders, but expressions of episodic, post-rift burial and exhumation: Global and Planetary Change: Geological Society of America Bulletin, v. 90–91, p. 73–86.

Japsen, P., Bonow, J.M., Green, P.F., Cobbold, P.R., Chiossi, D., Lilletveit, R., Magnavita, L.P., and Pedreira, A., 2012b, Episodic burial and exhumation in NE Brazil after opening of the South Atlantic: Geological Society of America Bulletin, v. 124, p. 800–816.

Kay, G.M., 1942., Ottawa-Bonnechere graben and Lake Ontario homocline: Geological Society of America Bulletin, v. 53, p. 585–646.

Kumarapeli, P.S., 1985., Vestiges of Iapetan rifting in the craton west of the northern Appalachians: Geoscience Canada, v. 12, p. 54–59.

Liberty, B.A., 1960. Belleville and Wellington Map areas, Ontario. Geological Survey of Canada, Paper 60–31, p. 9.

Lohest, M., 1909, De l'origine des veines et des géodes des terraines primaires de Belgique: Annales de la société géologique de la Belgique, v. 36B, p. 275–282.

Lo, K.Y., 1978, Regional distribution of in situ horizontal stresses in rocks of southern Ontario: Canadian Geotechnical Journal, v. 15, p. 371– 381.

Ludwig, K.R., 2003, User's manual for Isoplot 3.00 a geochronological toolkit for Excel: Berkeley Geochronological Center Special Publication no 4, p. 71–75.

Matthews, K.J., Müller, R.D., Wessel, P., and Whittaker, J.M., 2011, The tectonic fabric of the ocean basins: Journal of Geophysical Research: Solid Earth, v. 116, B12109.

Matthews, K., Seton, M., Muller, D.R., 2012. A global-scale plate reorganization event at 105 - 100 Ma: Earth and Planetary Science Letters, v. 355–356, p. 283–298.

Mitchell, F., 2007, Structural analysis of brittle deformation features along Grenvillian Shear Zones in southeastern Ontario [MSc thesis]: Kingston, Queen's University, 160 p.

McFall, G.H., and Allam, A., 1990, Neotectonic investigations in southern Ontario: Prince Edward county - Phase II: Atomic Energy Control Board, Open-File Report 3.131.2, 116 p.,

McFall, G.H., 1991, Faulting of a Middle Jurassic, ultramafic dyke in the Picton Quarry, Picton, southern Ontario: Canadian Journal of Earth Sciences, v. 27, p. 1536–1540.

McFall, G.H. 1993, Structural elements and neotectonics of Prince Edward County, southern Ontario: Géographie Physique et Quaternaire, v. 47, p. 303–312.

Miller, D. S., and Lakatos, S., 1983, Uplift rate of Adirondack anorthosite measured by fission-track analysis of apatite: Geology, v. 11, p. 284–286.

Mood, A.M.F., Graybill, F.A., and Boes, D.C., 1974, Introduction to the Theory of Statistics: New York, McGraw-Hill, v. 3, 577 p.

Mucci, A., and Morse, J. W., 1990, Chemistry of low-temperature abiotic calcites: Experimental studies on coprecipitation, stability, and fractionation: Reviews in Aquatic Science, v. 3, p. 217–254.

Ogliore, R.C. Huss, G.R., and Nagashima, K., 2011, Ratio estimation in SIMS analysis: Nuclear Instruments and Methods in Physics Research, B. 269, p. 1910–1918.

Ontario Geological Survey, 1991a, Bedrock geology of Ontario, southern sheet: Ontario Geological Survey, Map 2544, scale 1:1 000 000.

Ontario Geological Survey, 1991b, Total-field aeromagnetic of Ontario-southern sheet: Ontario Geological Survey, Map 2587, scale 1:100 000.

Palmer, J.H.L., and Lo, K.Y., 1976, In situ stress measurements in some near surface rock formations in Thorold Ontario: Canadian Geotechnical Journal, v. 13, p. 1–7.

Paquette, J., and Reeder, R., 1995, Relationship between surface structure, growth mechanism, and trace element incorporation in calcite: Geochimica et Cosmochimica, v. 59, p. 735–749.

Parker, J. M., 1942, Regional systematic jointing in slightly deformed sedimentary rocks: Geological Society of America Bulletin, v. 53, p. 381–408.

Pazzaglia, F.J., and Brandon, M.T., 1996, Macrogeomorphic evolution of the post-Triassic Appalachian Mountains determined by deconvolution of the offshore basin sedimentary record: Basin Research, v. 8, p. 255–278.

Piper, J.D.A., 1975, Proterozoic supercontinent: Time duration and the Grenville problem: Nature, v. 256, p. 519–520.

Poag, C.W., 1989, A record of Appalachian denudation in post-rift Mesozoic and Cenozoic sedimentary deposits of the U.S. Middle Atlantic Continental Margin: Geomorphology, v. 2, p. 119–157.

Powell, R. L., 1976, Some geomorphic and hydrologic implications of jointing in carbonate strata of Mississippian age in south-central- Indiana [Ph.D. thesis]: Lafayette, Purdue University, 169 p.

Rimando, R.E., and Benn, L., 2005, Evolution of faulting and paleo-stress field within the Ottawa graben: Canada. Journal of Geodynamics, v. 39, p. 337–360.

Reed, N.M., Cairns, R.O., and Hutton, R.C., 1994, Characterization of polyatomic ion interferences in inductively coupled plasma mass spectrometry using a high-resolution mass spectrometer: Journal of Analytical Atomic Spectrometry, v. 9, p. 888–896.

Roden-Tice, M.K., and Tice, S.J., 2005, Regional-Scale mid-Jurassic to Late Cretaceous unroofing from the Adirondack Mountains through central New England based on apatite fission-track and (U-Th)/He thermochronology: Journal of Geology, v. 113, p. 535–552.

Roden-Tice, M. K., Tice, S. J., and Schofield, I. S., 2000, Evidence for differential unroofing in the Adirondack Mountains, New York State determined by apatite fission-track thermochronology: Geology, v. 108, p. 155–169.

Roden-Tice, M.K., West Jr., D.P., Potter, J.K., Raymond, S.M., Winch, J.L., 2009, Presence of a long-term lithospheric thermal anomaly: evidence from apatite fission-track analysis in northern New England: Journal of Geology, v. 117, p. 627–641.

Rutty, A.L., and Cruden A.R., 1993, Pop-Up Structures and the Fracture Pattern in the Balsam Lake Area, Southern Ontario: Géographie physique et Quaternaire, v. 47, p. 379–388.

Sanford, B.V., 1993, Stratigraphic and structural framework of upper Middle Ordovician rocks in the Head Lake-Burleigh Falls area of south-central Ontario: Géographie Physique et Quaternaire, v. 47: p. 253–268.

Sbar, M. L., and Sykes, L. R., 1973, Contemporary compressive stress and seismicity in eastern North America—an example of intra-plate tectonics: *Geological Society* of America *Bulletin*, v. 84, p. 1861–1882.

Stacey, J.C., and Kramers, J.D., 1975, Approximation of terrestrial lead isotope evolution by a two-stage model: Earth and Planetary Science Letters, v. 26, p. 207–221.

Sun S. S., and McDonough, D. F., 1989, Chemical and isotopic systematics of oceanic basalts: implications for mantle composition and processes: Special publication from the Geological Society of London, v. 42, p. 313–345.

Taylor, J.P., and Fitzgerald, P.G., 2011, Low-temperature thermal history and landscape development of the eastern Adirondack Mountains, New York: Constraints from apatite fission-track thermochronology and apatite (U-Th)/He dating: Geological Society of America Bulletin, v. 123, p. 412–426.

Turner, F.J., and Ch'ih, C.S., 1953, Nature and dynamic interpretation of deformation lamellae in calcite of three Marbles: American Journal of Science, v. 251, p. 276–298.

Vernon, R. H., 1981, Optical microstructure of partly recrystallized calcite in some naturally deformed marbles: Tectonophysics, v. 78, p. 601–612.

Wallach, J.L., Mohajer, A.A., and Thomas, R.L., 1998, Linear zones, seismicity, and the possibility of a major earthquake in the intraplate western Lake Ontario area of eastern North America: Canadian Journal of Earth Sciences, v. 35, p. 762–786.

Wang, Y., and Merino, E., 1992, Dynamic model of oscillatory zoning of trace elements in calcite: Double layer, inhibition and self-organization: Geochimica et Cosmochimica, v. 56, p. 587–596.

Watson, E., 1996, Surface enrichment and trace-element uptake during crystal growth: Geochimica et Cosmochimica, v. 60, p. 5013–5020.

West, D. P., Jr., and Roden-Tice, M. K., 2003, Late Cretaceous reactivation of the Norumbega fault zone, Maine: evidence from apatite fission-track ages: Geology, v. 31, p. 649–652.

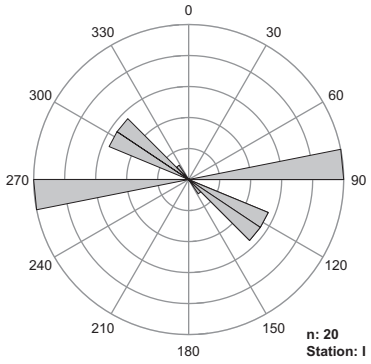
Wilson, A.W.G., 1902, Some recent folds in the Lorraine shales: Canadian Record of Science, v. 8, p. 525– 531.

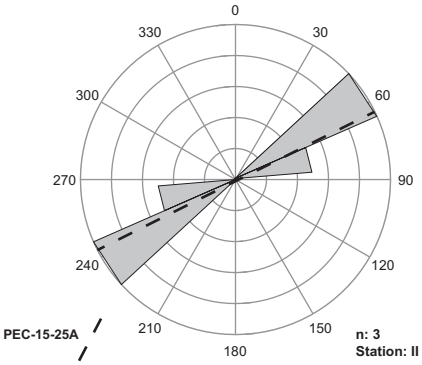
Winder, C.G., 1955, Preliminary Report on the Paleozoic Geology of the Peterborough Cairpbellford Area, Southern Ontario: Ontario Geologic Survey Open-File Report 5331, 12 p.,

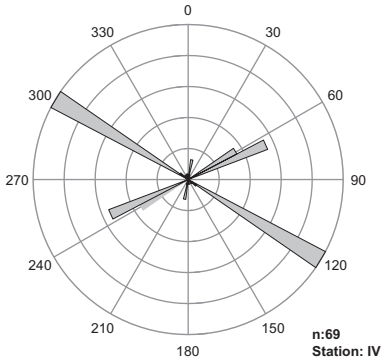
Zorina, S.O., Dzyuba, O.S., Shurygin, B.N., Ruban, D.A., 2008, How global are the Jurassic Cretaceous unconformities?: Terra Nova, v. 20, p. 341–346.

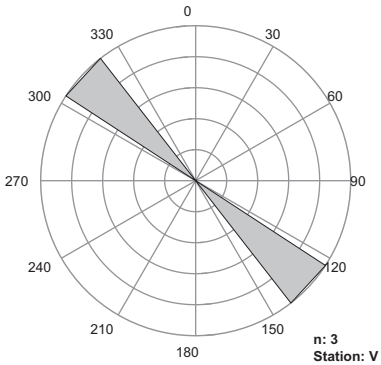
16. Appendix

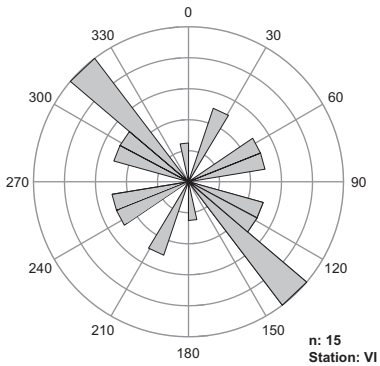
Figure DR-1

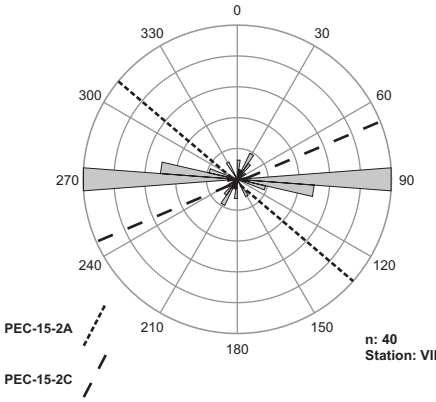


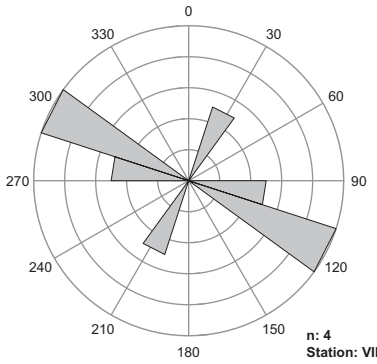


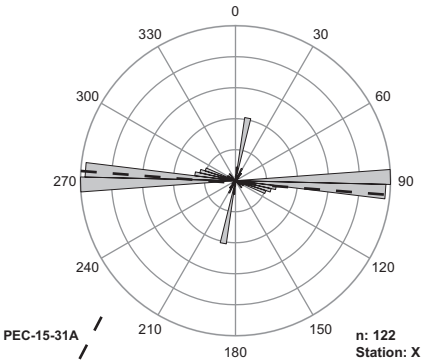


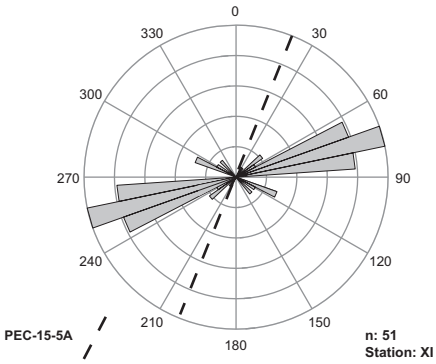


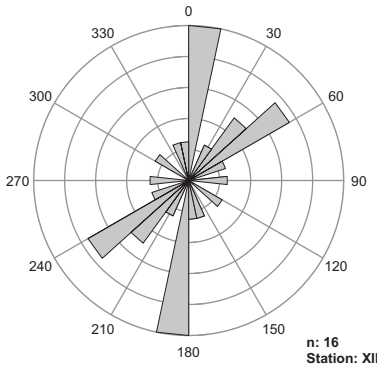


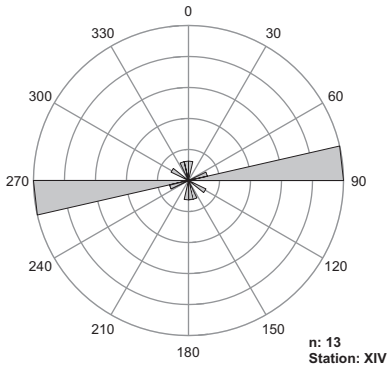












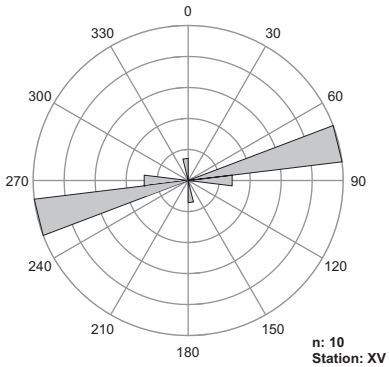
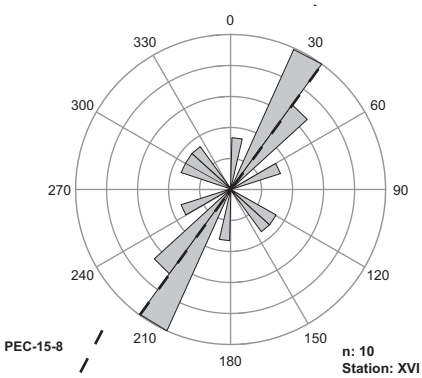
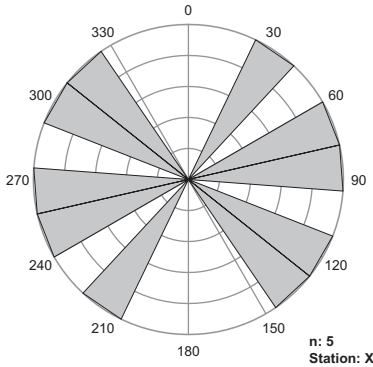


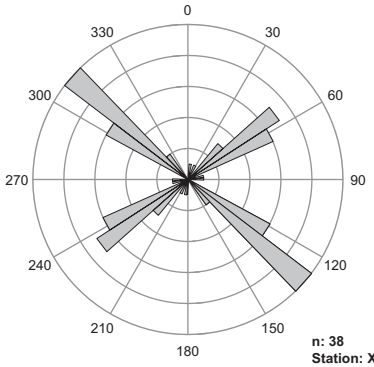
Figure DR-2



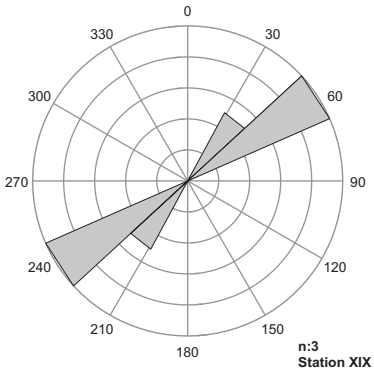
n: 10
Station: XVI



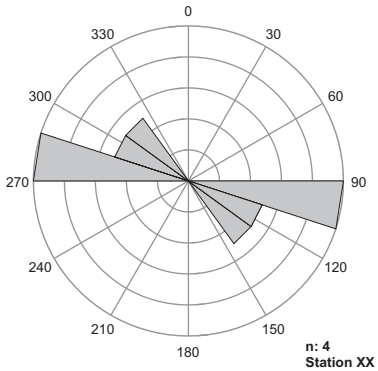
n: 5
Station: XVII



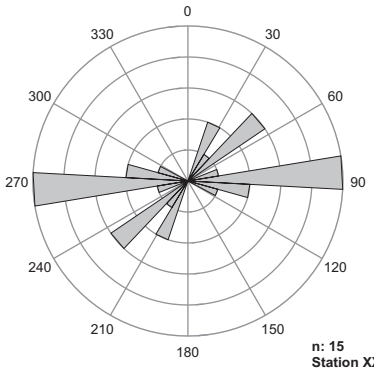
n: 38
Station: XVIII



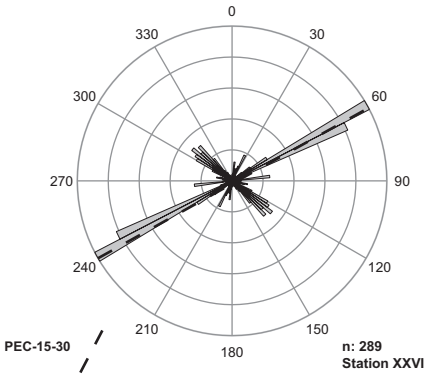
n:3
Station XIX



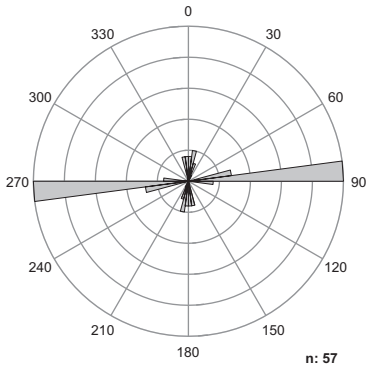
n: 4
Station XX



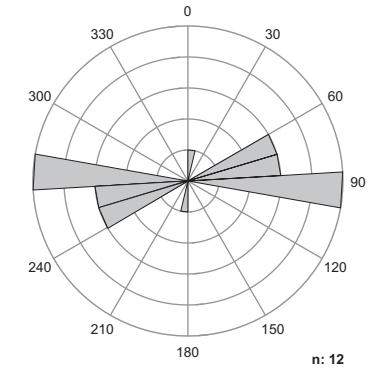
n: 15
Station XXV



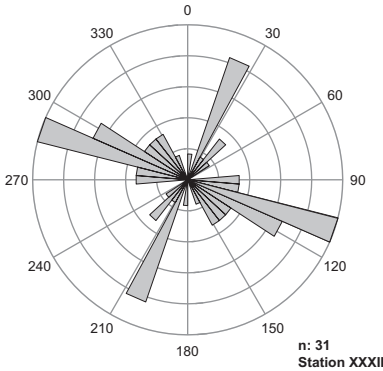
n: 289
Station XXVI



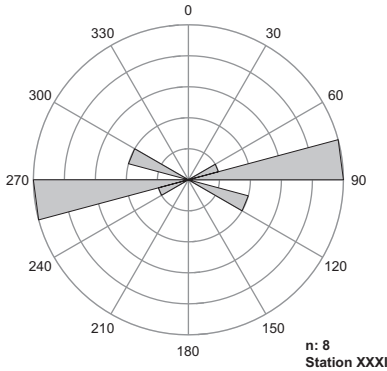
n: 57
Station XXIX



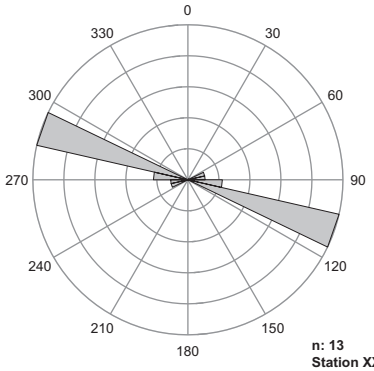
n: 12
Station XXXI



n: 31
Station XXXII



n: 8
Station XXXIII



n: 13
Station XXXIV

Figure 2C

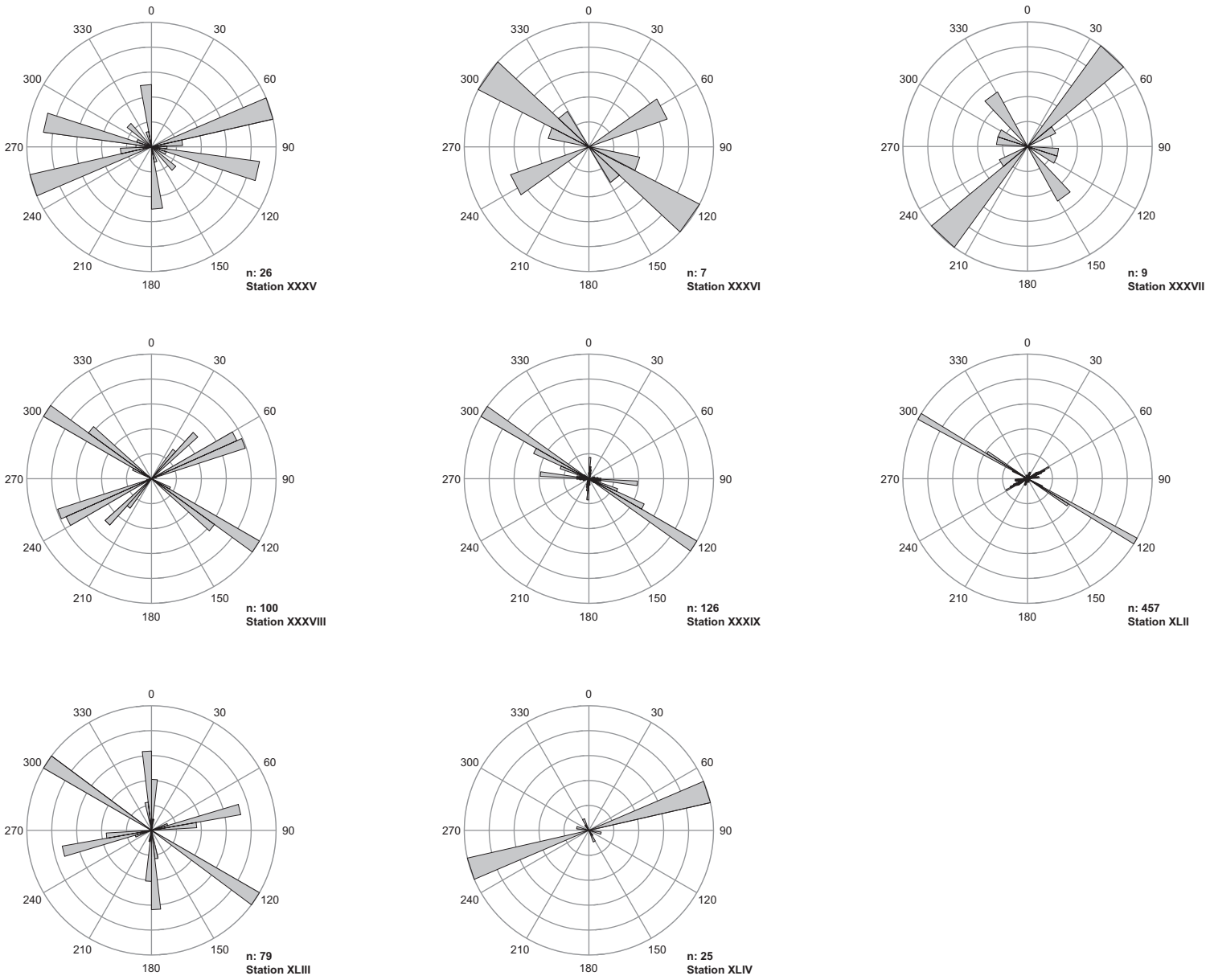


Figure DR-1 | Rose diagrams projecting the frequency of sub-vertical joints measured from all 32 stations. Roman numerals correspond to stations represented in Figure 2. Calcite veins dated via U-Pb are projected as dashed lines at their respective stations. Two prominent joint populations are identified: trending NW-SE and broadly E-W. Bin-sizes are proportional to the square root of the total number of joint measurements (n), a complete description is available in section 7. New field observations of the report

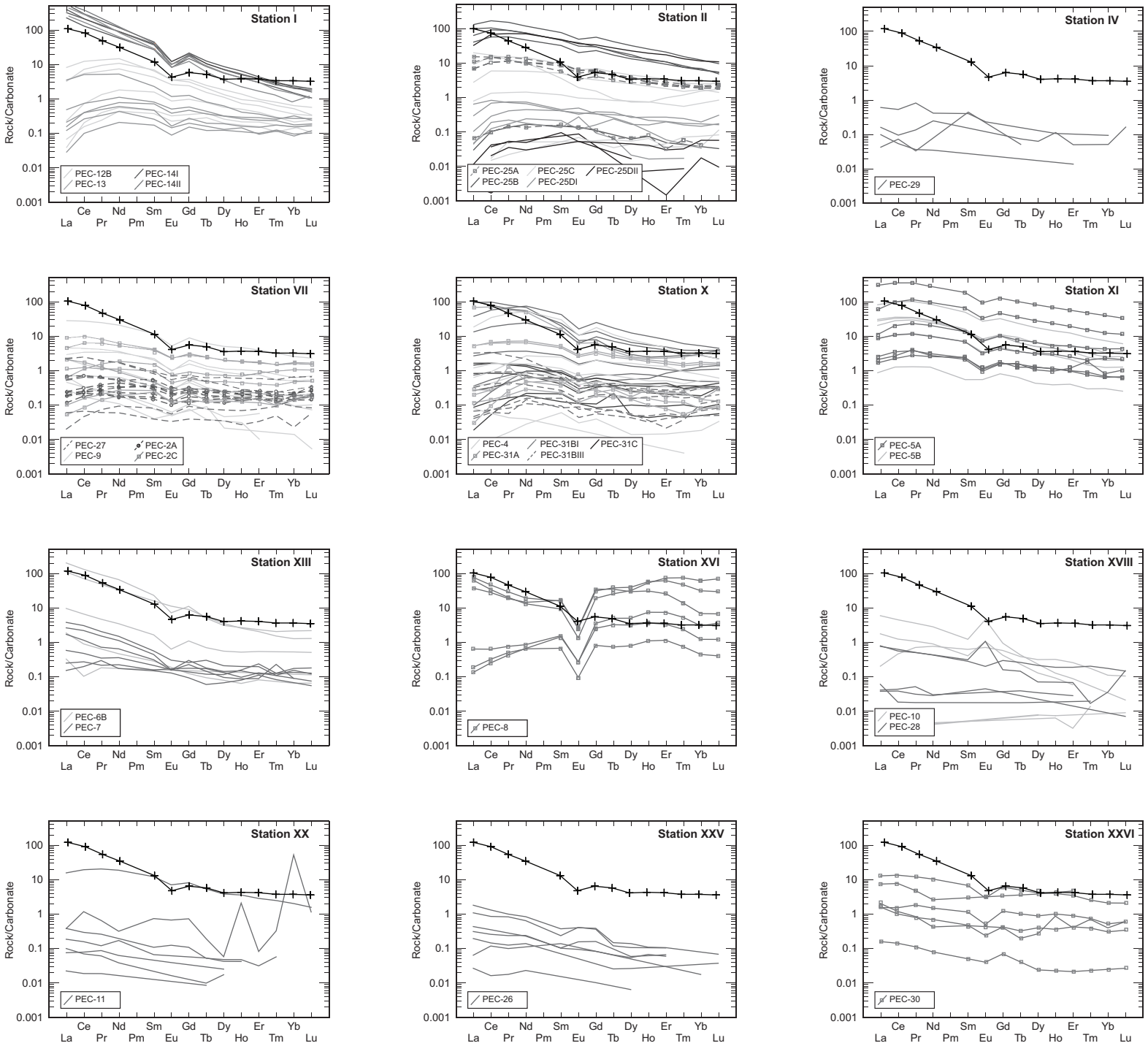


Figure DR-2 | Spider plots of calcite veins measured via LA-ICP-MS. Each plot represents a station, identified by roman numerals corresponding to the locations illustrated in Figure 2. Theoretical values of the upper continental crust are projected on each plot as a thick black line with " + "symbols. Stations where multiple samples were collected are differentiated by different increments of grey. Each line corresponds to a point analysis; three to seven measurements were taken on each sample. Calcite veins dated via U-Pb are represented by symbols. Samples with an enriched δ13C signature (refer to Figure 11) are represented by dashed lines. All samples were collected in 2015, and the "15" has been removed from sample numbers.

Table DR-1: Trace element geochemisry of vein calcite

Station	Sample number	Point analysis	Ca Wt%*	Ca	σCa	Mg	σMg	Si	σSi	Mn	σMn	Fe	σFe	Sr	σSr
I	PEC-15-12B	G1@1	53.78	384326.94	12159.72	2994.66	107.85	364.22	15.60	407.43	12.90	3281.27	440.98	188.56	6.06
		G1@2	53.50	382365.06	12097.71	2289.81	82.47	373.26	15.89	363.77	11.52	2820.37	379.04	226.33	7.27
		G2@1	54.95	392728.25	12426.44	2334.26	84.07	377.72	16.24	304.92	9.66	2393.35	321.65	134.82	4.33
		G3@1	54.07	386438.88	12226.33	2852.60	102.74	375.31	16.03	418.72	13.26	3246.21	436.27	209.02	6.71
		G4@1	54.18	387225.00	12250.13	2544.03	91.62	337.18	14.28	399.30	12.64	3109.85	417.94	223.90	7.19
		G5@1	54.39	388725.88	12298.1	2753.75	99.17	367.75	15.62	412.38	13.06	3173.19	426.45	190.23	6.11
	PEC-15-13	G1@1	55.78	398660.19	12610.51	1179.27	41.75	345.73	15.31	548.14	17.81	2026.78	68.90	171.06	5.28
		G2@1	55.17	394300.50	12472.47	2309.08	81.75	337.31	14.94	567.37	18.43	2862.36	97.31	195.24	6.03
		G2@2	55.37	395729.91	12517.67	2377.52	84.17	347.60	15.38	606.57	19.71	2911.98	98.99	173.24	5.35
		G3@1	55.90	399517.84	12637.41	631.92	22.38	379.00	16.69	545.49	17.72	1756.72	59.72	169.71	5.24
		G4@1	55.58	397230.78	12565.18	2483.44	87.92	353.09	15.62	608.09	19.75	3091.02	105.08	188.36	5.82
		G5@1	55.52	396801.97	12551.51	2400.96	85.00	334.28	14.79	591.33	19.21	2916.56	99.15	187.39	5.79
	PEC-15-14I	G1@1	47.74	341198.25	10837.9	34310.43	1282.97	28811.31	3593.78	1008.25	40.75	14463.41	1586.45	572.10	23.59
		G2@1	55.72	398231.34	12611.02	4004.95	149.61	2084.21	260.06	1485.77	59.98	1961.51	215.13	485.18	19.98
		G3@1	55.69	398016.97	12605.38	4520.43	168.87	2389.52	298.14	1201.81	48.52	2034.38	223.12	716.66	29.52
	PEC-15-14II	G1@1	55.13	394014.63	12468.56	1587.59	59.29	439.94	55.00	1407.20	56.79	444.43	48.74	485.25	19.98
		G2@1	56.00	400232.53	12675.33	1514.73	56.60	573.04	71.68	1367.41	55.20	529.85	58.11	399.37	16.45
		G3@1	55.06	393514.31	12451.88	3035.68	113.36	2019.15	251.88	1234.10	49.81	840.44	92.17	534.54	22.01
		G4@1	56.12	401090.16	12702.29	3650.46	136.37	2722.27	339.64	1196.59	48.31	1226.92	134.56	508.01	20.92

* All values are in ppm unless otherwise indicated
* Ca wt% values were measured via microprobe
* Hyphens indicate where no measurement was taken
* Sample codes beginning with "*" were measured during the in-situ analysis

Table DR-1: Trace element geochemisry of vein calcite

Station	Sample number	Point analysis	Y	σY	Ba	σBa	Zr	σZr	La	σLa	Ce	σCe	Pr	σPr	Nd	σNd	Sm	σSm	Eu	σEu
I	PEC-15-12B	G1@1	0.23	87.00	1.71	0.07	-	-	0.02	13.00	0.10	45.00	0.02	15.00	0.21	0.01	0.06	55.00	0.01	14.00
		G1@2	1.30	0.04	4.06	0.16	-	-	0.85	0.03	3.38	0.12	0.61	0.02	3.52	0.15	0.66	0.03	0.15	73.00
		G2@1	1.72	0.06	2.06	0.09	-	-	1.97	0.07	7.66	0.28	1.30	0.05	6.97	0.28	1.00	0.05	0.21	97.00
		G3@1	0.33	0.01	1.43	0.06	-	-	935.00	94.00	0.13	55.00	0.04	21.00	0.26	0.02	0.07	63.00	0.02	17.00
		G4@1	0.68	0.02	1.41	0.06	-	-	0.06	27.00	0.45	0.02	0.13	55.00	0.86	0.04	0.25	0.01	0.05	3.00
		G5@1	2.11	0.07	0.36	0.02	-	-	0.78	0.03	4.49	0.16	0.91	0.04	5.10	0.21	1.08	0.05	0.21	93.00
	PEC-15-13	G1@1	0.45	0.02	2.22	0.08	-	-	0.12	45.00	0.46	0.02	0.09	35.00	0.53	0.02	0.13	77.00	0.03	19.00
		G2@1	0.42	0.01	0.20	0.01	-	-	0.04	19.00	0.25	9.00	0.06	24.00	0.37	0.02	0.11	7.00	0.02	16.00
		G2@2	0.16	58.00	0.33	0.02	-	-	681.00	69.00	0.06	27.00	0.01	94.00	0.10	63.00	0.03	32.00	519.00	76.00
		G3@1	0.73	0.02	7.67	0.25	-	-	0.84	0.03	3.15	0.10	0.50	0.02	2.49	0.09	0.36	0.02	0.07	33.00
		G4@1	0.25	88.00	1.27	0.05	-	-	0.05	23.00	0.25	89.00	0.05	21.00	0.28	0.01	0.07	54.00	95.00	97.00
		G5@1	0.18	65.00	0.80	0.03	-	-	0.03	16.00	0.16	61.00	0.03	16.00	0.20	0.01	0.04	38.00	849.00	93.00
	PEC-15-14I	G1@1	7.11	0.26	9.83	0.87	-	-	158.19	6.82	245.47	15.25	21.86	1.05	60.99	2.66	6.74	0.33	0.49	0.03
		G2@1	8.25	0.30	0.62	0.06	-	-	66.54	2.87	107.30	6.66	10.17	0.49	30.72	1.33	4.29	0.20	0.62	0.03
		G3@1	4.30	0.16	3.08	0.27	-	-	115.47	4.97	181.53	11.27	15.61	0.74	41.27	1.78	4.56	0.21	0.50	0.03
	PEC-15-14II	G1@1	7.54	0.27	1.04	0.09	-	-	54.06	2.33	80.82	5.02	8.41	0.40	27.50	1.19	4.17	0.19	0.49	0.02
		G2@1	10.42	0.37	0.41	0.05	-	-	77.03	3.32	130.91	8.13	13.55	0.65	43.09	1.86	6.16	0.28	0.71	0.04
		G3@1	8.83	0.31	5.04	0.43	-	-	95.25	4.10	132.99	8.26	12.82	0.61	42.21	1.82	5.74	0.25	0.59	0.03
		G4@1	8.92	0.32	1.54	0.14	-	-	123.88	5.34	183.67	11.40	17.83	0.85	55.35	2.39	6.97	0.32	0.72	0.04

* All values are in ppm unless otherwise indicated
* Ca wt% values were measured via microprobe
* Hyphens indicate where no measurement was taken
* Sample codes beginning with "*" were measured during the in-situ analysis

Table DR-1: Trace element geochemisry of vein calcite

Station	Sample number	Point analysis	Gd	σGd	Tb	σTb	Dy	σDy	Ho	σHo	Er	σEr	Tm	σTm	Yb	σYb	Lu	σLu
I	PEC-15-12B	G1@1	0.05	53.00	0.01	91.00	0.05	41.00	992.00	91.00	0.03	24.00	285.00	45.00	0.02	3.00	469.00	58.00
		G1@2	0.50	0.02	0.06	3.00	0.29	0.01	0.04	24.00	0.11	62.00	0.01	97.00	0.06	5.00	845.00	81.00
		G2@1	0.65	0.03	0.08	39.00	0.34	0.02	0.05	31.00	0.14	81.00	0.02	12.00	0.09	66.00	879.00	88.00
		G3@1	0.07	63.00	0.01	11.00	0.07	48.00	0.01	1.00	0.04	29.00	446.00	53.00	0.03	31.00	274.00	52.00
		G4@1	0.20	0.01	0.03	17.00	0.15	81.00	0.03	17.00	0.07	42.00	754.00	67.00	0.04	33.00	619.00	62.00
		G5@1	0.77	0.03	0.09	44.00	0.47	0.02	0.08	39.00	0.16	84.00	0.02	13.00	0.11	7.00	0.01	11.00
	PEC-15-13	G1@1	0.12	74.00	0.02	11.00	0.08	5.00	0.02	11.00	0.05	31.00	658.00	62.00	0.06	42.00	619.00	61.00
		G2@1	0.10	62.00	0.01	93.00	0.08	48.00	0.02	98.00	0.04	28.00	599.00	56.00	0.03	28.00	482.00	51.00
		G2@2	0.03	32.00	457.00	47.00	0.03	27.00	638.00	6.00	0.02	17.00	321.00	42.00	0.02	21.00	26.00	39.00
		G3@1	0.26	0.01	0.03	16.00	0.16	79.00	0.02	13.00	0.06	36.00	728.00	63.00	0.05	35.00	692.00	63.00
		G4@1	0.06	46.00	742.00	64.00	0.05	35.00	913.00	72.00	0.03	21.00	448.00	47.00	0.03	26.00	425.00	49.00
		G5@1	0.04	36.00	603.00	58.00	0.03	28.00	824.00	69.00	0.02	16.00	299.00	39.00	0.01	2.00	304.00	4.00
	PEC-15-14I	G1@1	3.76	0.19	0.35	0.02	1.47	0.09	0.24	0.02	0.63	0.04	0.07	69.00	0.37	0.04	0.05	6.00
		G2@1	3.18	0.14	0.36	0.02	1.53	0.07	0.24	0.01	0.52	0.03	0.05	38.00	0.25	0.02	0.03	27.00
		G3@1	2.64	0.12	0.23	0.01	0.92	0.05	0.13	78.00	0.28	0.02	0.03	31.00	0.14	0.01	0.03	29.00
	PEC-15-14II	G1@1	3.10	0.13	0.33	0.02	1.44	0.06	0.23	0.01	0.50	0.02	0.06	33.00	0.26	0.02	0.03	21.00
		G2@1	4.48	0.20	0.48	0.02	2.22	0.10	0.37	0.02	0.72	0.04	0.08	54.00	0.37	0.03	0.04	35.00
		G3@1	3.89	0.16	0.40	0.02	1.80	0.08	0.29	0.01	0.65	0.03	0.07	39.00	0.35	0.02	0.05	28.00
		G4@1	4.25	0.19	0.40	0.02	1.85	0.09	0.30	0.02	0.64	0.03	0.08	52.00	0.41	0.03	0.05	4.00

* All values are in ppm unless otherwise indicated
* Ca wt% values were measured via microprobe
* Hyphens indicate where no measurement was taken
* Sample codes beginning with "*" were measured during the in-situ analysis

Table DR-1: Trace element geochemisry of vein calcite

Station	Sample number	Point analysis	Pb206 (ppb)	σPb206	Pb207 (ppb)	σPb207	Pb208 (ppb)	σPb208	Th232 (ppb)	σTh232	U238 (ppb)	σU238	ΣREE	Eu/Eu*
I	PEC-15-12B	G1@1	61.00	22.00	0.04	31.00	67.00	19.00	0.03	17.00	41.00	15.00	1746.58	0.24
		G1@2	0.01	24.00	0.01	22.00	0.01	2.00	0.07	36.00	49.00	24.00	855.24	0.27
		G2@1	0.01	25.00	0.01	22.00	0.01	21.00	0.04	2.00	0	18.00	899.48	0.26
		G3@1	0	22.00	0	2.00	62.00	17.00	0.01	78.00	0	18.00	1655.75	0.26
		G4@1	61.00	18.00	56.00	16.00	0.01	18.00	0.25	0.01	7.00	18.00	1375.30	0.23
		G5@1	0	2.00	0	18.00	63.00	16.00	0.04	21.00	0	21.00	14.28	0.23
	PEC-15-13	G1@1	76.00	19.00	0.01	18.00	68.00	16.00	0.02	12.00	25.00	1.00	1278.69	0.24
		G2@1	46.00	16.00	0	15.00	8.00	13.00	0.06	26.00	0	12.00	1082.12	0.22
		G2@2	0	17.00	44.00	15.00	59.00	14.00	0.01	84.00	0	15.00	2642.30	17896.02
		G3@1	0.02	22.00	0.03	21.00	0.03	22.00	0.05	2.00	0	17.00	1427.99	0.22
		G4@1	0	16.00	0	15.00	5.00	13.00	451.00	41.00	34.00	14.00	2623.86	1480.69
		G5@1	59.00	16.00	72.00	15.00	58.00	13.00	0.01	79.00	0	16.00	2879.57	21069.33
	PEC-15-14I	G1@1	0.02	64.00	0.02	69.00	0.03	66.00	0.44	0.02	23.20	57.00	500.68	0.10
		G2@1	61.00	32.00	95.00	32.00	0	25.00	15.00	48.00	2.00	66.00	225.79	0.17
		G3@1	5.00	31.00	0.01	35.00	71.00	26.00	292.00	76.00	1.00	48.00	363.34	0.14
	PEC-15-14II	G1@1	5.00	22.00	0.01	25.00	0.06	76.00	691.00	76.00	3.23	82.00	181.38	0.13
		G2@1	7.00	3.00	82.00	33.00	46.00	23.00	507.00	9.00	3.32	97.00	280.20	0.13
		G3@1	98.00	27.00	64.00	25.00	0	2.00	0.04	25.00	4.10	1.00	297.08	0.12
		G4@1	0.03	5.00	0.03	47.00	0.02	41.00	0.04	31.00	4.20	12.00	396.40	0.13

* All values are in ppm unless otherwise indicated
* Ca wt% values were measured via microprobe
* Hyphens indicate where no measurement was taken
* Sample codes beginning with "*" were measured during the in-situ analysis

Table DR-1: Trace element geochemisry of vein calcite

Station	Sample number	Point analysis	Ca Wt%*	Ca	σCa	Mg	σMg	Si	σSi	Mn	σMn	Fe	σFe	Sr	σSr
II	PEC-15-25A	G1@1	55.77	398588.72	12609.51	861.89	32.19	193.01	24.23	279.74	11.29	1227.93	134.67	165.07	6.80
		G2@1	55.00	393085.53	12436.59	625.50	23.36	208.30	26.18	228.91	9.24	1129.33	123.85	155.13	6.39
		G3@1	55.43	396158.72	12539.74	685.22	25.60	213.71	26.94	206.41	8.33	1203.57	132.00	216.54	8.92
		G4@1	55.36	395658.47	12518.39	761.15	28.43	203.24	25.57	286.86	11.58	1255.65	137.71	75.52	3.11
		G5@1	55.30	395229.63	12503.66	676.38	25.26	203.32	25.53	209.86	8.47	1181.64	129.59	202.46	8.34
	PEC-15-25B	G1@1	54.65	390584.06	12358.81	1881.02	70.24	217.41	27.35	424.82	17.15	1529.78	167.77	341.52	14.06
		G2@1	55.25	394872.28	12495.77	1194.48	44.61	221.93	27.93	522.79	21.10	1288.07	141.26	411.95	16.96
		G3@1	55.25	394872.28	12509.15	1705.16	63.72	241.35	30.63	426.10	17.21	1649.76	180.94	402.20	16.57
		G4@1	55.25	394872.28	12494.9	1879.48	70.19	239.30	30.14	471.48	19.03	1729.11	189.63	462.26	19.03
		G5@1	55.25	394872.28	12518.45	1857.19	69.43	217.33	28.12	1281.61	51.76	1627.94	178.56	342.16	14.10
		G5@2	55.25	394872.31	12501.08	1968.14	73.52	246.00	31.23	451.46	18.23	1554.97	170.54	333.67	13.74
	PEC-15-25C	G1@1	55.58	397230.81	12566.45	593.69	21.39	351.04	14.83	310.89	9.84	870.78	117.03	99.97	3.21
		G2@1	55.25	394872.31	12493.18	609.12	21.94	388.87	16.55	339.13	10.74	1472.75	197.93	80.43	2.58
		G3@1	55.20	394515.00	12481.32	602.23	21.70	368.18	15.65	333.37	10.55	1449.32	194.78	80.57	2.59
		G4@1	55.40	395944.34	12526.42	388.97	14.02	385.96	16.37	210.22	6.66	858.95	115.44	151.28	4.86
		G5@1	54.81	391727.63	12393.53	482.75	17.39	364.84	15.53	339.39	10.75	1751.74	235.42	108.78	3.49
		G5@2	55.66	397802.59	12585.22	441.50	15.91	368.58	15.69	325.41	10.30	1725.48	231.89	109.59	3.52
	PEC-15-25DI	G1@1	55.70	398088.47	12594.62	546.08	19.67	381.70	16.21	484.90	15.35	869.77	116.89	173.72	5.58
		G2@1	55.07	393585.88	12452.21	1264.79	45.56	377.93	16.05	528.83	16.74	1239.09	166.53	257.32	8.26
		G3@1	55.37	395729.97	12519.96	1503.68	54.16	369.34	15.76	556.41	17.62	1438.81	193.37	312.41	10.03
		G4@1	55.69	398017.03	12593.09	621.28	22.38	374.52	16.08	493.38	15.62	873.45	117.39	153.56	4.93
		G5@1	55.15	394157.59	12471.25	2964.92	106.78	376.82	16.20	584.92	18.52	2207.34	296.65	360.43	11.57
		G5@2	55.41	396015.81	12529.78	2763.79	99.54	362.04	15.56	587.06	18.59	2173.40	292.09	365.62	11.74
	PEC-15-25DII	G1@1	54.68	390798.50	12370.02	1372.53	49.45	340.40	14.95	560.46	17.75	1328.38	178.53	341.35	10.97
		G2@1	54.70	390941.44	12369.18	1803.67	64.96	362.93	15.61	1026.92	32.51	1810.37	243.30	421.77	13.54
		G3@1	54.42	388940.28	12305.54	1921.26	69.20	377.70	16.08	873.27	27.65	1628.22	218.82	294.62	9.46
		G4@1	54.92	392513.78	12418.23	1264.31	45.54	367.12	15.66	559.61	17.72	1297.41	174.36	291.05	9.35
		G5@1	54.87	392156.44	12407.08	871.02	31.38	373.98	15.94	515.62	16.32	1049.88	141.10	192.02	6.17
		G5@2	55.37	395729.94	12520.57	1082.26	38.98	395.06	16.82	502.16	15.90	1221.10	164.11	521.50	16.75
IV	PEC-15-29	G1@1	56.15	401304.59	12706.12	754.66	28.20	270.51	34.15	514.23	20.76	1449.98	159.03	411.22	16.94
		G2@1	56.01	400304.00	12670.08	702.83	26.26	273.51	34.62	549.93	22.20	1269.40	139.22	231.76	9.54
		G3@1	56.52	403948.97	12804.26	865.07	32.36	274.33	34.90	622.74	25.15	1164.00	127.67	99.42	4.10
		G4@1	56.45	403448.69	12819.66	292.84	11.02	223.23	29.37	396.65	16.04	664.06	72.85	112.61	4.65
		G5@1	55.57	397159.31	12600.27	683.50	25.59	262.81	33.62	524.62	21.20	1318.28	144.60	322.67	13.30
		G5@2	56.54	404091.91	12844.34	552.15	20.73	378.18	48.23	472.92	19.13	1000.65	109.77	219.17	9.05

* All values are in ppm unless otherwise indicated
* Ca wt% values were measured via microprobe
* Hyphens indicate where no measurement was taken
* Sample codes beginning with "*" were measured during the in-situ analysis

Table DR-1: Trace element geochemisry of vein calcite

Station	Sample number	Point analysis	Y	σY	Ba	σBa	Zr	σZr	La	σLa	Ce	σCe	Pr	σPr	Nd	σNd	Sm	σSm	Eu	σEu
II	PEC-15-25A	G1@1	2.97	0.11	0.50	0.05	-	-	2.80	0.12	7.02	0.44	0.90	0.04	3.46	0.15	0.69	0.03	0.15	79.00
		G2@1	3.68	0.13	0.12	0.02	-	-	1.95	0.09	6.77	0.42	1.08	0.05	4.74	0.21	1.10	0.05	0.27	0.01
		G3@1	4.37	0.16	0.07	0.01	-	-	1.22	0.06	4.94	0.31	0.84	0.04	3.73	0.17	1.12	0.06	0.28	0.02
		G4@1	0.06	33.00	0	9.00	-	-	0.01	12.00	0.05	36.00	0.01	11.00	0.05	52.00	0.02	35.00	33.00	11.00
		G5@1	4.09	0.15	0.17	0.02	-	-	1.27	0.06	4.88	0.30	0.83	0.04	3.70	0.16	0.98	0.05	0.23	0.01
	PEC-15-25B	G1@1	13.91	0.49	0.73	0.07	-	-	7.62	0.33	27.66	1.72	4.29	0.20	17.18	0.74	3.89	0.17	0.92	0.04
		G2@1	0.09	49.00	0.04	84.00	-	-	559.00	95.00	0.05	39.00	0.01	12.00	0.06	68.00	0.02	42.00	62.00	13.00
		G3@1	15.87	0.57	1.08	0.11	-	-	11.84	0.51	44.33	2.75	6.68	0.32	27.51	1.20	5.58	0.26	1.42	0.07
		G4@1	32.65	1.16	0.17	0.02	-	-	24.57	1.06	81.75	5.08	11.36	0.54	43.40	1.87	9.23	0.40	2.24	0.10
		G5@1	17.07	0.61	0.22	0.03	-	-	18.62	0.81	50.37	3.13	6.60	0.32	27.14	1.19	5.54	0.27	1.78	0.09
		G5@2	0.04	33.00	0.12	0.02	-	-	0	12.00	0.03	32.00	36.00	94.00	0.03	64.00	0	23.00	29.00	11.00
	PEC-15-25C	G1@1	5.51	0.18	91.00	41.00	-	-	1.69	0.06	7.63	0.28	1.12	0.04	5.24	0.21	1.15	0.05	0.29	0.01
		G2@1	0.05	24.00	0	4.00	-	-	0	39.00	715.00	82.00	163.00	38.00	65.00	22.00	0	21.00	312.00	65.00
		G3@1	0.05	25.00	9.00	4.00	-	-	1.00	38.00	827.00	84.00	397.00	53.00	0.02	28.00	0	15.00	237.00	58.00
		G4@1	0.99	0.03	0.03	55.00	-	-	3.69	0.13	8.19	0.30	0.94	0.04	3.74	0.15	0.43	0.02	0.09	45.00
		G5@1	0.82	0.03	0.13	0.01	-	-	0.15	62.00	0.64	0.02	0.10	47.00	0.52	0.03	0.14	97.00	0.04	28.00
		G5@2	2.39	0.08	0.09	88.00	-	-	0.52	0.02	2.83	0.10	0.44	0.02	2.12	0.09	0.61	0.03	0.17	78.00
	PEC-15-25DI	G1@1	0.03	17.00	0.01	42.00	-	-	829.00	89.00	0.09	42.00	0.02	12.00	0.07	58.00	0.02	31.00	0.01	13.00
		G2@1	0.17	65.00	0.02	48.00	-	-	0.06	28.00	0.33	0.01	0.06	28.00	0.27	0.02	0.05	51.00	0.02	18.00
		G3@1	54.00	7.00	0.06	72.00	-	-	0	26.00	346.00	53.00	6.00	27.00	0	22.00	0	13.00	641.00	88.00
		G4@1	0.21	8.00	0.07	84.00	-	-	0.12	52.00	0.40	0.02	0.05	28.00	0.24	0.01	0.05	52.00	0.02	17.00
		G5@1	0.21	8.00	0.05	72.00	-	-	881.00	92.00	0.06	31.00	0.01	11.00	0.09	73.00	0.03	38.00	533.00	94.00
		G5@2	0.35	0.01	0.23	0.02	-	-	0.02	14.00	0.14	6.00	0.03	19.00	0.16	0.01	0.05	52.00	0.01	15.00
	PEC-15-25DII	G1@1	0.01	13.00	0.04	78.00	-	-	158.00	61.00	98.00	13.00	262.00	62.00	0.01	3.00	56.00	24.00	241.00	8.00
		G2@1	26.36	0.86	0.07	78.00	-	-	6.09	0.22	32.97	1.20	5.34	0.20	25.93	1.04	5.82	0.24	1.67	0.07
		G3@1	0.06	3.00	0.02	54.00	-	-	137.00	53.00	0.02	13.00	396.00	54.00	0.02	3.00	0.01	24.00	236.00	6.00
		G4@1	211.00	45.00	0.02	49.00	-	-	5.00	19.00	8.00	24.00	3.00	14.00	0	11.00	0	9.00	0	54.00
		G5@1	206.00	47.00	0.02	38.00	-	-	0	34.00	244.00	49.00	75.00	22.00	0	22.00	0	1.00	0	39.00
		G5@2	696.00	95.00	0.08	9.00	-	-	216.00	49.00	0.02	15.00	365.00	55.00	0.02	32.00	38.00	17.00	395.00	77.00
IV	PEC-15-29	G1@1	68.00	13.00	0.63	0.06	-	-	0.02	22.00	0.03	29.00	273.00	74.00	0.01	42.00	0	23.00	26.00	11.00
		G2@1	0.01	15.00	1.05	0.10	-	-	0.04	3.00	0.03	27.00	253.00	61.00	0	53.00	0	24.00	25.00	12.00
		G3@1	34.00	13.00	0.05	0.01	-	-	8.00	19.00	0.04	45.00	25.00	1.00	0	4.00	0.05	0.01	23.00	18.00
		G4@1	0.11	0.01	31.14	2.69	-	-	0.11	0.01	0.26	0.02	0.06	75.00	0.15	0.03	0.05	0.02	0.01	4.00
		G5@1	0	27.00	0.05	0.02	-	-	11.00	1.00	17.00	13.00	0	13.00	0	15.00	0	0	33.00	19.00
		G5@2	0.02	47.00	3.32	0.32	-	-	0.03	54.00	0.05	71.00	0.01	3.00	0.09	0.02	0	17.00	0	0

* All values are in ppm unless otherwise indicated
* Ca wt% values were measured via microprobe
* Hyphens indicate where no measurement was taken
* Sample codes beginning with "*" were measured during the in-situ analysis

Table DR-1: Trace element geochemisry of vein calcite

Station	Sample number	Point analysis	Gd	σGd	Tb	σTb	Dy	σDy	Ho	σHo	Er	σEr	Tm	σTm	Yb	σYb	Lu	σLu
II	PEC-15-25A	G1@1	0.65	0.03	0.09	45.00	0.53	0.03	0.11	53.00	0.31	0.02	0.04	24.00	0.25	0.01	0.04	22.00
		G2@1	1.01	0.05	0.13	63.00	0.75	0.03	0.14	66.00	0.36	0.02	0.05	27.00	0.27	0.02	0.04	24.00
		G3@1	0.96	0.05	0.13	69.00	0.77	0.04	0.12	66.00	0.32	0.02	0.04	31.00	0.28	0.02	0.05	32.00
		G4@1	0.02	32.00	186.00	42.00	0.01	23.00	338.00	61.00	4.00	1.00	115.00	31.00	56.00	15.00	0	32.00
		G5@1	0.93	0.04	0.12	58.00	0.71	0.03	0.12	57.00	0.28	0.01	0.04	23.00	0.25	0.01	0.04	21.00
	PEC-15-25B	G1@1	3.72	0.16	0.50	0.02	2.64	0.11	0.50	0.02	1.20	0.05	0.15	72.00	0.84	0.04	0.11	54.00
		G2@1	0.02	42.00	16.00	57.00	0.01	25.00	328.00	67.00	63.00	15.00	0	36.00	2.00	13.00	65.00	27.00
		G3@1	4.79	0.21	0.63	0.03	3.06	0.14	0.58	0.03	1.40	0.07	0.17	97.00	0.85	0.05	0.11	71.00
		G4@1	9.11	0.37	1.23	0.05	6.41	0.27	1.14	0.05	2.70	0.11	0.31	0.01	1.64	0.07	0.19	9.00
		G5@1	4.77	0.22	0.66	0.03	3.49	0.16	0.55	0.03	1.41	0.07	0.15	99.00	0.93	0.06	0.10	73.00
		G5@2	0.01	48.00	0	74.00	41.00	23.00	105.00	59.00	31.00	17.00	0	52.00	0	23.00	0	52.00
	PEC-15-25C	G1@1	1.12	0.05	0.16	7.00	0.90	0.04	0.18	8.00	0.44	0.02	0.05	26.00	0.33	0.02	0.05	27.00
		G2@1	73.00	24.00	102.00	25.00	88.00	16.00	165.00	36.00	59.00	12.00	141.00	29.00	0.01	18.00	163.00	37.00
		G3@1	71.00	18.00	174.00	32.00	0.01	17.00	285.00	42.00	468.00	9.00	105.00	31.00	5.00	12.00	223.00	37.00
		G4@1	0.25	0.01	0.03	16.00	0.15	83.00	0.03	19.00	0.13	69.00	0.02	15.00	0.21	0.01	0.03	2.00
		G5@1	0.15	95.00	0.02	15.00	0.16	89.00	0.03	2.00	0.08	51.00	0.01	91.00	0.09	63.00	0.02	12.00
		G5@2	0.52	0.02	0.08	4.00	0.50	0.02	0.09	46.00	0.23	0.01	0.03	17.00	0.23	0.01	0.03	17.00
	PEC-15-25DI	G1@1	0.01	24.00	191.00	37.00	42.00	11.00	72.00	21.00	147.00	67.00	34.00	14.00	0	11.00	0	16.00
		G2@1	0.05	54.00	751.00	76.00	0.04	32.00	458.00	57.00	76.00	14.00	81.00	3.00	45.00	11.00	67.00	22.00
		G3@1	29.00	15.00	26.00	16.00	0	61.00	0	2.00	0	39.00	0	11.00	0	73.00	0	15.00
		G4@1	0.05	52.00	924.00	86.00	0.06	46.00	957.00	91.00	0.03	25.00	355.00	52.00	0.02	29.00	321.00	49.00
		G5@1	0.03	43.00	696.00	74.00	0.03	35.00	707.00	76.00	0.03	25.00	318.00	47.00	0.02	29.00	343.00	52.00
		G5@2	0.06	58.00	0.01	97.00	0.05	43.00	0.01	1.00	0.03	3.00	487.00	6.00	0.03	3.00	605.00	67.00
	PEC-15-25DII	G1@1	0	17.00	0	3.00	33.00	13.00	0	3.00	0	58.00	0	2.00	0	62.00	0	0
		G2@1	5.45	0.22	0.81	0.03	4.51	0.19	0.86	0.04	2.26	0.10	0.27	0.01	1.53	0.07	0.22	98.00
		G3@1	0.01	26.00	139.00	33.00	89.00	17.00	181.00	39.00	39.00	96.00	64.00	19.00	76.00	16.00	113.00	26.00
		G4@1	0	16.00	0	22.00	0	72.00	0	16.00	0	0	17.00	1.00	0	58.00	0	15.00
		G5@1	0	18.00	0	15.00	0	41.00	0	24.00	0	0	0	27.00	0	59.00	0	18.00
		G5@2	39.00	19.00	4.00	22.00	224.00	89.00	55.00	25.00	19.00	19.00	0	24.00	233.00	83.00	19.00	11.00
IV	PEC-15-29	G1@1	0	37.00	65.00	42.00	0	16.00	0	29.00	18.00	1.00	0	0	0	19.00	0	33.00
		G2@1	0	24.00	0	54.00	0	16.00	0	46.00	2.00	12.00	0	34.00	62.00	23.00	0	24.00
		G3@1	71.00	52.00	152.00	76.00	0	0	0	21.00	0	6.00	0	14.00	0	2.00	0	28.00
		G4@1	0	0	2.00	14.00	56.00	44.00	48.00	2.00	61.00	41.00	0	0	0.01	71.00	0	11.00
		G5@1	0	14.00	0	0	0	12.00	0	56.00	0	55.00	0	29.00	0	1.00	51.00	51.00
		G5@2	0	91.00	22.00	14.00	0.01	67.00	51.00	21.00	66.00	44.00	69.00	84.00	69.00	54.00	33.00	16.00

* All values are in ppm unless otherwise indicated
* Ca wt% values were measured via microprobe
* Hyphens indicate where no measurement was taken
* Sample codes beginning with "*" were measured during the in-situ analysis

Table DR-1: Trace element geochemisry of vein calcite

Station	Sample number	Point analysis	Pb206 (ppb)	σPb206	Pb207 (ppb)	σPb207	Pb208 (ppb)	σPb208	Th232 (ppb)	σTh232	U238 (ppb)	σU238	ΣREE	Eu/Eu*
II	PEC-15-25A	G1@1	0	19.00	49.00	19.00	0	16.00	0	29.00	1.79	47.00	17.03	0.22
		G2@1	88.00	23.00	0	2.00	0	18.00	45.00	51.00	17.30	38.00	18.65	0.25
		G3@1	0	23.00	8.00	29.00	92.00	25.00	0	22.00	169.00	57.00	14.79	0.27
		G4@1	79.00	23.00	0	23.00	0	2.00	0	27.00	9.40	21.00	732.17	1779.29
		G5@1	54.00	21.00	0	19.00	51.00	16.00	0	14.00	3.38	81.00	14.37	0.24
	PEC-15-25B	G1@1	85.00	31.00	0.01	29.00	0.02	31.00	0.37	0.02	197.00	6.00	71.21	0.24
		G2@1	0.01	31.00	57.00	24.00	83.00	24.00	51.00	26.00	0	26.00	1095.17	3753.79
		G3@1	0.02	49.00	0.02	45.00	0.02	44.00	0.39	0.02	7.30	19.00	108.95	0.27
		G4@1	0	31.00	0.02	34.00	0.01	31.00	0.26	0.01	0	29.00	195.28	0.24
		G5@1	0.01	56.00	0.01	54.00	0.02	52.00	0.11	73.00	103.00	72.00	122.11	0.35
		G5@2	0	37.00	91.00	42.00	0	32.00	121.00	52.00	79.00	43.00	242.07	0
	PEC-15-25C	G1@1	0.03	25.00	0	15.00	5.00	15.00	969.00	7.00	61.00	17.00	20.34	0.26
		G2@1	0	22.00	48.00	18.00	71.00	18.00	485.00	5.00	0	17.00	2046.01	0
		G3@1	53.00	19.00	0	19.00	71.00	16.00	351.00	44.00	0	17.00	2793.03	0
		G4@1	0	2.00	0	19.00	0.02	23.00	0.02	12.00	3.79	43.00	17.92	0.27
		G5@1	0	53.00	46.00	18.00	72.00	16.00	0.03	17.00	28.50	17.00	2.16	0.30
		G5@2	0	2.00	86.00	19.00	0	16.00	0.02	12.00	19.70	12.00	8.40	0.30
	PEC-15-25DI	G1@1	0	21.00	0	19.00	64.00	16.00	0	13.00	0	15.00	1315.22	0.81
		G2@1	0.03	27.00	0.01	21.00	0	18.00	432.00	45.00	22.00	12.00	1478.87	0.42
		G3@1	0.01	21.00	47.00	18.00	0	17.00	7.00	23.00	0	11.00	1048.00	0
		G4@1	0	22.00	0	22.00	54.00	18.00	0	21.00	0	16.00	2558.03	0.32
		G5@1	88.00	22.00	79.00	22.00	63.00	18.00	48.00	17.00	0	14.00	3478.29	20699.38
		G5@2	67.00	23.00	0.01	22.00	0.01	19.00	4.00	19.00	36.00	15.00	1092.61	0.27
	PEC-15-25DII	G1@1	0	23.00	73.00	24.00	0	2.00	0	15.00	0	14.00	848.01	0
		G2@1	0.02	28.00	0.02	25.00	0.02	25.00	0.26	0.01	0.94	19.00	93.72	0.30
		G3@1	0.02	26.00	72.00	21.00	0.01	18.00	0	15.00	34.00	18.00	1470.06	21171.24
		G4@1	71.00	21.00	0	19.00	0	17.00	0	14.00	0	14.00	33.00	0
		G5@1	0	21.00	73.00	2.00	62.00	17.00	0	17.00	0	12.00	319.00	0
		G5@2	0.01	23.00	69.00	22.00	0.02	25.00	37.00	16.00	44.00	18.00	1607.04	10.26
IV	PEC-15-29	G1@1	0	36.00	93.00	36.00	96.00	33.00	7.00	37.00	0	39.00	382.06	0
		G2@1	0	39.00	0	38.00	0	33.00	0	41.00	314.00	93.00	342.07	0
		G3@1	0	41.00	0.01	44.00	0.02	5.00	147.00	73.00	32.00	3.00	279.09	11.75
		G4@1	0.03	89.00	92.00	6.00	0.05	94.00	36.00	14.00	98.00	86.00	167.66	0
		G5@1	0	46.00	0	44.00	0	4.00	0	21.00	0	41.00	112.00	0
		G5@2	0.03	86.00	0.03	85.00	0.06	0.01	0.01	25.00	7.50	24.00	310.19	0

* All values are in ppm unless otherwise indicated
* Ca wt% values were measured via microprobe
* Hyphens indicate where no measurement was taken
* Sample codes beginning with "*" were measured during the in-situ analysis

Table DR-1: Trace element geochemisry of vein calcite

Station	Sample number	Point analysis	Ca Wt%*	Ca	σCa	Mg	σMg	Si	σSi	Mn	σMn	Fe	σFe	Sr	σSr
VII	PEC-15-2A	G1@1	54.63	390441.13	12352.4	394.79	14.75	239.05	29.99	932.43	37.63	3276.45	359.32	110.59	4.55
		G1@2	54.98	392942.59	12431.38	401.18	14.99	246.85	30.96	920.97	37.17	3217.11	352.82	110.56	4.55
		G2@1	54.21	387439.38	12257.37	381.08	14.23	235.52	29.55	953.09	38.46	3194.46	350.33	94.13	3.88
		G3@1	54.60	390226.75	12346.09	251.30	9.39	239.06	30.01	1434.60	57.89	2139.19	234.60	56.79	2.34
		G3@2	54.30	388082.63	12278.12	234.50	8.76	241.62	30.32	1459.52	58.90	2056.02	225.48	54.34	2.24
		G4@1	55.12	393943.16	12462.85	270.78	10.12	251.74	31.55	1989.08	80.27	2035.98	223.28	52.90	2.18
		G5@1	54.24	387653.81	12263.77	408.49	15.26	238.37	29.88	847.26	34.19	2995.19	328.48	76.35	3.14
		*1	56.37	402841.25	12746.23	419.41	14.86	257.71	11.65	851.38	26.35	772.13	30.59	146.27	4.54
		*2	55.22	394679.38	12487.68	854.46	30.26	264.53	11.84	3163.00	97.87	1760.93	69.76	84.15	2.61
		*3	55.38	395794.31	12523.68	326.09	11.56	283.01	12.71	1992.00	61.64	2245.78	88.97	52.23	1.62
		*4	55.12	393964.63	12465.15	328.31	11.63	322.89	14.07	1248.23	38.62	2039.99	80.82	226.84	7.03
		*5	55.78	398674.50	12613.85	352.72	12.50	269.90	12.06	2109.42	65.27	2377.71	94.20	58.24	1.81
		*6	56.14	401204.59	12695.78	357.48	12.67	1004.68	41.12	938.59	29.05	766.08	30.35	44.00	1.37
		*7	55.38	395815.75	12523.47	357.92	12.68	275.25	12.23	1923.58	59.52	2302.72	91.23	64.60	2.00
	PEC-15-2C	G1@1	55.00	393085.53	12435.43	208.35	7.78	206.00	25.87	1425.66	57.53	1950.47	213.91	56.64	2.33
		G2@1	55.53	396873.44	12554.83	268.19	10.02	205.33	25.77	1462.98	59.04	2098.48	230.14	55.26	2.28
		G2@2	54.94	392656.69	12421.25	284.01	10.61	202.00	25.35	1796.26	72.49	2191.36	240.32	56.58	2.33
		G3@1	54.69	390869.94	12364.88	387.64	14.48	188.23	23.64	693.07	27.97	1999.84	219.32	136.38	5.62
		G4@1	54.94	392656.69	12422.38	263.48	9.84	221.75	27.85	1897.82	76.59	1925.62	211.18	43.33	1.79
		G5@1	54.91	392442.25	12416.32	241.11	9.01	222.53	27.99	1885.39	76.09	1825.26	200.18	47.96	1.98
		G5@2	55.09	393728.75	12456.56	252.34	9.43	230.53	28.96	1391.37	56.15	1972.32	216.30	95.28	3.92
	PEC-15-9	G1@1	56.26	402090.78	12719.92	420.70	15.71	258.60	32.40	882.39	35.61	1269.79	139.26	58.00	2.39
		G1@2	54.52	389654.97	12326.5	254.58	9.51	225.79	28.31	748.33	30.20	866.43	95.02	30.02	1.24
		G2@1	54.69	390869.94	12365.11	1089.59	40.69	223.93	28.09	717.67	28.96	1756.62	192.65	85.54	3.52
		G3@1	55.08	393657.28	12453.12	974.69	36.40	219.33	27.51	561.19	22.65	1420.23	155.76	77.21	3.18
		G4@1	55.51	396730.50	12550.55	1721.87	64.29	229.95	28.83	792.11	31.97	2384.58	261.51	82.82	3.41
		G5@1	54.57	390012.31	12337.64	1570.12	58.63	211.65	26.55	1006.37	40.61	2371.26	260.05	70.26	2.89
		G5@2	54.76	391370.25	12380.53	1236.20	46.16	214.83	26.94	982.14	39.63	2173.26	238.34	77.87	3.21
		G6@1	54.40	388797.31	12298.66	459.06	17.14	204.83	25.67	905.05	36.52	1360.74	149.23	92.44	3.81
	PEC-15-27	G1@1	54.91	392442.28	12414.27	384.19	13.61	349.95	15.48	409.44	13.30	2014.61	68.49	198.53	6.13
		G2@1	54.78	391513.19	12387.04	219.13	7.77	338.86	15.16	1412.82	45.90	2533.38	86.13	64.75	2.00
		G3@1	54.77	391441.72	12382.68	332.05	11.76	359.34	15.88	909.01	29.53	2311.92	78.60	62.12	1.92
		G3@2	54.01	386009.97	12210.72	270.60	9.59	347.49	15.37	634.84	20.62	1854.99	63.06	50.65	1.56
		G4@1	55.12	393943.16	12462.13	282.18	10.00	359.64	15.98	617.60	20.06	2169.77	73.77	50.00	1.55
		G5@1	53.47	382150.59	12088.52	351.81	12.46	344.54	15.23	501.45	16.29	1798.66	61.15	80.86	2.50

* All values are in ppm unless otherwise indicated
* Ca wt% values were measured via microprobe
* Hyphens indicate where no measurement was taken
* Sample codes beginning with "*" were measured during the in-situ analysis

Table DR-1: Trace element geochemisry of vein calcite

Station	Sample number	Point analysis	Y	σY	Ba	σBa	Zr	σZr	La	σLa	Ce	σCe	Pr	σPr	Nd	σNd	Sm	σSm	Eu	σEu
VII	PEC-15-2A	G1@1	0.37	0.01	0.01	34.00	-	-	0.04	23.00	0.15	96.00	0.03	19.00	0.11	82.00	0.03	47.00	0.01	13.00
		G1@2	0.40	0.02	0.02	38.00	-	-	0.06	34.00	0.20	0.01	0.03	22.00	0.14	96.00	0.04	48.00	97.00	13.00
		G2@1	0.31	0.01	0.03	56.00	-	-	0.06	31.00	0.18	0.01	0.03	18.00	0.10	79.00	0.03	4.00	78.00	11.00
		G3@1	0.48	0.02	0.03	6.00	-	-	0.06	33.00	0.18	0.01	0.03	23.00	0.20	0.01	0.07	69.00	0.02	17.00
		G3@2	0.47	0.02	0.05	79.00	-	-	0.07	4.00	0.20	0.01	0.04	28.00	0.21	0.01	0.07	69.00	0.02	18.00
		G4@1	0.27	0.01	0.04	67.00	-	-	0.08	4.00	0.25	0.02	0.05	29.00	0.27	0.02	0.06	61.00	0.01	15.00
		G5@1	0.59	0.02	67.00	31.00	-	-	0.22	0.01	0.58	0.04	0.08	45.00	0.33	0.02	0.11	86.00	0.03	21.00
		*1	7.93	0.25	0.23	0.02	0.02	49.00	2.92	0.09	7.67	0.24	0.99	0.03	0	0.16	0.99	0.04	0	8.00
		*2	21.70	0.69	0.17	0.01	0.01	43.00	8.36	0.26	19.12	0.60	2.43	0.08	11.20	0.36	2.46	0.08	0.46	0.02
		*3	0.37	0.01	0.11	0.01	96.00	45.00	0.06	32.00	0.22	82.00	0.04	23.00	0	0.02	0.08	7.00	0.01	15.00
		*4	7.22	0.23	0.17	0.01	0.01	49.00	4.38	0.14	10.50	0.33	1.34	0.04	0	0.20	0	0.04	0.21	85.00
		*5	0.59	0.02	0.10	97.00	0.02	5.00	0.08	37.00	0	99.00	0.05	24.00	0.34	0.02	0.12	83.00	0	17.00
		*6	1.18	0.04	0.97	0.04	0.17	0.02	0.41	0.01	1.05	0.03	0.15	57.00	0.67	0.03	0	0.01	0	24.00
		*7	0.89	0.03	0.08	87.00	0.04	69.00	0.10	44.00	0.43	0.02	0.09	38.00	0.61	0.03	0.17	0.01	0.04	25.00
	PEC-15-2C	G1@1	0.28	0.01	0.14	0.02	-	-	0.02	13.00	0.07	49.00	0.02	14.00	0.12	81.00	0.05	53.00	0.01	12.00
		G2@1	1.59	0.06	0.14	0.01	-	-	0.20	95.00	0.93	0.06	0.20	0.01	1.18	0.05	0.31	0.02	0.06	36.00
		G2@2	0.41	0.02	0.18	0.02	-	-	0.67	0.03	1.45	0.09	0.16	82.00	0.57	0.03	0.09	72.00	0.02	17.00
		G3@1	4.56	0.16	0.12	0.01	-	-	2.83	0.12	8.17	0.51	1.03	0.05	3.91	0.17	0.86	0.04	0.18	93.00
		G4@1	0.75	0.03	0.05	77.00	-	-	0.36	0.02	1.02	0.06	0.14	75.00	0.71	0.04	0.20	0.01	0.03	26.00
		G5@1	0.21	87.00	0.03	57.00	-	-	0.03	22.00	0.13	88.00	0.03	19.00	0.17	0.01	0.05	59.00	89.00	13.00
		G5@2	4.69	0.17	0.06	87.00	-	-	1.47	0.06	5.19	0.32	0.80	0.04	3.30	0.15	0.81	0.04	0.18	93.00
	PEC-15-9	G1@1	2.02	0.07	0.45	0.04	-	-	1.36	0.06	3.36	0.21	0.49	0.02	2.10	0.09	0.39	0.02	0.07	44.00
		G1@2	0.74	0.03	0.14	0.02	-	-	0.63	0.03	1.15	0.07	0.14	72.00	0.58	0.03	0.09	73.00	0.02	17.00
		G2@1	0.10	44.00	0.08	99.00	-	-	0.08	42.00	0.13	86.00	0.02	12.00	0.06	54.00	77.00	18.00	235.00	6.00
		G3@1	2.37	0.09	0.23	0.02	-	-	0.87	0.04	2.63	0.16	0.41	0.02	1.94	0.09	0.43	0.02	0.07	42.00
		G4@1	0.62	0.02	0.23	0.02	-	-	0.21	97.00	0.55	0.04	0.08	43.00	0.38	0.02	0.06	59.00	0.02	19.00
		G5@1	0.21	84.00	0.08	96.00	-	-	0.13	65.00	0.25	0.02	0.03	2.00	0.13	84.00	0.02	31.00	45.00	78.00
		G5@2	0.13	55.00	58.00	29.00	-	-	0.19	9.00	0.26	0.02	0.03	18.00	0.11	75.00	88.00	21.00	354.00	61.00
		G6@1	10.09	0.36	0.11	0.01	-	-	8.44	0.36	21.10	1.31	2.95	0.14	12.26	0.53	2.25	0.10	0.38	0.02
	PEC-15-27	G1@1	1.75	0.06	0.07	7.00	-	-	0.69	0.02	2.01	0.07	0.25	89.00	1.08	0.04	0.19	0.01	0.05	29.00
		G2@1	0.58	0.02	0.41	0.02	-	-	0.16	66.00	0.52	0.02	0.08	35.00	0.35	0.02	0.08	7.00	0.02	16.00
		G3@1	0.17	62.00	0	29.00	-	-	631.00	7.00	0.04	2.00	933.00	77.00	0.06	5.00	0.02	3.00	425.00	74.00
		G3@2	0.08	33.00	0	29.00	-	-	0.02	12.00	0.05	25.00	764.00	7.00	0.04	38.00	79.00	17.00	256.00	52.00
		G4@1	0.46	0.02	0	28.00	-	-	0.17	64.00	0.59	0.02	0.08	32.00	0.33	0.02	0.06	51.00	0.02	15.00
		G5@1	1.04	0.03	0.02	34.00	-	-	0.72	0.02	2.01	0.07	0.25	87.00	1.05	0.04	0.16	93.00	0.04	25.00

* All values are in ppm unless otherwise indicated
* Ca wt% values were measured via microprobe
* Hyphens indicate where no measurement was taken
* Sample codes beginning with "*" were measured during the in-situ analysis

Table DR-1: Trace element geochemisry of vein calcite

Station	Sample number	Point analysis	Gd	σGd	Tb	σTb	Dy	σDy	Ho	σHo	Er	σEr	Tm	σTm	Yb	σYb	Lu	σLu
VII	PEC-15-2A	G1@1	0.03	43.00	71.00	76.00	0.05	44.00	0.01	11.00	0.04	33.00	666.00	75.00	0.03	36.00	474.00	63.00
		G1@2	0.05	54.00	79.00	82.00	0.06	48.00	0.01	1.00	0.04	33.00	406.00	57.00	0.04	41.00	624.00	72.00
		G2@1	0.04	44.00	601.00	71.00	0.04	37.00	0.01	97.00	0.03	29.00	513.00	63.00	0.03	36.00	631.00	76.00
		G3@1	0.06	64.00	0.01	11.00	0.09	63.00	0.02	13.00	0.04	35.00	672.00	76.00	0.05	48.00	0.01	11.00
		G3@2	0.09	76.00	0.01	1.00	0.08	57.00	0.02	13.00	0.05	38.00	556.00	72.00	0.05	45.00	876.00	89.00
		G4@1	0.06	61.00	935.00	87.00	0.06	47.00	0.01	1.00	0.03	29.00	419.00	6.00	0.03	35.00	666.00	74.00
		G5@1	0.07	66.00	0.01	96.00	0.08	56.00	0.02	14.00	0.06	4.00	823.00	81.00	0.05	44.00	851.00	83.00
		*1	0	0.04	0.14	55.00	0	0.03	0.18	68.00	0	0.02	0.05	27.00	0	0.02	0	26.00
		*2	2.80	0.10	0	0.02	0	0.10	0	0.02	0	0.06	0.19	72.00	0	0.04	0.13	53.00
		*3	0	69.00	946.00	93.00	0	49.00	0.01	11.00	0.03	3.00	582.00	71.00	0.03	37.00	909.00	9.00
		*4	0	0.04	0.16	6.00	0.96	0.04	0.19	74.00	0.57	0.02	0	34.00	0.54	0.02	0.08	34.00
		*5	0.10	75.00	0	12.00	0	6.00	0	14.00	0	39.00	725.00	75.00	0	5.00	0.01	1.00
		*6	0.13	95.00	0	17.00	0.18	97.00	0.04	22.00	0.12	7.00	0	13.00	0.11	75.00	0	13.00
		*7	0.17	0.01	0.03	16.00	0.16	83.00	0.03	18.00	0.09	52.00	0.02	12.00	0.11	71.00	0	12.00
	PEC-15-2C	G1@1	0.06	59.00	693.00	72.00	0.05	41.00	0.01	97.00	0.03	29.00	33.00	5.00	0.03	35.00	713.00	77.00
		G2@1	0.26	0.01	0.04	22.00	0.25	0.01	0.05	28.00	0.19	96.00	0.03	19.00	0.25	0.01	0.04	2.00
		G2@2	0.09	68.00	0.01	11.00	0.08	54.00	0.02	13.00	0.05	35.00	686.00	69.00	0.04	39.00	723.00	71.00
		G3@1	0.78	0.04	0.12	56.00	0.69	0.03	0.14	65.00	0.39	0.02	0.05	27.00	0.37	0.02	0.05	27.00
		G4@1	0.16	0.01	0.02	16.00	0.17	96.00	0.03	21.00	0.09	57.00	0.01	11.00	0.11	75.00	0.02	13.00
		G5@1	0.04	5.00	609.00	77.00	0.04	42.00	95.00	1.00	0.03	27.00	338.00	55.00	0.03	36.00	6.00	74.00
		G5@2	0.86	0.04	0.12	59.00	0.68	0.03	0.14	65.00	0.37	0.02	0.05	29.00	0.40	0.02	0.06	31.00
	PEC-15-9	G1@1	0.40	0.02	0.05	27.00	0.28	0.01	0.06	29.00	0.16	82.00	0.02	12.00	0.11	71.00	0.02	12.00
		G1@2	0.14	93.00	0.02	11.00	0.08	54.00	0.02	12.00	0.05	34.00	518.00	59.00	0.02	24.00	231.00	42.00
		G2@1	0.01	28.00	419.00	53.00	68.00	15.00	81.00	31.00	33.00	11.00	0	2.00	297.00	9.00	17.00	1.00
		G3@1	0.52	0.03	0.06	32.00	0.35	0.02	0.07	37.00	0.20	0.01	0.02	16.00	0.13	82.00	0.02	15.00
		G4@1	0.12	84.00	0.01	1.00	0.06	46.00	0.01	1.00	0.04	31.00	399.00	54.00	0.02	26.00	321.00	46.00
		G5@1	0.03	36.00	355.00	46.00	0.01	2.00	345.00	53.00	0.01	15.00	79.00	24.00	0	14.00	0	22.00
		G5@2	0.02	31.00	178.00	32.00	54.00	13.00	218.00	36.00	212.00	59.00	0	16.00	0	99.00	0	15.00
		G6@1	2.31	0.10	0.29	0.01	1.60	0.07	0.33	0.01	0.82	0.03	0.10	48.00	0.55	0.03	0.07	35.00
	PEC-15-27	G1@1	0.20	0.01	0.03	17.00	0.22	0.01	0.04	22.00	0.13	65.00	0.02	12.00	0.15	82.00	0.02	14.00
		G2@1	0.08	68.00	0.02	12.00	0.09	61.00	0.02	14.00	0.05	41.00	802.00	84.00	0.07	55.00	0.01	11.00
		G3@1	0.03	3.00	381.00	47.00	0.02	25.00	519.00	59.00	0.02	18.00	312.00	46.00	0.03	31.00	613.00	64.00
		G3@2	0.01	2.00	102.00	27.00	0.01	18.00	202.00	38.00	73.00	12.00	166.00	31.00	51.00	11.00	195.00	32.00
		G4@1	0.08	62.00	937.00	8.00	0.06	44.00	996.00	88.00	0.03	27.00	407.00	52.00	0.02	25.00	279.00	45.00
		G5@1	0.18	98.00	0.02	14.00	0.13	7.00	0.02	13.00	0.06	35.00	665.00	62.00	0.04	36.00	624.00	6.00

* All values are in ppm unless otherwise indicated
* Ca wt% values were measured via microprobe
* Hyphens indicate where no measurement was taken
* Sample codes beginning with "*" were measured during the in-situ analysis

Table DR-1: Trace element geochemisry of vein calcite

Station	Sample number	Point analysis	Pb206 (ppb)	σPb206	Pb207 (ppb)	σPb207	Pb208 (ppb)	σPb208	Th232 (ppb)	σTh232	U238 (ppb)	σU238	ΣREE	Eu/Eu*
VII	PEC-15-2A	G1@1	0	21.00	0	2.00	0	18.00	119.00	3.00	5.20	12.00	1211.53	0.33
		G1@2	63.00	23.00	0.01	23.00	0	18.00	21.00	33.00	7.60	17.00	1206.68	2158.14
		G2@1	0	21.00	0	2.00	49.00	19.00	544.00	55.00	22.10	48.00	1823.54	2354.65
		G3@1	87.00	24.00	0	21.00	0	19.00	5.00	15.00	69.00	0.02	672.84	0.26
		G3@2	0.01	25.00	53.00	22.00	0	19.00	145.00	3.00	80.00	0.02	1432.91	0.24
		G4@1	0.01	26.00	0	3.00	72.00	2.00	0	15.00	209.00	0.05	2020.93	0.23
		G5@1	0.01	25.00	0.04	53.00	0.08	91.00	46.00	17.00	5.80	13.00	1675.63	0.28
		*1	0.01	22.00	45.00	2.00	34.00	14.00	106.00	27.00	72.40	3.00	12.93	0
		*2	0.01	24.00	0.02	25.00	0.01	14.00	814.00	65.00	0	13.00	47.15	0.17
		*3	0.02	28.00	0.01	25.00	69.00	14.00	579.00	6.00	167.80	63.00	2437.50	0
		*4	0.02	26.00	85.00	24.00	0.07	35.00	83.00	21.00	5.32	51.00	18.93	0
		*5	0.03	3.00	0.01	23.00	45.00	15.00	529.00	56.00	270.70	98.00	725.71	0
		*6	0.41	0.02	0.25	0.01	0.34	0.01	0.02	12.00	104.00	42.00	2.84	0
		*7	0.04	35.00	0.02	26.00	0.02	15.00	512.00	51.00	393.00	0.01	2.05	0.23
	PEC-15-2C	G1@1	0	21.00	82.00	21.00	94.00	2.00	885.00	72.00	56.00	0.01	1439.47	0.18
		G2@1	0.01	25.00	86.00	19.00	5.00	17.00	368.00	42.00	200.00	0.04	4.00	0.21
		G2@2	61.00	18.00	0	16.00	35.00	14.00	202.00	35.00	41.40	89.00	1412.26	0.23
		G3@1	82.00	2.00	88.00	19.00	81.00	17.00	0	27.00	8.50	19.00	19.58	0.22
		G4@1	72.00	24.00	0.04	51.00	0	19.00	0.03	16.00	110.00	0.02	3.08	0.19
		G5@1	0.02	34.00	0	23.00	72.00	21.00	988.00	83.00	113.00	0.02	1137.56	1923.76
		G5@2	0	24.00	0	19.00	61.00	2.00	0	19.00	19.30	42.00	14.42	0.21
	PEC-15-9	G1@1	0.01	22.00	47.00	18.00	41.00	17.00	166.00	29.00	13.20	29.00	8.85	0.19
		G1@2	0	17.00	44.00	18.00	0	14.00	0	14.00	57.00	22.00	751.93	0.17
		G2@1	69.00	19.00	7.00	18.00	45.00	16.00	0	18.00	1.95	5.00	1227.30	244.47
		G3@1	0	19.00	65.00	17.00	0	16.00	0.02	11.00	56.00	0.01	7.73	0.15
		G4@1	53.00	17.00	0	17.00	48.00	16.00	0	15.00	0.68	22.00	721.56	0.26
		G5@1	0	17.00	0	16.00	0	16.00	65.00	2.00	0	12.00	824.62	1959.93
		G5@2	0	17.00	43.00	16.00	0	15.00	0	17.00	0	14.00	1104.61	270.24
		G6@1	75.00	17.00	54.00	15.00	0	14.00	0	13.00	6.80	15.00	53.46	0.17
	PEC-15-27	G1@1	79.00	18.00	62.00	16.00	0	13.00	0	16.00	0	14.00	5.08	0.28
		G2@1	0.01	23.00	55.00	18.00	48.00	16.00	791.00	72.00	33.00	17.00	803.53	0.21
		G3@1	47.00	16.00	0	14.00	49.00	14.00	22.00	31.00	69.00	21.00	3814.21	20842.35
		G3@2	44.00	16.00	63.00	16.00	42.00	15.00	0	19.00	0	16.00	1888.13	278.44
		G4@1	0	17.00	0	17.00	41.00	15.00	28.00	12.00	0	12.00	2620.42	0.23
		G5@1	0	18.00	59.00	14.00	0	14.00	0	2.00	0	15.00	1293.69	0.24

* All values are in ppm unless otherwise indicated
* Ca wt% values were measured via microprobe
* Hyphens indicate where no measurement was taken
* Sample codes beginning with "*" were measured during the in-situ analysis

Table DR-1: Trace element geochemisry of vein calcite

Station	Sample number	Point analysis	Ca Wt%*	Ca	σCa	Mg	σMg	Si	σSi	Mn	σMn	Fe	σFe	Sr	σSr
X	PEC-15-4	G1@1	54.25	387725.31	12268.96	716.94	25.83	396.80	17.14	4077.05	129.08	1112.18	149.47	32.73	1.05
		G2@1	54.50	389512.09	12324.92	584.35	21.06	369.76	16.11	725.26	22.96	1158.80	155.74	100.67	3.23
		G3@1	54.31	388154.16	12282.47	1593.52	57.40	409.19	17.66	809.35	25.63	2095.32	281.60	132.68	4.26
		G4@1	55.04	393371.47	12448.01	388.63	14.01	387.67	16.92	856.86	27.13	1111.10	149.33	78.15	2.51
		G5@1	55.08	393657.31	12456.66	376.20	13.56	376.86	16.43	818.21	25.91	706.60	94.96	38.37	1.23
		G5@2	54.36	388511.50	12294.23	721.25	25.99	369.37	16.22	3946.60	124.95	1234.24	165.87	32.18	1.04
	PEC-15-31A	G1@1	54.54	389797.97	12332.48	530.90	19.13	400.60	16.96	1705.69	54.00	1218.62	163.77	133.33	4.28
		G2@1	54.90	392370.84	12417.83	579.09	20.87	373.28	16.04	831.91	26.34	952.16	127.97	52.63	1.69
		G3@1	53.70	383794.47	12142.36	552.52	19.91	377.68	16.07	1527.06	48.34	1406.72	189.05	90.97	2.92
		G4@1	55.01	393157.06	12439.41	201.03	7.25	394.38	16.87	1377.71	43.62	474.74	63.80	22.03	0.71
		G4@2	55.12	393943.19	12463.68	804.84	28.99	573.45	23.83	1867.88	59.13	1319.15	177.28	45.93	1.48
		G5@1	55.21	394586.44	12483.76	806.67	29.06	371.59	15.84	1594.32	50.47	1334.39	179.33	34.01	1.09
		G5@2	54.93	392585.25	12420.91	823.64	29.67	382.08	16.26	1487.35	47.09	1361.88	183.03	31.71	1.02
		*1	57.33	409752.25	12963.23	467.86	17.02	300.01	12.57	608.84	19.17	857.87	76.35	124.07	3.79
		*2	57.14	408387.19	12920.8	540.81	19.69	295.87	12.53	849.79	26.77	841.92	75.90	50.14	1.53
		*3	57.14	408387.19	12919.81	913.56	33.30	300.52	12.64	1599.89	50.45	2111.16	193.10	201.40	6.15
		*4	56.91	406714.78	12867.85	182.54	6.67	307.15	12.97	828.87	26.17	482.10	44.82	20.76	0.63
		*5	56.56	404270.53	12797.77	737.67	26.99	303.85	13.36	2162.82	68.40	1227.40	116.15	61.99	1.90
		*6	57.53	411188.84	13008.57	857.01	31.59	295.49	12.48	1882.51	59.94	1397.71	143.85	40.96	1.26
		*7	57.36	409981.00	12970.25	182.09	6.74	301.41	12.75	1589.10	50.70	574.03	60.49	18.40	0.56
		*8	57.28	409359.19	12950.84	894.21	33.14	314.19	13.30	4996.17	159.79	1723.84	186.15	50.08	1.54
		*9	56.06	400647.00	12675.01	954.78	35.48	290.84	12.34	1777.23	56.98	2329.60	257.95	133.81	4.11
		*10	56.67	405049.63	12814.84	1387.62	51.72	601.78	24.32	1800.19	57.88	2430.46	276.11	172.08	5.29
		*11	56.59	404477.84	12796.75	539.78	20.40	304.72	13.05	1811.90	58.97	976.59	123.42	31.93	0.99
		*12	55.94	399832.38	12649.84	2132.12	80.87	311.16	13.29	955.51	31.21	2838.06	368.56	156.19	4.83
		*13	55.90	399496.44	12639.21	2153.11	81.99	323.96	13.77	1284.07	42.09	2797.70	373.38	139.29	4.32
		*14	56.50	403813.19	12775.84	444.20	16.99	293.25	12.68	1991.71	65.52	943.19	129.37	30.50	0.95
		*15	55.95	399896.66	12651.67	440.42	16.92	292.66	12.57	2217.11	73.22	1130.13	159.31	36.45	1.13
		*16	58.13	415484.38	13144.9	512.60	20.06	302.58	13.08	649.28	21.81	978.19	153.75	101.00	3.16
		*17	57.92	413933.44	13095.53	436.75	17.18	291.76	12.57	2279.95	76.91	1046.06	168.91	35.79	1.12
		*18	56.93	406843.59	12871.28	751.47	29.70	292.52	12.60	3864.77	130.98	1448.61	240.25	46.18	1.45
		*19	56.59	404470.78	12795.84	1162.55	46.18	270.34	11.71	2071.81	70.55	2605.00	443.67	140.63	4.43
	PEC-15-31BI	G1@1	54.29	388011.19	12279.26	1388.95	50.04	409.98	18.12	2988.91	94.63	1915.72	257.46	84.06	2.70
		G2@1	55.17	394300.53	12479.07	471.63	17.00	427.88	18.93	786.16	24.89	1044.79	140.42	135.81	4.36
		G3@1	55.23	394729.38	12492.25	338.30	12.20	447.74	19.65	1901.81	60.22	784.01	105.37	30.63	0.99
		G4@1	54.64	390512.63	12361.16	506.59	18.26	465.74	20.84	2687.26	85.09	1258.97	169.20	35.63	1.15
		G5@1	54.71	391012.91	12376.96	1073.62	38.69	473.39	21.46	2221.03	70.33	1762.84	236.92	45.78	1.47
		G5@2	55.48	396516.13	12551.02	202.98	7.33	485.57	21.86	841.08	26.64	517.18	69.51	20.62	0.67
		G6@1	54.28	387939.72	12284.15	1270.32	45.79	476.40	22.16	1442.75	45.70	1909.15	256.58	279.72	8.99

* All values are in ppm unless otherwise indicated
* Ca wt% values were measured via microprobe
* Hyphens indicate where no measurement was taken
* Sample codes beginning with "*" were measured during the in-situ analysis

Table DR-1: Trace element geochemisry of vein calcite

Station	Sample number	Point analysis	Y	σY	Ba	σBa	Zr	σZr	La	σLa	Ce	σCe	Pr	σPr	Nd	σNd	Sm	σSm	Eu	σEu
X	PEC-15-4	G1@1	1.24	0.04	0.07	89.00	-	-	0.17	72.00	0.55	0.02	0.12	56.00	0.83	0.04	0.21	0.01	0.05	32.00
		G2@1	0.03	21.00	0.01	56.00	-	-	0.04	23.00	0.07	36.00	835.00	88.00	0.04	52.00	0	22.00	0	46.00
		G3@1	19.23	0.63	2.41	0.10	-	-	9.11	0.32	44.01	1.61	8.88	0.34	50.93	2.04	9.47	0.39	1.25	0.05
		G4@1	2.47	0.08	0.08	95.00	-	-	0.59	0.02	1.97	0.07	0.31	0.01	1.51	0.07	0.36	0.02	0.09	51.00
		G5@1	0.04	24.00	0.02	44.00	-	-	0	56.00	0.01	12.00	315.00	64.00	0.03	45.00	0.02	36.00	361.00	8.00
		G5@2	5.62	0.18	0.03	55.00	-	-	0.31	0.01	1.17	0.04	0.32	0.01	2.58	0.11	0.78	0.04	0.17	83.00
	PEC-15-31A	G1@1	8.61	0.28	0.05	68.00	-	-	2.56	0.09	7.74	0.28	1.24	0.05	6.07	0.25	1.43	0.06	0.30	0.01
		G2@1	0.27	0.01	0.18	0.02	-	-	0.01	14.00	0.12	59.00	0.05	3.00	0.44	0.02	0.16	0.01	0.03	26.00
		G3@1	9.37	0.31	9.00	35.00	-	-	2.51	0.09	8.17	0.30	1.37	0.05	6.84	0.28	1.58	0.07	0.33	0.01
		G4@1	5.58	0.18	0.05	74.00	-	-	32.94	1.16	87.82	3.21	11.19	0.43	47.63	1.91	4.77	0.20	0.73	0.03
		G4@2	0.37	0.01	0.35	0.02	-	-	0.13	56.00	0.34	0.01	0.25	0.01	0.47	0.02	0.11	83.00	0.09	49.00
		G5@1	0.64	0.02	0	42.00	-	-	0.09	42.00	0.34	0.01	0.08	39.00	0.63	0.03	0.16	0.01	0.06	36.00
		G5@2	0.38	0.01	0	4.00	-	-	0.06	29.00	0.18	75.00	0.04	21.00	0.27	0.02	0.07	62.00	0.01	14.00
		*1	12.08	0.37	0.09	82.00	0.03	6.00	2.13	0.07	6.26	0.20	0	0.03	5.26	0.17	0	0.05	0.29	0.01
		*2	0.23	78.00	0.01	4.00	0.01	43.00	0.01	11.00	0.08	35.00	0.03	16.00	0.25	0.01	0.10	76.00	0	16.00
		*3	4.07	0.12	1.35	0.05	0.03	49.00	2.67	0.08	8.41	0.26	1.37	0.04	0	0.22	0	0.05	0.23	84.00
		*4	4.63	0.14	79.00	33.00	0.33	0.02	26.98	0.82	75.83	2.37	9.80	0.30	41.98	1.35	3.96	0.14	0.55	0.02
		*5	1.40	0.04	0.17	0.02	0.03	8.00	1.40	0.05	0	0.10	0.41	0.02	1.99	0.08	0	0.02	0.05	4.00
		*6	0.11	4.00	0.01	39.00	0	25.00	0.01	1.00	0.05	24.00	0.01	94.00	0.08	63.00	0.02	28.00	321.00	63.00
		*7	4.89	0.15	0.07	71.00	0.22	0.01	27.29	0.83	59.36	1.87	0	0.22	31.30	1.02	3.55	0.13	0.52	0.02
		*8	0.19	66.00	0.14	0.01	0	67.00	0.02	15.00	0.10	4.00	0	13.00	0	82.00	0	47.00	0	94.00
		*9	1.29	0.04	3.71	0.12	0.01	43.00	1.05	0.03	2.27	0.07	0.35	0.01	1.73	0.06	0	0.01	0.07	34.00
		*10	2.56	0.08	2.14	0.08	0.09	92.00	1.55	0.05	4.86	0.16	0.81	0.03	4.30	0.15	0	0.03	0	69.00
		*11	0.03	15.00	0.01	59.00	76.00	31.00	411.00	63.00	0.01	11.00	19.00	4.00	0		32.00	14.00	0	23.00
		*12	1.09	0.03	99.00	47.00	0.02	45.00	0.12	46.00	0.77	0.03	0	7.00	0	0.05	0	0.02	0	3.00
		*13	0.56	0.02	3.05	0.10	0.01	41.00	0.07	3.00	0.36	0.01	0	36.00	0.63	0.03	0	99.00	0.02	18.00
		*14	0.02	12.00	0.04	67.00	62.00	3.00	0	65.00	0.01	11.00	0	41.00	0.02	3.00	24.00	14.00	85.00	43.00
		*15	0.05	22.00	0.01	43.00	0.01	34.00	0	81.00	0.03	17.00	465.00	57.00	0	31.00	48.00	21.00	145.00	51.00
		*16	4.48	0.14	0.04	59.00	0.01	39.00	0.90	0.03	3.07	0.10	0.55	0.02	0	0.11	0.76	0.04	0.15	62.00
		*17	0.06	23.00	0.04	68.00	99.00	38.00	862.00	91.00	0.04	21.00	0	84.00	0	68.00	0.02	31.00	0	82.00
		*18	0.68	0.02	1.16	0.05	0.04	59.00	0.58	0.02	0	0.05	0.20	7.00	0	0.04	0	0.01	0	21.00
		*19	0.60	0.02	1.81	0.07	8.00	28.00	0.42	0.01	0.94	0.03	0	54.00	0.75	0.03	0	89.00	0	21.00
	PEC-15-31BI	G1@1	33.03	1.08	0	45.00	-	-	18.48	0.65	72.58	2.65	13.14	0.50	72.18	2.89	13.37	0.55	1.94	0.08
		G2@1	5.05	0.17	0.03	67.00	-	-	1.31	0.05	4.16	0.15	0.71	0.03	3.52	0.15	0.87	0.04	0.19	93.00
		G3@1	13.97	0.46	0.12	0.01	-	-	51.47	1.82	100.12	3.66	12.12	0.46	52.74	2.11	7.37	0.31	1.28	0.05
		G4@1	2.42	0.08	0.01	41.00	-	-	0.05	31.00	0.31	0.01	0.10	53.00	0.94	0.05	0.28	0.02	0.06	43.00
		G5@1	1.91	0.07	0	54.00	-	-	0.17	8.00	0.69	0.03	0.14	69.00	0.91	0.05	0.31	0.02	0.07	47.00
		G5@2	5.81	0.19	0	68.00	-	-	46.59	1.64	123.29	4.50	15.60	0.60	65.67	2.63	6.23	0.26	0.89	0.04
		G6@1	16.71	0.55	0.06	0.01	-	-	6.54	0.23	23.72	0.87	4.32	0.17	23.35	0.95	4.66	0.20	0.75	0.03

* All values are in ppm unless otherwise indicated
* Ca wt% values were measured via microprobe
* Hyphens indicate where no measurement was taken
* Sample codes beginning with "*" were measured during the in-situ analysis

Table DR-1: Trace element geochemisry of vein calcite

Station	Sample number	Point analysis	Gd	σGd	Tb	σTb	Dy	σDy	Ho	σHo	Er	σEr	Tm	σTm	Yb	σYb	Lu	σLu
X	PEC-15-4	G1@1	0.20	0.01	0.03	21.00	0.21	0.01	0.04	26.00	0.12	72.00	0.01	12.00	0.10	74.00	0.02	13.00
		G2@1	82.00	25.00	0	37.00	0	13.00	0	34.00	145.00	7.00	21.00	12.00	0	66.00	0	24.00
		G3@1	7.54	0.30	0.85	0.04	4.07	0.17	0.69	0.03	1.58	0.07	0.17	74.00	0.94	0.04	0.12	57.00
		G4@1	0.35	0.02	0.05	31.00	0.31	0.02	0.06	33.00	0.17	96.00	0.02	16.00	0.18	0.01	0.03	18.00
		G5@1	0.02	34.00	157.00	43.00	72.00	17.00	204.00	56.00	49.00	12.00	0	37.00	64.00	17.00	173.00	38.00
		G5@2	0.86	0.04	0.13	62.00	0.85	0.04	0.16	79.00	0.45	0.02	0.05	28.00	0.27	0.02	0.03	21.00
	PEC-15-31A	G1@1	1.33	0.06	0.19	83.00	1.11	0.05	0.21	95.00	0.53	0.02	0.07	34.00	0.53	0.03	0.08	39.00
		G2@1	0.12	97.00	0.02	14.00	0.08	63.00	0.01	12.00	0.03	3.00	279.00	54.00	0.03	37.00	415.00	66.00
		G3@1	1.51	0.06	0.22	94.00	1.22	0.05	0.23	0.01	0.62	0.03	0.08	38.00	0.60	0.03	0.08	42.00
		G4@1	2.71	0.11	0.27	0.01	1.30	0.06	0.26	0.01	0.77	0.03	0.13	57.00	1.08	0.05	0.19	88.00
		G4@2	0.10	73.00	0.02	14.00	0.09	59.00	0.03	2.00	0.06	39.00	0.01	1.00	0.05	43.00	0.02	12.00
		G5@1	0.16	98.00	0.02	15.00	0.12	72.00	0.03	17.00	0.08	49.00	0.01	9.00	0.05	43.00	669.00	71.00
		G5@2	0.08	63.00	0.01	1.00	0.08	57.00	0.02	13.00	0.04	33.00	624.00	67.00	0.03	31.00	475.00	63.00
		*1	1.29	0.05	0.23	8.00	0	0.05	0.31	0.01	0	0.03	0	49.00	0.83	0.03	0.12	44.00
		*2	0.08	67.00	0.01	1.00	0.05	42.00	0.01	97.00	0	25.00	229.00	46.00	0	22.00	0	52.00
		*3	0	0.04	0.12	47.00	0	0.02	0.11	42.00	0	0.01	0	17.00	0	89.00	0	14.00
		*4	2.36	0.08	0.21	75.00	0	0.04	0.21	75.00	0.60	0.02	0	39.00	0.83	0.03	0.15	55.00
		*5	0.26	0.02	0	24.00	0	0.01	0.04	28.00	0.10	74.00	0.02	17.00	0.10	87.00	0	16.00
		*6	0.01	28.00	0	42.00	0.01	2.00	47.00	59.00	0	17.00	229.00	41.00	0.02	27.00	0	57.00
		*7	2.25	0.08	0.22	78.00	1.16	0.04	0	78.00	0.66	0.02	0	44.00	0.94	0.03	0.18	63.00
		*8	0.04	44.00	543.00	63.00	0	33.00	774.00	78.00	0	18.00	331.00	5.00	0	21.00	349.00	49.00
		*9	0.28	0.01	0.03	16.00	0.17	83.00	0.03	18.00	0	45.00	856.00	77.00	0.04	38.00	0	6.00
		*10	0.69	0.03	0.08	34.00	0.43	0.02	0	32.00	0	78.00	0.02	14.00	0.11	67.00	0	11.00
		*11	0	13.00	45.00	21.00	243.00	95.00	13.00	35.00	0	93.00	61.00	26.00	0	12.00	143.00	33.00
		*12	0	0.02	0	22.00	0.22	0.01	0.04	21.00	0.10	53.00	0.01	89.00	0.06	48.00	0	8.00
		*13	0	93.00	0.02	12.00	0.11	66.00	0.02	13.00	0.05	36.00	612.00	67.00	0.03	33.00	669.00	71.00
		*14	41.00	2.00	45.00	19.00	44.00	15.00	48.00	23.00	233.00	88.00	47.00	21.00	3.00	13.00	114.00	3.00
		*15	73.00	2.00	0	29.00	9.00	17.00	19.00	39.00	269.00	8.00	0	23.00	0	15.00	71.00	24.00
		*16	0.77	0.03	0	42.00	0	0.02	0.11	46.00	0.29	0.01	0.04	21.00	0.27	0.01	0.04	21.00
		*17	0.02	29.00	0	43.00	0.02	24.00	2.00	42.00	0	98.00	0	28.00	71.00	16.00	108.00	33.00
		*18	0	93.00	0	12.00	0.09	56.00	0.02	13.00	0.05	33.00	586.00	64.00	0.05	42.00	907.00	81.00
		*19	0.14	88.00	0.01	1.00	0	5.00	0	1.00	0	29.00	0	49.00	0	24.00	342.00	52.00
	PEC-15-31BI	G1@1	10.60	0.42	1.33	0.06	6.49	0.27	1.16	0.05	2.71	0.11	0.32	0.01	1.84	0.08	0.23	0.01
		G2@1	0.85	0.04	0.12	61.00	0.70	0.03	0.14	71.00	0.36	0.02	0.05	3.00	0.37	0.02	0.06	34.00
		G3@1	5.91	0.24	0.70	0.03	3.44	0.14	0.65	0.03	1.66	0.07	0.21	92.00	1.34	0.06	0.20	96.00
		G4@1	0.26	0.02	0.04	27.00	0.29	0.02	0.07	41.00	0.29	0.02	0.05	33.00	0.45	0.02	0.07	43.00
		G5@1	0.31	0.02	0.06	35.00	0.42	0.02	0.09	49.00	0.22	0.01	0.03	22.00	0.17	0.01	0.02	2.00
		G5@2	3.36	0.14	0.32	0.01	1.54	0.07	0.29	0.01	0.88	0.04	0.14	7.00	1.08	0.05	0.20	99.00
		G6@1	4.07	0.17	0.54	0.02	2.89	0.13	0.54	0.03	1.36	0.06	0.14	74.00	0.97	0.05	0.11	64.00

* All values are in ppm unless otherwise indicated
* Ca wt% values were measured via microprobe
* Hyphens indicate where no measurement was taken
* Sample codes beginning with "*" were measured during the in-situ analysis

Table DR-1: Trace element geochemisry of vein calcite

Station	Sample number	Point analysis	Pb206 (ppb)	σPb206	Pb207 (ppb)	σPb207	Pb208 (ppb)	σPb208	Th232 (ppb)	σTh232	U238 (ppb)	σU238	ΣREE	Eu/Eu*
X	PEC-15-4	G1@1	0.02	29.00	0	24.00	0	21.00	0	16.00	124.70	63.00	2.65	0.23
		G2@1	0	28.00	0	25.00	73.00	21.00	25.00	14.00	0	19.00	1083.15	0
		G3@1	0.01	29.00	0	24.00	0	22.00	0.05	27.00	147.80	73.00	139.60	0.15
		G4@1	0	27.00	0	23.00	0	23.00	0	24.00	109.00	32.00	6.00	0.25
		G5@1	0.01	27.00	0	23.00	0	21.00	132.00	31.00	71.60	38.00	1395.07	20496.81
		G5@2	79.00	28.00	0.02	28.00	0	24.00	0	29.00	98.30	51.00	8.13	0.21
	PEC-15-31A	G1@1	73.00	22.00	0.03	25.00	82.00	18.00	95.00	25.00	5.65	52.00	23.38	0.22
		G2@1	0.02	3.00	69.00	2.00	0.01	19.00	0	1.00	142.90	72.00	695.08	0.21
		G3@1	0	2.00	0	19.00	0	16.00	35.00	14.00	1.86	31.00	25.37	0.21
		G4@1	0.01	25.00	9.00	2.00	0	18.00	0.01	1.00	106.90	54.00	191.79	0.20
		G4@2	0.85	0.04	0.32	0.02	0.61	0.03	0.07	36.00	70.40	36.00	1.77	0.91
		G5@1	0.02	26.00	0	19.00	0	17.00	0.03	18.00	237.00	0.01	670.83	0.40
		G5@2	89.00	22.00	47.00	18.00	0	16.00	0.03	15.00	64.20	33.00	1099.89	0.19
		*1	89.00	31.00	69.00	3.00	9.00	17.00	512.00	5.00	106.00	38.00	16.72	0
		*2	0.03	38.00	67.00	27.00	44.00	18.00	0.24	79.00	542.00	0.02	229.62	0
		*3	72.00	29.00	69.00	27.00	56.00	19.00	51.00	17.00	2.93	37.00	12.91	0
		*4	68.00	27.00	64.00	28.00	43.00	18.00	105.00	3.00	42.20	18.00	163.46	0.18
		*5	63.00	34.00	68.00	35.00	44.00	22.00	85.00	3.00	94.90	41.00	4.37	0
		*6	0.02	28.00	72.00	27.00	57.00	17.00	39.00	18.00	115.20	41.00	597.22	23830.79
		*7	0.02	31.00	79.00	28.00	71.00	18.00	184.00	29.00	234.90	78.00	127.44	0.18
		*8	0.02	33.00	0.01	3.00	99.00	19.00	46.00	2.00	0	65.00	1997.16	0
		*9	0.01	25.00	52.00	22.00	41.00	17.00	57.00	19.00	0.46	21.00	862.04	0
		*10	0.39	0.02	0.36	0.01	0.39	0.01	0.05	2.00	63.00	25.00	12.85	0
		*11	63.00	27.00	76.00	3.00	68.00	17.00	0	19.00	28.50	14.00	967.01	0
		*12	0.02	27.00	77.00	28.00	62.00	18.00	957.00	72.00	51.60	21.00	1.31	0
		*13	63.00	27.00	7.00	3.00	52.00	17.00	745.00	63.00	35.40	16.00	1282.31	0
		*14	63.00	26.00	82.00	29.00	44.00	17.00	47.00	17.00	46.90	2.00	684.03	2.71
		*15	6.00	26.00	78.00	23.00	43.00	17.00	21.00	12.00	12.18	77.00	1099.03	2.45
		*16	74.00	28.00	7.00	29.00	53.00	15.00	46.00	17.00	1.76	28.00	6.94	0.20
		*17	0.03	32.00	67.00	27.00	39.00	16.00	323.00	41.00	248.30	84.00	1043.09	0
		*18	0.05	42.00	0.04	37.00	0.03	25.00	283.00	37.00	243.30	83.00	1493.98	0
		*19	63.00	25.00	56.00	22.00	39.00	15.00	36.00	14.00	0.94	2.00	344.27	0
	PEC-15-31BI	G1@1	0.01	33.00	0	27.00	0	27.00	0.08	42.00	100.90	52.00	216.36	0.16
		G2@1	0	31.00	0	31.00	0	26.00	0	33.00	0	3.00	13.42	0.22
		G3@1	9.00	33.00	0	31.00	0	27.00	0.04	23.00	28.00	18.00	239.20	0.19
		G4@1	0.06	57.00	98.00	36.00	0	33.00	0.02	16.00	892.00	0.04	3.26	0.22
		G5@1	0.01	42.00	0	36.00	0.01	35.00	0.42	0.02	135.80	7.00	3.62	0.21
		G5@2	0.01	43.00	0	37.00	0	36.00	0.12	59.00	121.50	63.00	266.08	0.19
		G6@1	0.02	51.00	93.00	42.00	0	38.00	0.03	21.00	80.60	47.00	73.96	0.17

* All values are in ppm unless otherwise indicated
* Ca wt% values were measured via microprobe
* Hyphens indicate where no measurement was taken
* Sample codes beginning with "*" were measured during the in-situ analysis

Table DR-1: Trace element geochemisry of vein calcite

Station	Sample number	Point analysis	Ca Wt%*	Ca	σCa	Mg	σMg	Si	σSi	Mn	σMn	Fe	σFe	Sr	σSr
X	PEC-15-31BIII	G1@1	55.65	397731.09	12580.89	380.11	13.46	374.76	16.52	1071.73	34.82	1625.54	55.26	97.11	3.00
		G2@2	55.43	396158.75	12531.16	388.91	13.77	359.09	15.83	976.67	31.73	1509.11	51.30	106.13	3.28
		G2@1	56.03	400446.94	12667.07	402.01	14.24	380.66	16.82	879.16	28.56	1047.76	35.62	54.60	1.69
		G3@1	56.08	400804.28	12696.19	415.81	14.76	347.48	16.76	880.61	28.63	1125.21	38.29	55.87	1.73
		G4@1	55.65	397731.09	12581.13	426.74	15.11	361.79	16.00	1105.40	35.91	1206.98	41.03	64.54	1.99
		G5@1	55.93	399732.25	12644.55	113.22	4.01	381.34	16.84	577.73	18.77	327.65	11.14	17.24	0.53
	PEC-15-31C	G1@1	54.91	392442.34	12418.79	388.48	14.00	395.69	17.31	627.33	19.86	1359.23	182.67	106.90	3.43
		G2@1	55.37	395729.94	12523.86	398.42	14.36	396.61	17.61	754.06	23.88	1311.09	176.20	74.35	2.39
		G3@1	54.68	390798.53	12367.12	476.77	17.18	393.10	17.18	1243.10	39.36	1177.99	158.32	53.61	1.72
		G4@1	54.79	391584.72	12391.44	379.74	13.69	398.72	17.33	578.02	18.30	1286.33	172.88	107.88	3.47
		G5@1	54.72	391084.44	12376.3	482.64	17.40	411.18	17.89	1006.07	31.86	1282.66	172.38	65.34	2.10
		G5@2	54.78	391513.25	12389.27	424.92	15.32	424.93	18.37	778.57	24.65	1503.00	201.99	113.76	3.66
XI	PEC-15-5A	G1@1	53.82	384652.06	12180.14	2740.93	102.39	274.45	35.12	3327.52	134.32	3936.43	431.72	188.07	7.75
		G2@1	53.73	384008.81	12161.14	3847.78	143.74	246.01	31.71	3218.26	129.91	4456.87	488.80	116.32	4.79
		G3@1	53.42	381793.25	12120.58	3246.49	121.42	252.45	32.83	4084.50	165.01	4455.12	488.67	117.07	4.83
		G4@1	54.44	389083.19	12318.36	3246.11	121.25	227.07	29.16	3166.18	127.80	4198.77	460.49	150.05	6.18
		G5@1	54.18	387224.94	12258.53	3638.03	135.88	238.54	30.21	3470.37	140.07	4257.35	466.91	109.04	4.49
		G5@2	54.51	389583.50	12331.29	1445.77	54.00	231.51	29.40	1700.55	68.64	2251.66	246.94	637.07	26.23
		G6@1	55.17	394300.50	12482.35	3385.50	126.45	207.46	26.35	2563.04	103.45	4110.43	450.80	129.35	5.33
		*1	54.85	392034.94	12402.83	29212.35	3923.07	265.89	11.83	25515.11	1427.54	38742.93	4447.82	899.19	28.92
		*2	54.77	391456.00	12384.95	29305.23	3935.55	269.42	12.07	25515.36	1427.56	37845.33	4344.78	768.35	24.71
		*3	54.54	389826.53	12334.16	27348.63	3672.80	268.87	12.10	28007.10	1566.99	35750.26	4104.27	730.06	23.48
		*4	54.27	387861.06	12272.03	27401.10	3679.85	282.88	12.66	25013.94	1399.53	35505.52	4076.17	815.87	26.24
		*12	53.11	379584.84	12010.41	27109.54	3640.69	245.45	11.23	22633.55	1266.35	36511.68	4191.68	1260.18	40.53
		*5	54.94	392663.88	12423.43	23144.20	3108.16	251.46	11.39	22422.39	1254.52	31798.86	3650.62	1046.79	33.66
		*6	55.30	395251.09	12506.17	28961.04	3889.34	265.25	12.12	26349.39	1474.25	37200.55	4270.77	892.62	28.71
		*7	55.34	395515.53	12514.79	30834.11	4140.89	263.06	12.08	29302.30	1639.47	38932.71	4469.63	816.91	26.27
		*13	54.16	387082.06	12247.16	31042.43	4168.86	356.28	15.56	25133.39	1406.20	40388.38	4636.74	810.80	26.08
		*8	54.46	389247.66	12314.83	30269.74	4065.08	261.83	11.64	24979.17	1397.56	39929.28	4584.02	871.88	28.04
		*9	54.41	388861.66	12302.64	10914.11	1465.72	247.98	11.13	13536.43	757.35	20912.81	2400.86	4151.80	133.49
		*10	55.33	395479.81	12512.71	25512.39	3426.20	255.40	11.55	20337.17	1137.86	33571.87	3854.17	1081.00	34.76
		*11	54.78	391491.78	12387.76	16878.72	2266.75	302.44	13.71	17685.53	989.52	25058.01	2876.76	1911.74	61.48
	PEC-15-5B	G1@1	55.01	393157.00	12467.16	3010.91	112.55	258.46	34.60	2396.79	96.80	3694.21	405.18	144.44	5.96
		G2@1	54.19	387296.44	12268.43	2749.14	102.72	275.83	35.79	1712.04	69.12	3374.52	370.10	143.97	5.93
		G3@1	53.83	384723.53	12185.82	3711.67	138.67	264.01	34.08	2986.74	120.58	4326.69	474.53	103.31	4.26
		G4@1	54.47	389297.59	12327.98	3597.79	134.40	208.23	27.26	2594.48	104.73	4185.13	459.00	149.85	6.17
		G5@1	54.92	392513.75	12435.21	2430.21	90.81	236.27	30.90	1490.11	60.16	3002.90	329.35	215.36	8.87
		G5@2	54.92	392513.75	12434.68	1673.23	62.53	255.95	33.37	1631.09	65.85	2390.06	262.13	94.53	3.90

* All values are in ppm unless otherwise indicated
* Ca wt% values were measured via microprobe
* Hyphens indicate where no measurement was taken
* Sample codes beginning with "*" were measured during the in-situ analysis

Table DR-1: Trace element geochemisry of vein calcite

Station	Sample number	Point analysis	Y	σY	Ba	σBa	Zr	σZr	La	σLa	Ce	σCe	Pr	σPr	Nd	σNd	Sm	σSm	Eu	σEu
X	PEC-15-31BIII	G1@1	0.58	0.02	0.08	66.00	-	-	0.16	59.00	0.53	0.02	0.09	34.00	0.37	0.02	0.08	58.00	0.02	14.00
		G2@2	1.10	0.04	0.15	99.00	-	-	0.36	0.01	1.16	0.04	0.18	64.00	0.84	0.03	0.18	96.00	0.04	21.00
		G2@1	0.12	47.00	0.02	35.00	-	-	0.03	17.00	0.09	37.00	0.02	1.00	0.10	68.00	0.03	34.00	52.00	79.00
		G3@1	0.16	88.00	0.03	0.01	-	-	0.02	26.00	0.08	55.00	0.01	18.00	0.14	0.02	0.03	7.00	0.01	24.00
		G4@1	0.15	56.00	0.28	0.02	-	-	0.02	14.00	0.09	37.00	0.02	12.00	0.15	86.00	0.05	44.00	894.00	97.00
		G5@1	0.51	0.02	0.01	31.00	-	-	1.58	0.05	4.28	0.14	0.53	0.02	2.08	0.08	0.24	0.01	0.04	24.00
	PEC-15-31C	G1@1	1.90	0.06	0.13	0.01	-	-	0.80	0.03	2.08	0.08	0.29	0.01	1.27	0.06	0.20	0.01	0.05	32.00
		G2@1	1.62	0.06	0.03	59.00	-	-	0.40	0.02	1.06	0.04	0.16	73.00	0.68	0.03	0.13	0.01	0.03	24.00
		G3@1	0.65	0.02	0.01	56.00	-	-	0.13	59.00	0.41	0.02	0.09	43.00	0.60	0.03	0.19	0.01	0.04	28.00
		G4@1	1.91	0.06	0.10	0.01	-	-	0.71	0.03	2.07	0.08	0.31	0.01	1.39	0.06	0.27	0.02	0.06	4.00
		G5@1	0.12	55.00	0	49.00	-	-	92.00	11.00	0.07	37.00	0.03	19.00	0.21	0.01	0.07	72.00	0.01	16.00
		G5@2	0.41	0.02	0.02	49.00	-	-	0.04	26.00	0.16	72.00	0.03	21.00	0.18	0.01	0.04	51.00	0.01	15.00
XI	PEC-15-5A	G1@1	46.39	1.65	0.34	0.04	-	-	14.93	0.65	64.12	3.98	11.77	0.56	48.06	2.07	10.82	0.48	2.05	0.10
		G2@1	1.70	0.06	0.19	0.03	-	-	0.53	0.03	1.75	0.11	0.41	0.02	1.39	0.07	0.35	0.03	0.06	56.00
		G3@1	10.86	0.40	0.19	0.04	-	-	2.80	0.13	13.24	0.83	2.38	0.12	10.31	0.48	2.21	0.13	0.44	0.03
		G4@1	1.72	0.06	0.04	0.01	-	-	0.42	0.02	1.46	0.09	0.28	0.02	1.27	0.07	0.39	0.03	0.07	56.00
		G5@1	4.81	0.17	0	0.01	-	-	2.15	0.09	7.06	0.44	1.18	0.06	4.96	0.22	1.13	0.06	0.20	0.01
		G5@2	129.39	4.59	0.47	0.05	-	-	76.03	3.27	231.10	14.35	36.05	1.71	140.90	6.05	30.57	1.32	5.78	0.26
		G6@1	1.97	0.07	0.19	0.03	-	-	0.64	0.03	2.28	0.14	0.38	0.02	1.56	0.08	0.39	0.03	0.07	57.00
		*1	72.53	3.15	8.66	0.44	0.09	0.04	28.71	1.35	93.64	3.85	0	0.59	0	2.84	14.89	0.67	3.07	0.14
		*2	47.50	2.07	2.63	0.18	0.06	0.03	14.51	0.69	47.77	1.97	7.73	0.32	0	1.61	0	0.41	1.89	0.09
		*3	60.81	2.64	4.15	0.26	0.10	0.04	0	0.98	64.63	2.66	10.27	0.42	47.82	2.04	0	0.53	2.32	0.11
		*4	102.54	4.45	0	0.22	0.09	0.04	43.27	2.04	129.21	5.31	19.72	0.81	91.36	3.85	0	0.96	0	0.19
		*12	251.89	10.93	3.29	0.22	0.09	0.04	136.01	6.38	0	16.51	60.40	2.45	269.33	11.22	58.18	2.49	11.88	0.50
		*5	120.09	5.21	40.96	1.83	0.12	0.04	66.98	3.15	195.97	8.04	29.18	1.19	0	5.73	0	1.19	5.49	0.24
		*6	98.21	4.27	1.90	0.15	0.12	0.05	44.00	2.07	131.24	5.39	19.93	0.82	0	4.05	21.03	0.94	4.28	0.19
		*7	63.14	2.75	1.78	0.15	0.11	0.05	28.22	1.33	0	3.44	0	0.52	60.87	2.59	13.05	0.61	2.61	0.13
		*13	35.29	1.54	0	0.21	0.36	0.08	13.68	0.65	0	1.76	6.50	0.27	0	1.37	6.43	0.33	1.40	0.07
		*8	78.03	3.39	6.47	0.35	0.09	0.03	26.91	1.27	90.89	3.73	0	0.57	67.56	2.85	15.48	0.70	0	0.15
		*9	1703.03	73.85	4.89	0.28	0.08	0.03	767.16	35.94	0	103.56	0	15.20	0	71.62	373.84	15.58	77.80	3.19
		*10	200.67	8.71	0	0.10	0.04	0.02	79.69	3.74	251.77	10.33	39.36	1.60	186.26	7.77	40.84	1.76	8.72	0.37
		*11	302.70	13.13	10.71	0.56	0.08	0.03	203.40	9.54	520.72	21.35	73.86	2.99	330.76	13.77	0	2.87	14.23	0.60
	PEC-15-5B	G1@1	10.76	0.39	1.51	0.15	-	-	5.28	0.23	18.69	1.16	3.05	0.15	12.58	0.57	2.55	0.14	0.52	0.03
		G2@1	7.41	0.27	8.05	0.70	-	-	7.86	0.34	23.60	1.47	3.60	0.17	14.63	0.64	2.65	0.13	0.44	0.03
		G3@1	0.74	0.03	0.16	0.03	-	-	0.22	0.01	0.84	0.05	0.13	86.00	0.64	0.04	0.09	0.01	0.03	44.00
		G4@1	4.87	0.18	0.08	0.02	-	-	2.19	0.10	7.34	0.46	1.23	0.06	5.14	0.23	1.14	0.06	0.21	0.01
		G5@1	28.30	1.01	0.09	0.02	-	-	20.88	0.90	65.74	4.08	10.43	0.50	43.12	1.87	8.21	0.37	1.70	0.08
		G5@2	8.49	0.31	0.04	0.02	-	-	7.13	0.31	21.74	1.35	3.47	0.17	14.18	0.63	2.35	0.12	0.46	0.03

* All values are in ppm unless otherwise indicated
* Ca wt% values were measured via microprobe
* Hyphens indicate where no measurement was taken
* Sample codes beginning with "*" were measured during the in-situ analysis

Table DR-1: Trace element geochemisry of vein calcite

Station	Sample number	Point analysis	Gd	σGd	Tb	σTb	Dy	σDy	Ho	σHo	Er	σEr	Tm	σTm	Yb	σYb	Lu	σLu
X	PEC-15-31BIII	G1@1	0.08	56.00	0.02	99.00	0.08	48.00	0.02	12.00	0.06	36.00	845.00	68.00	0.06	42.00	0.01	79.00
		G2@2	0.16	88.00	0.03	17.00	0.16	81.00	0.03	17.00	0.09	48.00	0.01	96.00	0.11	64.00	0.02	11.00
		G2@1	0.02	32.00	374.00	45.00	0.02	22.00	37.00	5.00	0.01	15.00	238.00	4.00	0.02	21.00	26.00	38.00
		G3@1	0.03	68.00	56.00	13.00	0.03	58.00	41.00	11.00	73.00	26.00	196.00	75.00	0.04	71.00	7.00	14.00
		G4@1	0.03	36.00	535.00	56.00	0.03	25.00	562.00	57.00	0.02	18.00	259.00	36.00	0.02	24.00	427.00	5.00
		G5@1	0.17	93.00	0.02	14.00	0.15	78.00	0.03	16.00	0.09	47.00	0.01	88.00	0.11	65.00	0.02	11.00
	PEC-15-31C	G1@1	0.21	0.01	0.03	19.00	0.20	0.01	0.04	25.00	0.12	73.00	0.02	15.00	0.12	87.00	0.02	17.00
		G2@1	0.14	0.01	0.03	2.00	0.19	0.01	0.04	26.00	0.12	79.00	0.02	14.00	0.12	9.00	0.02	15.00
		G3@1	0.15	0.01	0.03	19.00	0.13	88.00	0.03	19.00	0.07	52.00	0.01	11.00	0.07	59.00	0.02	14.00
		G4@1	0.25	0.02	0.04	24.00	0.21	0.01	0.05	29.00	0.15	85.00	0.02	13.00	0.11	81.00	0.01	13.00
		G5@1	0.05	54.00	0.02	14.00	0.03	32.00	503.00	73.00	0.02	24.00	232.00	46.00	86.00	24.00	291.00	52.00
		G5@2	0.04	52.00	686.00	86.00	0.05	47.00	0.01	11.00	0.03	33.00	531.00	78.00	0.03	39.00	545.00	71.00
XI	PEC-15-5A	G1@1	10.13	0.42	1.44	0.06	7.69	0.33	1.43	0.06	3.42	0.14	0.42	0.02	2.24	0.11	0.31	0.02
		G2@1	0.34	0.03	0.06	47.00	0.29	0.02	0.06	44.00	0.21	0.01	0.05	4.00	0.15	0.01	0.03	28.00
		G3@1	2.25	0.13	0.31	0.02	1.83	0.10	0.32	0.02	0.93	0.06	0.12	99.00	0.78	0.06	0.12	96.00
		G4@1	0.35	0.03	0.06	42.00	0.35	0.02	0.07	46.00	0.17	0.01	0.02	21.00	0.12	0.01	0.02	21.00
		G5@1	0.95	0.05	0.14	77.00	0.85	0.04	0.18	93.00	0.44	0.02	0.05	38.00	0.42	0.03	0.06	39.00
		G5@2	28.03	1.14	4.08	0.17	22.55	0.93	4.15	0.17	10.09	0.41	1.30	0.06	7.28	0.31	0.91	0.04
		G6@1	0.39	0.03	0.05	35.00	0.34	0.02	0.07	45.00	0.18	0.01	0.02	23.00	0.12	0.01	0.02	18.00
		*1	13.40	0.61	0	0.10	12.68	0.59	0	0.11	5.69	0.27	0.67	0.04	4.19	0.22	0	0.03
		*2	7.88	0.38	1.32	0.07	8.34	0.40	1.52	0.08	4.14	0.21	0.53	0.03	3.07	0.17	0.47	0.03
		*3	10.27	0.49	1.62	0.08	0	0.53	2.12	0.10	0	0.28	0.71	0.04	4.98	0.26	0.67	0.04
		*4	18.52	0.84	3.00	0.14	0	0.84	0	0.17	8.38	0.40	1.15	0.06	7.39	0.36	1.08	0.06
		*12	0	2.15	0	0.33	0	1.94	7.87	0.36	0	0.83	2.13	0.10	0	0.60	0	0.08
		*5	23.14	1.03	0	0.16	22.00	1.00	4.01	0.19	10.17	0.47	0	0.07	0	0.41	0	0.06
		*6	0	0.80	2.85	0.13	18.05	0.83	0	0.16	0	0.42	1.12	0.06	0	0.36	0	0.05
		*7	11.16	0.53	0	0.09	11.50	0.55	2.18	0.11	0	0.28	0.82	0.05	0	0.27	0.80	0.04
		*13	5.94	0.30	0.93	0.05	0	0.30	1.15	0.06	2.60	0.14	0.32	0.02	2.25	0.13	0	0.02
		*8	0	0.66	0	0.10	0	0.64	0	0.12	6.26	0.30	0	0.04	4.43	0.23	0	0.03
		*9	323.68	13.74	49.00	2.12	286.11	12.62	50.21	2.23	115.67	5.14	13.60	0.62	75.38	3.33	9.51	0.42
		*10	35.60	1.56	0	0.26	0	1.57	0	0.31	16.29	0.75	2.02	0.10	12.11	0.57	1.71	0.08
		*11	57.46	2.50	8.85	0.39	51.44	2.31	9.18	0.42	22.14	1.01	0	0.13	0	0.71	0	0.10
	PEC-15-5B	G1@1	2.44	0.13	0.37	0.02	1.76	0.09	0.35	0.02	0.88	0.05	0.13	92.00	0.61	0.04	0.10	76.00
		G2@1	2.22	0.11	0.27	0.01	1.37	0.07	0.27	0.01	0.65	0.03	0.09	6.00	0.46	0.03	0.07	53.00
		G3@1	0.18	0.02	0.03	27.00	0.12	0.01	0.02	27.00	0.07	79.00	81.00	15.00	0.05	87.00	69.00	15.00
		G4@1	1.06	0.06	0.15	83.00	0.83	0.04	0.17	91.00	0.38	0.02	0.04	35.00	0.23	0.02	0.03	31.00
		G5@1	7.17	0.31	0.96	0.04	4.91	0.21	0.89	0.04	2.21	0.10	0.25	0.01	1.36	0.07	0.17	96.00
		G5@2	2.31	0.11	0.27	0.01	1.39	0.07	0.28	0.02	0.65	0.04	0.07	52.00	0.36	0.03	0.06	46.00

* All values are in ppm unless otherwise indicated
* Ca wt% values were measured via microprobe
* Hyphens indicate where no measurement was taken
* Sample codes beginning with "*" were measured during the in-situ analysis

Table DR-1: Trace element geochemisry of vein calcite

Station	Sample number	Point analysis	Pb206 (ppb)	σPb206	Pb207 (ppb)	σPb207	Pb208 (ppb)	σPb208	Th232 (ppb)	σTh232	U238 (ppb)	σU238	ΣREE	Eu/Eu*
X	PEC-15-31BIII	G1@1	0	18.00	43.00	16.00	48.00	14.00	0	15.00	0	14.00	846.57	0.21
		G2@2	0	17.00	47.00	15.00	31.00	13.00	0	15.00	3.00	11.00	3.38	0.21
		G2@1	0	18.00	0	17.00	0	15.00	126.00	25.00	1.26	23.00	727.35	1963.28
		G3@1	0.02	43.00	0	26.00	76.00	28.00	25.00	72.00	0	9.00	373.38	0.40
		G4@1	0	17.00	0	15.00	0	13.00	161.00	24.00	36.00	14.00	2677.43	22142.01
		G5@1	0	18.00	0	15.00	0	14.00	707.00	55.00	0	15.00	9.34	0.21
	PEC-15-31C	G1@1	0.25	0.01	0.06	44.00	0.16	87.00	33.00	5.00	54.00	24.00	5.45	0.22
		G2@1	0	32.00	0	31.00	0	26.00	53.00	26.00	2.99	5.00	3.14	0.19
		G3@1	0	3.00	0	25.00	0	24.00	228.00	42.00	26.50	17.00	1.94	0.21
		G4@1	0	29.00	0	76.00	0.01	24.00	254.00	45.00	0	33.00	5.64	0.24
		G5@1	0	29.00	0	26.00	0	23.00	294.00	54.00	0	36.00	1204.49	0.24
		G5@2	0	29.00	0	25.00	0.03	32.00	0	19.00	130.40	66.00	1762.63	0.35
XI	PEC-15-5A	G1@1	0.10	0.01	0.09	0.01	0.10	0.01	0.22	0.01	7.60	19.00	178.84	0.20
		G2@1	0.07	99.00	0.36	0.04	0.04	76.00	0.02	21.00	92.00	0.02	5.65	0.17
		G3@1	0.06	0.01	0.05	0.01	0.06	99.00	0.07	59.00	2.90	12.00	38.03	0.20
		G4@1	0.08	0.01	0.09	0.01	0.08	0.01	0.11	59.00	4.10	11.00	5.06	0.18
		G5@1	0.03	55.00	0.03	53.00	0.04	64.00	0.04	26.00	129.00	61.00	19.76	0.19
		G5@2	0.32	0.04	0.35	0.04	0.32	0.04	0.31	0.02	9.30	22.00	598.82	0.20
		G6@1	0.06	82.00	0.06	8.00	0.06	76.00	0.05	3.00	7.00	4.00	6.50	0.19
		*1	0.77	0.05	0.79	0.05	0.81	0.04	1.67	0.07	33.10	38.00	176.94	0.22
		*2	0.39	0.04	0.46	0.04	0.36	0.03	0.52	0.03	8.40	28.00	99.17	0
		*3	0.60	0.04	0.58	0.05	0.56	0.03	0	0.04	20.30	41.00	145.41	0
		*4	0.48	0.04	0.60	0.05	0.56	0.03	1.30	0.05	29.30	4.00	323.08	0
		*12	0.82	0.05	0.84	0.06	0.94	0.05	2.34	0.09	0	59.00	545.80	0
		*5	1.77	0.09	1.69	0.09	1.76	0.07	2.17	0.09	35.00	42.00	356.94	0
		*6	0.51	0.05	0.41	0.04	0.52	0.03	1.41	0.06	28.90	43.00	242.50	0
		*7	0.64	0.05	0.63	0.05	0.55	0.03	1.04	0.05	32.40	46.00	131.21	0.22
		*13	0.30	0.04	0.24	0.03	0.34	0.03	0.97	0.04	35.70	47.00	41.20	0.23
		*8	0.68	0.05	0.95	0.06	0.59	0.03	0.86	0.04	0	3.00	211.53	0
		*9	4.23	0.17	3.86	0.16	4.08	0.15	2.25	0.09	125.80	83.00	2141.96	0.22
		*10	0.59	0.04	1.07	0.06	0.61	0.03	2.13	0.08	0	54.00	674.36	0.23
		*11	1.84	0.09	1.74	0.09	1.85	0.08	0	0.06	0	75.00	1292.04	0
	PEC-15-5B	G1@1	0.12	0.02	0.11	0.02	0.13	0.02	0.14	88.00	49.00	17.00	49.30	0.21
		G2@1	0.16	0.02	0.12	0.02	0.14	0.02	0.17	93.00	10.10	26.00	58.17	0.18
		G3@1	0.03	78.00	0.04	72.00	0.03	63.00	58.00	14.00	161.00	76.00	152.43	0.27
		G4@1	0.05	9.00	0.04	78.00	0.05	8.00	0.07	46.00	155.00	72.00	20.13	0.19
		G5@1	0.10	0.01	0.06	0.01	0.07	0.01	0.14	79.00	19.70	46.00	167.99	0.22
		G5@2	0.03	95.00	0.03	8.00	0.03	74.00	0.03	26.00	9.00	23.00	54.72	0.20

* All values are in ppm unless otherwise indicated
* Ca wt% values were measured via microprobe
* Hyphens indicate where no measurement was taken
* Sample codes beginning with "*" were measured during the in-situ analysis

Table DR-1: Trace element geochemisry of vein calcite

Station	Sample number	Point analysis	Ca Wt%*	Ca	σCa	Mg	σMg	Si	σSi	Mn	σMn	Fe	σFe	Sr	σSr
XIII	PEC-15-6	G1@1	54.65	390584.06	12355.76	2280.13	85.14	185.82	23.31	422.88	17.07	2186.65	239.81	75.22	3.10
		G1@2	55.44	396230.22	12534.28	1022.91	38.20	186.97	23.45	304.31	12.28	1483.07	162.65	115.48	4.76
		G5@1	54.46	389226.13	12313.15	2034.47	75.97	186.59	23.42	350.49	14.14	2015.07	220.99	199.56	8.22
		G6@1	54.20	387367.91	12254.06	2365.10	88.31	181.79	22.80	392.96	15.86	2276.69	249.68	101.41	4.18
	PEC-15-7	G1@1	55.05	393442.94	12449.54	1635.88	58.92	452.83	19.35	333.42	10.56	993.51	133.52	44.68	1.44
		G2@1	55.34	395515.53	12520.19	1716.85	61.86	420.96	18.48	311.03	9.85	1021.47	137.28	63.13	2.03
		G3@1	54.96	392799.72	12429.42	1465.82	52.80	422.26	18.24	254.10	8.05	798.72	107.34	79.73	2.56
		G4@1	55.06	393514.41	12452.86	1742.59	62.77	433.79	18.88	297.51	9.42	952.51	128.01	65.89	2.12
		G5@2	55.25	394872.31	12495.9	1789.41	64.46	436.70	19.02	359.76	11.39	1079.48	145.08	47.30	1.52
XVI	PEC-15-8	G1@1	53.81	384580.59	12192.82	915.92	34.26	212.18	27.53	11057.95	446.53	3178.42	348.61	63.51	2.62
		G1@2	53.40	381650.31	12081.58	472.01	17.64	225.78	28.83	5794.93	233.90	1578.91	173.16	192.21	7.92
		G2@1	54.03	386152.97	12224.56	947.82	35.41	292.37	37.01	11076.23	447.06	3443.13	377.61	32.53	1.34
		G3@1	54.07	386438.81	12234.6	546.28	20.42	237.49	30.39	8173.94	329.93	2209.33	242.30	30.18	1.25
		G4@1	54.57	390012.34	12358.89	504.31	18.87	280.11	36.82	6689.75	270.10	2118.65	232.37	140.98	5.81
		G5@1	54.04	386224.41	12244.64	788.71	29.51	295.15	39.09	10281.17	415.16	2916.96	319.93	29.36	1.22
		*1	56.22	401790.53	12715.33	766.37	27.53	289.06	13.12	8588.75	283.57	2695.07	91.70	151.82	4.77
		*2	56.05	400625.56	12678.46	799.14	28.76	345.99	15.19	9489.41	315.36	2888.94	99.11	26.71	0.84
		*3	56.02	400396.88	12672.53	918.68	33.14	371.58	16.24	8844.20	296.39	2757.80	95.61	83.34	2.64
		*4	56.48	403648.81	12777.66	830.71	30.28	366.77	16.53	9630.71	334.10	2952.83	106.83	56.69	1.83
		*5	56.11	401033.03	12691	687.76	25.17	307.23	13.90	8504.05	299.23	2837.88	104.47	111.98	3.64
		*6	56.06	400668.50	12677.5	669.18	24.61	357.19	15.62	7903.09	282.42	2496.86	93.66	130.23	4.27
		*7	54.56	389926.53	12339.19	882.62	32.63	317.93	14.31	9497.93	345.12	2995.37	114.62	114.58	3.80
		*8	55.22	394607.84	12484.6	576.48	20.28	281.69	12.13	6872.80	208.19	2178.98	66.12	127.87	3.84
		*9	54.49	389440.53	12320.68	603.16	21.23	262.48	11.28	7356.58	222.84	2350.25	71.29	96.35	2.90
		*10	55.51	396701.91	12552.26	839.10	29.53	357.92	15.00	9489.93	287.50	2893.23	87.75	73.82	2.22
		*11	55.46	396358.88	12541.04	886.06	31.19	286.24	12.33	10596.63	321.03	3035.05	92.03	29.86	0.90
		*12	55.35	395625.59	12517.48	780.51	27.48	279.47	11.97	9609.60	291.13	2623.24	79.53	29.55	0.89
XVIII	PEC-15-10	G1@1	55.18	394371.94	12484.35	313.04	11.71	187.42	23.68	219.82	8.88	663.15	72.73	112.14	4.62
		G2@1	55.66	397802.56	12585.55	370.45	13.84	208.31	26.16	225.09	9.08	555.38	60.91	64.59	2.66
		G3@1	54.04	386224.41	12218.45	1905.89	71.17	188.02	23.61	460.84	18.60	2399.08	263.10	143.72	5.92
		G4@1	54.46	389226.13	60916.29	6244.65	734.54	330918.97	56416.65	808.97	104.47	3292.90	575.53	328.50	40.93
		G5@1	54.68	390798.47	12365.3	1795.63	67.06	196.78	24.77	479.15	19.34	2400.61	263.27	160.61	6.61
		G5@2	54.98	392942.59	12434.31	1849.63	69.08	250.56	31.48	501.40	20.24	2521.19	276.50	166.66	6.86
	PEC-15-28	G1@1	54.70	390941.38	12367.02	903.73	33.75	206.59	25.89	373.30	15.06	1237.19	135.68	407.59	16.78
		G2@1	55.09	393728.75	12455.44	689.44	25.75	193.54	24.27	367.77	14.84	1027.93	112.73	205.01	8.44
		G2@2	55.07	393585.81	12450.65	800.04	29.88	196.61	24.65	411.15	16.59	1209.00	132.59	222.28	9.15
		G3@1	54.82	391799.06	12403.73	977.02	36.50	187.58	23.66	444.68	17.95	1271.31	139.43	110.07	4.54
		G4@1	55.40	395944.31	12527.64	1436.14	53.63	184.58	23.19	465.48	18.79	1774.10	194.56	192.02	7.91
		G5@1	55.00	393085.53	12434.36	781.16	29.17	171.33	21.48	359.14	14.49	1081.45	118.60	354.86	14.61

* All values are in ppm unless otherwise indicated
* Ca wt% values were measured via microprobe
* Hyphens indicate where no measurement was taken
* Sample codes beginning with "*" were measured during the in-situ analysis

Table DR-1: Trace element geochemisry of vein calcite

Station	Sample number	Point analysis	Y	σY	Ba	σBa	Zr	σZr	La	σLa	Ce	σCe	Pr	σPr	Nd	σNd	Sm	σSm	Eu	σEu
XIII	PEC-15-6	G1@1	0.87	0.03	0.01	34.00	-	-	2.22	0.10	3.94	0.24	0.43	0.02	1.58	0.07	0.25	0.01	0.04	25.00
		G1@2	3.65	0.13	0.04	56.00	-	-	46.65	2.01	78.45	4.87	8.52	0.41	30.15	1.30	3.46	0.15	0.41	0.02
		G5@1	4.44	0.16	0.46	0.05	-	-	25.49	1.10	42.33	2.63	4.48	0.21	14.88	0.64	2.37	0.11	0.63	0.03
		G6@1	0.10	45.00	1.83	0.16	-	-	0.43	0.02	0.53	0.03	0.06	33.00	0.21	0.01	0.04	44.00	92.00	16.00
	PEC-15-7	G1@1	0.09	43.00	0	19.00	-	-	0.03	22.00	0.12	54.00	0.03	18.00	0.08	72.00	0.02	4.00	72.00	11.00
		G2@1	0.16	75.00	0	55.00	-	-	0.13	66.00	0.28	0.01	0.03	24.00	0.16	0.01	0.03	59.00	9.00	15.00
		G3@1	0.19	75.00	0.07	91.00	-	-	0.39	0.02	0.68	0.03	0.07	35.00	0.29	0.02	0.05	56.00	87.00	14.00
		G4@1	0.21	84.00	0	6.00	-	-	0.61	0.02	1.30	0.05	0.14	64.00	0.51	0.03	0.07	69.00	89.00	13.00
		G5@2	0.15	63.00	0	6.00	-	-	0.06	32.00	0.16	73.00	0.02	16.00	0.10	89.00	0.02	46.00	96.00	15.00
XVI	PEC-15-8	G1@1	75.60	2.69	0.11	0.02	-	-	1.93	0.09	6.86	0.43	1.39	0.07	8.49	0.39	4.11	0.20	0.67	0.04
		G1@2	404.49	14.34	1.22	0.11	-	-	42.45	1.83	80.29	4.99	9.57	0.46	37.96	1.64	10.42	0.46	1.50	0.07
		G2@1	100.58	3.57	0.40	0.04	-	-	4.23	0.18	10.86	0.68	1.85	0.09	9.64	0.42	4.27	0.20	0.67	0.03
		G3@1	229.65	8.15	0.17	0.02	-	-	32.59	1.41	72.61	4.51	9.21	0.44	39.92	1.72	13.97	0.61	2.13	0.10
		G4@1	376.50	13.36	1.28	0.13	-	-	46.79	2.02	93.56	5.81	11.55	0.55	46.03	1.99	13.62	0.61	2.06	0.10
		G5@1	40.64	1.45	0.22	0.04	-	-	2.29	0.10	7.76	0.48	1.51	0.08	8.38	0.38	2.80	0.15	0.40	0.03
		*1	177.80	5.55	2.18	0.08	0.01	54.00	16.60	0.53	34.12	1.07	4.50	0.14	0	0.75	7.07	0.24	1.09	0.04
		*2	27.26	0.86	0.12	0.01	0.02	6.00	2.01	0.07	0	0.17	0	0.03	0	0.20	1.80	0.07	0.29	0.01
		*3	59.41	1.87	0.57	0.03	0.06	91.00	2.69	0.09	8.38	0.26	1.74	0.06	11.92	0.41	3.83	0.14	0	0.02
		*4	62.71	2.01	0.68	0.04	0.03	76.00	3.52	0.12	0	0.26	0	0.04	6.79	0.25	2.54	0.10	0.39	0.02
		*5	125.79	4.05	0.61	0.03	0.05	8.00	11.02	0.37	0	0.77	3.27	0.11	17.43	0.62	0	0.21	0.95	0.03
		*6	186.06	6.04	1.32	0.05	0.05	66.00	11.59	0.39	25.67	0.83	0	0.12	18.68	0.67	0	0.24	1.04	0.03
		*7	144.04	4.72	1.52	0.06	0.02	65.00	11.53	0.40	24.71	0.80	0	0.11	0	0.65	6.00	0.23	0.89	0.03
		*8	112.34	3.38	1.17	0.05	0.02	43.00	9.03	0.27	0	0.60	0	0.09	0	0.42	0	0.13	0.69	0.02
		*9	98.79	2.97	0.54	0.03	0.05	63.00	8.72	0.26	0	0.55	0	0.08	12.36	0.38	3.25	0.10	0.55	0.02
		*10	89.10	2.68	0.63	0.03	0.04	66.00	0	0.17	0	0.37	1.84	0.06	10.36	0.32	3.69	0.12	0.60	0.02
		*11	77.03	2.32	0.16	0.01	0.06	76.00	7.71	0.23	16.06	0.49	2.11	0.07	0	0.34	3.70	0.12	0.62	0.02
		*12	191.42	5.75	0.21	0.01	0.09	89.00	7.30	0.22	18.73	0.57	0	0.10	0	0.65	9.01	0.28	1.50	0.05
XVIII	PEC-15-10	G1@1	79.00	13.00	0	56.00	-	-	0.01	18.00	0.01	16.00	17.00	56.00	54.00	26.00	32.00	25.00	0	53.00
		G2@1	0.32	0.01	0.41	0.04	-	-	0.18	87.00	0.39	0.03	0.05	3.00	0.20	0.01	0.04	55.00	0.01	14.00
		G3@1	0.19	79.00	0.09	0.01	-	-	0.19	89.00	0.35	0.02	0.05	29.00	0.20	0.01	0.05	53.00	0.06	39.00
		G4@1	0	2.47	0	29.15	-	-	0	1.55	0	1.36	1.88	1.10	0	8.41	5.44	3.90	0	2.45
		G5@1	0.04	24.00	0.09	0.01	-	-	9.00	11.00	0.02	21.00	297.00	57.00	0.01	3.00	0	14.00	261.00	66.00
		G5@2	0.05	33.00	0.20	0.02	-	-	98.00	12.00	0.03	24.00	491.00	82.00	0.01	31.00	0	26.00	0	67.00
	PEC-15-28	G1@1	0.49	0.02	0.08	94.00	-	-	1.42	0.06	2.79	0.17	0.34	0.02	1.34	0.06	0.19	0.01	0.27	0.01
		G2@1	387.00	59.00	0	28.00	-	-	0	27.00	0	31.00	0	19.00	0	11.00	0	15.00	0	29.00
		G2@2	201.00	48.00	0.03	42.00	-	-	115.00	34.00	209.00	39.00	59.00	24.00	29.00	11.00	0	1.00	84.00	35.00
		G3@1	5.00	11.00	0.06	0.01	-	-	111.00	62.00	258.00	76.00	8.00	45.00	0	25.00	56.00	31.00	49.00	47.00
		G4@1	0.47	0.02	0.02	52.00	-	-	0.05	3.00	0.28	0.02	0.07	4.00	0.36	0.02	0.10	87.00	0.04	32.00
		G5@1	0.25	97.00	0.05	65.00	-	-	0.42	0.02	0.77	0.05	0.10	54.00	0.42	0.02	0.06	54.00	0.06	37.00

* All values are in ppm unless otherwise indicated
* Ca wt% values were measured via microprobe
* Hyphens indicate where no measurement was taken
* Sample codes beginning with "*" were measured during the in-situ analysis

Table DR-1: Trace element geochemisry of vein calcite

Station	Sample number	Point analysis	Gd	σGd	Tb	σTb	Dy	σDy	Ho	σHo	Er	σEr	Tm	σTm	Yb	σYb	Lu	σLu
XIII	PEC-15-6	G1@1	0.22	0.01	0.03	16.00	0.14	79.00	0.03	17.00	0.09	52.00	0.01	1.00	0.09	6.00	0.01	1.00
		G1@2	2.21	0.09	0.18	8.00	0.77	0.03	0.15	67.00	0.37	0.02	0.05	27.00	0.35	0.02	0.05	28.00
		G5@1	1.80	0.08	0.20	87.00	0.87	0.04	0.14	65.00	0.33	0.02	0.04	22.00	0.21	0.01	0.03	19.00
		G6@1	0.02	32.00	339.00	49.00	0.02	24.00	35.00	48.00	0.01	16.00	137.00	36.00	0.01	19.00	16.00	32.00
	PEC-15-7	G1@1	0.02	36.00	215.00	43.00	0.02	25.00	436.00	63.00	0.02	22.00	203.00	41.00	66.00	19.00	135.00	32.00
		G2@1	0.01	44.00	43.00	79.00	0.03	4.00	86.00	12.00	0.04	41.00	312.00	67.00	0.03	44.00	442.00	79.00
		G3@1	0.05	53.00	523.00	67.00	0.02	31.00	475.00	69.00	0.01	19.00	563.00	7.00	0.01	24.00	101.00	37.00
		G4@1	0.06	65.00	652.00	84.00	0.04	4.00	815.00	93.00	0.02	25.00	17.00	5.00	0.02	32.00	313.00	55.00
		G5@2	0.04	48.00	622.00	8.00	0.03	36.00	528.00	74.00	0.02	26.00	146.00	41.00	91.00	27.00	184.00	46.00
XVI	PEC-15-8	G1@1	7.37	0.33	1.51	0.07	10.12	0.43	2.42	0.10	6.78	0.29	0.88	0.04	4.20	0.20	0.63	0.03
		G1@2	20.10	0.82	4.25	0.17	32.13	1.33	9.28	0.38	31.91	1.28	4.96	0.21	29.96	1.27	4.76	0.20
		G2@1	8.68	0.36	1.87	0.08	12.73	0.53	3.46	0.14	10.10	0.41	1.32	0.06	6.60	0.29	1.08	0.05
		G3@1	27.19	1.11	4.95	0.20	31.03	1.28	7.07	0.29	18.87	0.76	2.13	0.09	9.95	0.43	1.47	0.06
		G4@1	25.75	1.06	5.19	0.21	35.89	1.49	9.64	0.40	29.24	1.18	3.93	0.17	21.37	0.92	3.11	0.13
		G5@1	4.14	0.20	0.72	0.03	5.05	0.23	1.33	0.06	3.96	0.17	0.49	0.03	2.53	0.13	0.36	0.02
		*1	13.06	0.46	2.45	0.08	17.21	0.57	4.08	0.13	0	0.37	1.42	0.05	0	0.26	1.28	0.04
		*2	0	0.11	0.52	0.02	3.54	0.12	0.89	0.03	0	0.08	0	99.00	0	0.04	0.18	74.00
		*3	5.50	0.20	0	0.03	6.76	0.23	1.66	0.06	4.61	0.15	0	0.02	0	0.10	0	0.02
		*4	4.48	0.18	0	0.03	0	0.23	1.56	0.05	4.67	0.15	0	0.02	0	0.11	0	0.02
		*5	0	0.37	0	0.06	0	0.43	0	0.10	7.72	0.25	0.84	0.03	0	0.14	0.59	0.02
		*6	0	0.48	2.33	0.07	0	0.61	0	0.14	12.13	0.39	0	0.05	0	0.24	1.08	0.04
		*7	11.06	0.44	2.15	0.07	14.85	0.55	3.51	0.12	10.19	0.33	0	0.04	0	0.25	0	0.04
		*8	7.30	0.23	1.37	0.04	9.76	0.30	2.34	0.07	6.83	0.21	0.82	0.03	4.37	0.14	0.62	0.02
		*9	5.64	0.18	1.11	0.03	0	0.25	2.08	0.06	6.12	0.19	0	0.02	3.68	0.12	0	0.02
		*10	7.08	0.22	0	0.04	9.59	0.29	0	0.07	6.45	0.20	0.78	0.03	4.13	0.13	0	0.02
		*11	0	0.22	0	0.04	9.41	0.29	0	0.07	5.91	0.18	0.60	0.02	0	0.09	0	0.01
		*12	17.41	0.53	0	0.10	23.43	0.71	0	0.17	14.66	0.45	1.55	0.05	6.94	0.21	0.99	0.03
XVIII	PEC-15-10	G1@1	26.00	2.00	66.00	33.00	35.00	19.00	0	14.00	0	92.00	5.00	29.00	0	77.00	0	3.00
		G2@1	0.06	61.00	983.00	95.00	0.05	46.00	0.01	1.00	0.03	3.00	521.00	69.00	0.03	34.00	373.00	54.00
		G3@1	0.03	4.00	545.00	65.00	0.02	23.00	397.00	59.00	0.01	16.00	43.00	17.00	61.00	15.00	385.00	54.00
		G4@1	0	9.69	0	0	0	0	0	1.05	0	2.25	0	1.13	0	5.74	0	1.33
		G5@1	0.01	33.00	0	3.00	0	16.00	1.00	34.00	0	9.00	0	24.00	0	13.00	18.00	13.00
		G5@2	99.00	32.00	147.00	4.00	88.00	2.00	106.00	38.00	47.00	12.00	106.00	5.00	61.00	2.00	112.00	38.00
	PEC-15-28	G1@1	0.20	0.01	0.02	12.00	0.06	44.00	728.00	72.00	0.01	17.00	116.00	32.00	0	11.00	54.00	17.00
		G2@1	0	2.00	0	1.00	0	48.00	42.00	16.00	0	54.00	0	1.00	0	91.00	23.00	11.00
		G2@2	0	11.00	59.00	24.00	197.00	66.00	0	16.00	0	58.00	3.00	17.00	0	94.00	0	2.00
		G3@1	0	29.00	0	8.00	32.00	16.00	36.00	26.00	53.00	53.00	35.00	25.00	0	0	0	24.00
		G4@1	0.12	97.00	0.01	13.00	0.08	62.00	0.02	15.00	0.04	37.00	45.00	65.00	0.02	29.00	268.00	51.00
		G5@1	0.09	63.00	869.00	76.00	0.03	3.00	524.00	56.00	98.00	14.00	56.00	19.00	33.00	13.00	56.00	26.00

* All values are in ppm unless otherwise indicated
* Ca wt% values were measured via microprobe
* Hyphens indicate where no measurement was taken
* Sample codes beginning with "*" were measured during the in-situ analysis

Table DR-1: Trace element geochemisry of vein calcite

Station	Sample number	Point analysis	Pb206 (ppb)	σPb206	Pb207 (ppb)	σPb207	Pb208 (ppb)	σPb208	Th232 (ppb)	σTh232	U238 (ppb)	σU238	ΣREE	Eu/Eu*
XIII	PEC-15-6	G1@1	73.00	2.00	0	16.00	0	14.00	0.07	34.00	16.60	36.00	9.05	0.15
		G1@2	6.00	17.00	0	16.00	48.00	15.00	0.28	0.01	53.00	0.01	171.77	0.15
		G5@1	0.02	32.00	0.02	25.00	0.02	26.00	307.00	43.00	58.00	21.00	93.80	0.31
		G6@1	0	24.00	0	42.00	0	21.00	88.00	21.00	0	19.00	620.34	2858.77
	PEC-15-7	G1@1	0.10	65.00	0	25.00	0	22.00	0.02	12.00	6.00	61.00	1127.33	3568.91
		G2@1	0	28.00	0.88	0.04	53.00	23.00	572.00	77.00	2.57	51.00	892.75	444.75
		G3@1	0	29.00	0	25.00	0	22.00	185.00	37.00	7.28	69.00	1750.57	1908.01
		G4@1	0	27.00	0.04	36.00	0	24.00	0.02	12.00	8.95	83.00	1888.76	1426.84
		G5@2	0	0.01	0.07	5.00	0.09	54.00	646.00	69.00	12.80	11.00	1667.45	3364.14
XVI	PEC-15-8	G1@1	0.01	59.00	0	47.00	0	41.00	0.28	0.02	139.00	0.03	57.35	0.12
		G1@2	0	42.00	0	43.00	0.01	37.00	0.10	55.00	15.60	35.00	319.54	0.10
		G2@1	0.01	43.00	0	42.00	0	36.00	0.04	27.00	70.00	0.02	77.37	0.11
		G3@1	0	52.00	0	44.00	0	41.00	0.04	26.00	131.00	0.03	273.09	0.11
		G4@1	0	86.00	0	85.00	0	69.00	0.03	28.00	80.00	0.02	347.73	0.11
		G5@1	0.02	97.00	0	92.00	0	84.00	0	95.00	58.00	0.01	41.71	0.12
		*1	0.01	34.00	0.01	34.00	0.01	2.00	0.03	19.00	74.50	33.00	102.87	0.11
		*2	0.02	31.00	0.01	3.00	49.00	18.00	64.00	22.00	22.90	14.00	9.22	0
		*3	0.03	42.00	0.02	37.00	0.02	26.00	0.09	39.00	0	58.00	47.08	0
		*4	0.04	49.00	0.04	51.00	0.04	36.00	0.02	13.00	47.20	26.00	23.95	0.11
		*5	84.00	25.00	0.01	31.00	4.00	17.00	104.00	28.00	16.10	11.00	41.82	0
		*6	0.01	26.00	77.00	24.00	37.00	16.00	0	62.00	42.30	21.00	72.52	0
		*7	0.02	34.00	0.03	37.00	0.02	23.00	0.04	21.00	67.20	31.00	84.89	0.11
		*8	0.02	27.00	68.00	25.00	99.00	16.00	92.00	29.00	7.82	61.00	43.13	0
		*9	0.01	24.00	0.01	24.00	0.03	21.00	487.00	51.00	0	26.00	43.51	0.13
		*10	0.16	81.00	0.18	89.00	0.13	54.00	0	16.00	71.40	28.00	44.52	0.12
		*11	0.04	39.00	71.00	24.00	41.00	18.00	947.00	81.00	39.90	18.00	46.12	0
		*12	0.02	26.00	69.00	28.00	69.00	15.00	836.00	69.00	56.80	23.00	101.51	0.12
XVIII	PEC-15-10	G1@1	0	24.00	0.06	76.00	43.00	2.00	0	25.00	0.52	24.00	235.03	0
		G2@1	0.01	29.00	0.01	25.00	0.01	24.00	0.03	17.00	17.70	39.00	1878.06	0.23
		G3@1	0.03	43.00	0.01	24.00	0.06	66.00	312.00	43.00	0	19.00	1431.96	1.56
		G4@1	0	10.42	0	9.31	0	8.20	0	1.02	0	0.92	7.32	0
		G5@1	0	23.00	97.00	23.00	0	21.00	0	25.00	166.00	52.00	586.05	0
		G5@2	0	25.00	67.00	23.00	0	2.00	487.00	65.00	1.84	53.00	1355.04	0
	PEC-15-28	G1@1	53.00	17.00	83.00	18.00	0.05	56.00	0	18.00	2.41	59.00	904.63	1.39
		G2@1	39.00	17.00	4.00	17.00	39.00	16.00	0	16.00	0	15.00	65.00	0
		G2@2	0.14	0.02	0.14	0.02	0.14	0.02	0	14.00	79.00	27.00	755.00	0
		G3@1	0.10	0.01	0.13	0.02	0.12	0.01	0	17.00	0	16.00	638.00	0
		G4@1	0.03	38.00	0.03	4.00	0.03	4.00	0	2.00	58.00	23.00	314.19	0.39
		G5@1	7.00	17.00	45.00	15.00	39.00	13.00	0	11.00	1.55	42.00	1637.96	0.84

* All values are in ppm unless otherwise indicated
* Ca wt% values were measured via microprobe
* Hyphens indicate where no measurement was taken
* Sample codes beginning with "*" were measured during the in-situ analysis

Table DR-1: Trace element geochemisry of vein calcite

Station	Sample number	Point analysis	Ca Wt%*	Ca	σCa	Mg	σMg	Si	σSi	Mn	σMn	Fe	σFe	Sr	σSr
XX	PEC-15-11	G1@1	54.05	386295.88	12221.43	1539.07	57.47	213.76	26.84	487.86	19.69	2423.74	265.81	105.83	4.36
		G2@2	54.09	386581.75	12238.32	1688.89	63.09	253.21	31.86	534.72	21.59	2679.88	293.91	88.54	3.65
		G3@1	54.03	386152.94	12217.21	1628.38	60.81	201.25	25.30	502.19	20.27	2543.64	278.96	98.01	4.04
		G4@1	54.48	389369.06	12323.57	884.77	33.05	229.01	28.79	226.76	9.15	1143.03	125.36	181.35	7.47
		G5@1	54.15	387010.53	12243.63	1662.95	62.10	210.31	26.40	515.33	20.80	2609.05	286.13	127.35	5.24
		G6@1	54.37	388582.91	12294.53	1555.37	58.08	225.32	28.30	476.17	19.22	2413.96	264.74	105.19	4.33
XXV	PEC-15-26	G1@1	55.44	396230.22	12535.54	1868.42	69.77	216.80	27.20	464.67	18.75	2254.50	247.25	134.80	5.55
		G1@2	55.51	396730.50	12552.13	1771.24	66.14	236.66	29.70	514.86	20.78	2420.19	265.42	150.83	6.21
		G2@1	55.38	395801.41	12524.46	1528.95	57.10	221.08	27.79	473.10	19.09	2249.81	246.74	172.67	7.11
		G3@1	54.93	392585.22	12421.15	1549.94	57.88	230.33	28.92	468.58	18.91	2142.98	235.02	152.68	6.29
		G4@1	55.42	396087.28	12532.96	1573.56	58.76	233.83	29.40	491.79	19.85	2287.90	250.91	136.92	5.64
		G5@1	55.62	397516.66	12598.88	1943.73	72.65	210.41	26.92	452.98	18.30	2255.39	247.37	164.96	6.80
		G5@2	55.28	395086.69	12519.65	1981.76	74.07	205.18	26.31	452.04	18.26	2375.03	260.49	124.40	5.13
XXVI	PEC-15-30	G1@1	56.07	400732.78	12678.54	1075.75	40.17	218.40	27.42	312.45	12.61	1386.77	152.09	216.36	8.91
		G2@1	56.75	405592.78	12831.5	477.82	17.85	212.33	26.66	197.58	7.97	628.50	68.93	449.57	18.51
		G3@1	55.31	395301.09	12580.85	6165.60	230.80	424.50	53.97	153.11	6.21	878.26	96.36	327.47	13.52
		G3@2	54.38	388654.38	12302.69	6551.54	244.68	311.17	39.00	130.10	5.25	142.72	15.65	333.02	13.71
		G4@1	54.42	388940.25	16217.51	2244.19	98.81	6557.60	1042.51	236.05	11.57	1754.33	196.50	245.36	11.94
		G5@1	55.52	396801.97	12553.02	1786.31	66.70	412.75	51.56	374.49	15.11	2001.56	219.51	187.57	7.72
		*1	55.20	394486.34	12481.55	13634.29	1826.22	264.91	11.79	4079.18	228.62	17313.56	3541.27	2204.97	69.64
		*2	56.31	402440.97	12733.11	19077.49	2555.29	267.31	11.85	4939.40	276.83	21778.88	4454.59	1452.17	45.87
		*3	55.71	398138.47	12596.28	16665.38	2232.20	271.34	11.81	4720.56	264.56	20611.29	4215.78	2166.20	68.41
		*4	56.33	402569.59	12736.45	11784.89	1578.50	253.78	11.15	3885.26	217.75	16201.97	3313.91	2652.48	83.77
XXIX	PEC-15-32A	G1@1	55.86	399231.94	12634.36	1228.74	45.89	879.16	109.79	544.74	21.99	2214.16	242.83	170.69	7.03
		G2@1	54.56	389940.84	12341.71	2248.26	83.97	360.04	45.23	1033.07	41.70	2992.78	328.22	159.03	6.55
		G2@2	54.81	391727.63	12398.08	1674.59	62.55	243.43	30.84	616.95	24.90	2533.88	277.89	123.10	5.07
		G3@1	52.40	374503.31	11865.11	2033.21	75.98	224.65	28.77	650.83	26.28	2448.44	268.54	134.89	5.56
		G4@1	55.64	397659.56	12587.67	1716.43	64.11	322.30	40.68	633.38	25.57	2571.66	282.04	113.76	4.69
		G5@1	55.81	398874.59	12635.54	1551.97	58.00	285.72	36.89	632.13	25.52	2525.03	276.94	101.43	4.18
		G6@1	53.78	384366.16	12236.43	4685.86	175.45	457.93	58.69	81.03	3.30	1477.59	162.10	349.50	14.43
	PEC-15-32B	G1@1	54.43	389011.72	12305.39	2202.76	77.98	405.83	17.89	1306.86	42.45	2713.43	92.25	186.85	5.77
		G1@2	54.52	389654.97	12325.61	2438.16	86.32	410.80	18.06	1802.76	58.56	2709.11	92.10	131.96	4.08
		G2@1	54.49	389440.59	12320.96	2323.81	82.28	366.91	16.30	1242.23	40.36	2844.31	96.70	187.97	5.81
		G3@1	55.06	393514.34	12454	1943.27	68.82	402.29	18.12	832.72	27.06	2475.87	84.19	150.31	4.64
		G4@1	54.67	390727.00	12359.74	2429.07	86.00	382.77	16.96	891.25	28.95	2931.42	99.66	171.20	5.29
		G5@1	54.80	391656.13	12389.07	1838.12	65.08	390.59	17.25	2727.57	88.61	2737.14	93.05	65.58	2.03

* All values are in ppm unless otherwise indicated
* Ca wt% values were measured via microprobe
* Hyphens indicate where no measurement was taken
* Sample codes beginning with "*" were measured during the in-situ analysis

Table DR-1: Trace element geochemisry of vein calcite

Station	Sample number	Point analysis	Y	σY	Ba	σBa	Zr	σZr	La	σLa	Ce	σCe	Pr	σPr	Nd	σNd	Sm	σSm	Eu	σEu
XX	PEC-15-11	G1@1	0.11	5.00	0.19	0.02	-	-	0.04	27.00	0.10	66.00	0.01	11.00	0.08	67.00	0.01	23.00	171.00	58.00
		G2@2	0.05	38.00	0.05	0.01	-	-	0.02	2.00	0.05	42.00	83.00	13.00	0.03	56.00	0	25.00	228.00	9.00
		G3@1	0.04	24.00	0.25	0.02	-	-	0.02	17.00	0.04	33.00	582.00	72.00	0.02	3.00	68.00	23.00	95.00	36.00
		G4@1	6.47	0.23	0.22	0.03	-	-	3.77	0.16	12.02	0.75	1.97	0.10	8.88	0.39	1.89	0.09	0.41	0.02
		G5@1	0.15	62.00	0.02	45.00	-	-	0.09	47.00	0.18	0.01	0.02	17.00	0.09	73.00	0.02	28.00	723.00	99.00
		G6@1	0.02	15.00	63.00	26.00	-	-	529.00	72.00	0.01	13.00	178.00	44.00	61.00	28.00	0	11.00	0	29.00
XXV	PEC-15-26	G1@1	0.44	0.02	0.21	0.02	-	-	0.43	0.02	0.81	0.05	0.10	52.00	0.40	0.02	0.06	58.00	0.02	21.00
		G1@2	0.07	35.00	0.28	0.03	-	-	0.05	29.00	0.09	62.00	0.01	12.00	0.07	61.00	63.00	21.00	142.00	66.00
		G2@1	0.27	0.01	0.16	0.02	-	-	0.10	56.00	0.22	0.01	0.03	21.00	0.11	92.00	0.02	34.00	91.00	16.00
		G3@1	0.01	13.00	94.00	42.00	-	-	634.00	9.00	0.01	12.00	169.00	38.00	0.01	24.00	0	14.00	0	62.00
		G4@1	0.20	86.00	0.07	0.01	-	-	0.07	42.00	0.16	0.01	0.02	18.00	0.11	94.00	0.02	37.00	55.00	11.00
		G5@1	0.28	0.02	0.19	0.03	-	-	0.26	0.02	0.53	0.04	0.08	65.00	0.30	0.03	0.04	95.00	0.02	41.00
		G5@2	0.04	4.00	0.12	0.02	-	-	0.02	25.00	0.07	68.00	95.00	18.00	0.02	65.00	0.02	76.00	0	12.00
XXVI	PEC-15-30	G1@1	8.02	0.29	0.12	0.02	-	-	3.08	0.13	8.34	0.52	1.16	0.06	4.90	0.22	1.05	0.05	0.17	92.00
		G2@1	0.08	39.00	0.03	75.00	-	-	0.04	24.00	0.09	6.00	0.01	1.00	0.04	42.00	56.00	25.00	233.00	61.00
		G3@1	0.95	0.05	4.06	0.40	-	-	0.49	0.03	0.73	0.05	0.08	98.00	0.20	0.04	0.07	0.02	0	19.00
		G3@2	0.78	0.03	0.64	0.06	-	-	0.38	0.02	0.62	0.04	0.08	5.00	0.33	0.02	0.07	94.00	0.01	21.00
		G4@1	5.76	0.66	3.10	1.46	-	-	1.78	0.34	4.77	0.62	0.46	0.16	1.23	0.62	0.84	0.67	0.22	0.18
		G5@1	1.69	0.06	0.02	56.00	-	-	0.37	0.02	0.94	0.06	0.18	9.00	0.70	0.03	0.18	0.01	0.03	23.00
		*1	88.44	3.14	1.40	0.13	0.06	0.03	15.73	0.74	0	1.72	5.99	0.25	31.76	1.38	8.66	0.43	1.39	0.08
		*2	24.93	0.89	0.40	0.07	0.07	0.03	2.10	0.11	0	0.31	1.18	0.06	7.00	0.35	2.04	0.14	0.29	0.03
		*3	112.95	4.01	6.91	0.37	0.17	0.04	17.60	0.83	52.55	2.18	7.93	0.32	41.30	1.76	11.73	0.56	1.71	0.09
		*4	70.27	2.50	1.82	0.14	0.08	0.03	19.00	0.89	43.23	1.80	0	0.23	27.02	1.17	0	0.32	1.06	0.06
XXIX	PEC-15-32A	G1@1	5.16	0.18	0.55	0.05	-	-	2.36	0.10	8.78	0.55	1.58	0.08	7.91	0.35	1.52	0.07	0.30	0.02
		G2@1	1.02	0.04	0.27	0.03	-	-	0.40	0.02	2.25	0.14	0.51	0.03	2.84	0.13	0.61	0.04	0.19	0.01
		G2@2	1.69	0.06	0.05	99.00	-	-	0.65	0.03	2.05	0.13	0.39	0.02	2.20	0.10	0.43	0.03	0.14	84.00
		G3@1	0.61	0.03	0.04	0.01	-	-	0.22	0.01	0.57	0.04	0.10	7.00	0.63	0.04	0.08	0.01	0.07	7.00
		G4@1	1.27	0.05	0.10	0.02	-	-	0.45	0.02	1.73	0.11	0.37	0.02	1.86	0.09	0.39	0.03	0.10	71.00
		G5@1	0.89	0.04	0	0.02	-	-	0.41	0.02	1.14	0.07	0.22	0.01	1.12	0.06	0.22	0.02	0.06	65.00
		G6@1	1.67	0.08	1.41	0.17	-	-	2.18	0.11	3.19	0.21	0.41	0.03	1.54	0.12	0.20	0.04	0.04	83.00
	PEC-15-32B	G1@1	2.70	0.09	0.27	0.02	-	-	0.56	0.02	3.20	0.11	0.82	0.03	5.11	0.18	1.20	0.05	0.21	83.00
		G1@2	1.48	0.05	0.03	4.00	-	-	0.17	61.00	1.09	0.04	0.30	0.01	2.17	0.08	0.63	0.03	0.12	5.00
		G2@1	6.59	0.21	0.01	45.00	-	-	1.32	0.04	8.55	0.28	1.99	0.07	12.31	0.43	2.89	0.11	0.51	0.02
		G3@1	0.05	33.00	0.02	54.00	-	-	57.00	95.00	0.04	29.00	81.00	11.00	0.07	8.00	0.01	39.00	72.00	14.00
		G4@1	0.74	0.03	0.06	68.00	-	-	0.09	36.00	0.63	0.02	0.16	61.00	1.11	0.04	0.26	0.01	0.06	3.00
		G5@1	5.27	0.17	0.01	32.00	-	-	4.42	0.14	17.58	0.58	3.32	0.11	19.22	0.66	3.28	0.12	0.43	0.02

* All values are in ppm unless otherwise indicated
* Ca wt% values were measured via microprobe
* Hyphens indicate where no measurement was taken
* Sample codes beginning with "*" were measured during the in-situ analysis

Table DR-1: Trace element geochemisry of vein calcite

Station	Sample number	Point analysis	Gd	σGd	Tb	σTb	Dy	σDy	Ho	σHo	Er	σEr	Tm	σTm	Yb	σYb	Lu	σLu
XX	PEC-15-11	G1@1	0.01	32.00	199.00	38.00	0.01	18.00	238.00	51.00	39.00	11.00	47.00	22.00	0	12.00	65.00	28.00
		G2@2	9.00	37.00	0	22.00	64.00	22.00	119.00	52.00	0	12.00	58.00	35.00	22.00	17.00	0	2.00
		G3@1	0	27.00	37.00	17.00	44.00	13.00	0	3.00	209.00	9.00	0	19.00	0	13.00	76.00	3.00
		G4@1	1.69	0.08	0.20	97.00	0.99	0.05	0.20	99.00	0.48	0.02	0.06	39.00	0.35	0.02	0.04	28.00
		G5@1	0.02	34.00	195.00	43.00	0.01	2.00	27.00	46.00	52.00	12.00	146.00	32.00	42.00	14.00	0	36.00
		G6@1	0	17.00	32.00	16.00	25.00	11.00	0	35.00	0	11.00	0	27.00	0	96.00	0	28.00
XXV	PEC-15-26	G1@1	0.08	73.00	555.00	73.00	0.04	37.00	621.00	77.00	0.02	21.00	131.00	39.00	55.00	18.00	174.00	35.00
		G1@2	74.00	24.00	96.00	28.00	67.00	15.00	104.00	33.00	3.00	12.00	0	32.00	0	14.00	95.00	28.00
		G2@1	0.03	5.00	229.00	58.00	0.02	26.00	352.00	7.00	0.01	19.00	6.00	29.00	45.00	18.00	93.00	49.00
		G3@1	21.00	11.00	0	33.00	163.00	73.00	0	24.00	0	7.00	0	17.00	0	1.00	0	16.00
		G4@1	0.02	35.00	246.00	49.00	0.01	27.00	382.00	63.00	99.00	18.00	107.00	4.00	39.00	19.00	0	31.00
		G5@1	0.08	0.01	45.00	13.00	0.03	65.00	33.00	13.00	0.02	45.00	0	69.00	0	27.00	0	31.00
		G5@2	0	42.00	0	66.00	0	16.00	219.00	91.00	0	18.00	0	48.00	3.00	21.00	0	52.00
XXVI	PEC-15-30	G1@1	1.27	0.06	0.19	85.00	1.06	0.05	0.23	0.01	0.58	0.03	0.07	35.00	0.36	0.02	0.05	3.00
		G2@1	0.01	29.00	13.00	41.00	61.00	13.00	92.00	33.00	355.00	87.00	0	4.00	173.00	97.00	68.00	22.00
		G3@1	0.08	0.02	74.00	29.00	0.07	0.02	0.05	75.00	0.07	0.02	0.02	43.00	0.07	0.02	0.02	4.00
		G3@2	0.09	0.01	0.01	15.00	0.10	9.00	0.02	2.00	0.07	64.00	0.01	13.00	0.05	65.00	87.00	12.00
		G4@1	0	0.55	0	0.01	0.98	0.50	0	0.01	0.78	0.37	0	0.02	0	0.30	0	0.01
		G5@1	0.25	0.01	0.04	22.00	0.23	0.01	0.06	3.00	0.15	8.00	0.02	14.00	0.09	63.00	0.02	12.00
		*1	10.74	0.48	1.98	0.09	13.67	0.60	3.18	0.14	0	0.37	0	0.05	5.85	0.28	0.79	0.04
		*2	2.78	0.16	0	0.03	3.92	0.20	0	0.05	2.34	0.12	0	0.02	0	0.12	0.36	0.02
		*3	13.76	0.60	2.63	0.11	18.33	0.79	4.10	0.18	11.20	0.47	0	0.06	7.88	0.36	1.17	0.06
		*4	7.66	0.35	0	0.06	9.33	0.42	2.10	0.10	0	0.24	0.65	0.03	3.51	0.18	0	0.03
XXIX	PEC-15-32A	G1@1	1.39	0.07	0.16	78.00	0.78	0.04	0.15	75.00	0.36	0.02	0.05	31.00	0.26	0.02	0.03	24.00
		G2@1	0.45	0.03	0.04	3.00	0.21	0.01	0.03	24.00	0.06	56.00	512.00	92.00	0.03	55.00	525.00	95.00
		G2@2	0.45	0.03	0.04	3.00	0.22	0.01	0.04	29.00	0.11	81.00	0.01	12.00	0.05	69.00	0.01	13.00
		G3@1	0.14	0.02	94.00	18.00	0.06	92.00	0.02	22.00	0.03	52.00	3.00	1.00	0.01	47.00	137.00	62.00
		G4@1	0.33	0.02	0.03	28.00	0.20	0.01	0.03	28.00	0.06	61.00	62.00	11.00	0.03	51.00	7.00	12.00
		G5@1	0.25	0.02	0.02	28.00	0.14	0.01	0.02	3.00	0.06	77.00	56.00	14.00	0.06	9.00	37.00	11.00
		G6@1	0.24	0.04	0.03	54.00	0.17	0.03	0.04	71.00	0.10	0.02	0.02	42.00	0.07	0.02	0.02	44.00
	PEC-15-32B	G1@1	1.08	0.04	0.12	5.00	0.63	0.03	0.10	41.00	0.23	0.01	0.03	14.00	0.15	79.00	0.02	13.00
		G1@2	0.58	0.02	0.07	32.00	0.34	0.02	0.06	26.00	0.13	65.00	0.02	11.00	0.08	53.00	0.01	94.00
		G2@1	2.38	0.09	0.29	0.01	1.33	0.05	0.21	83.00	0.46	0.02	0.05	26.00	0.31	0.02	0.04	22.00
		G3@1	0.03	54.00	121.00	41.00	85.00	22.00	128.00	46.00	34.00	14.00	36.00	26.00	17.00	12.00	0	22.00
		G4@1	0.25	0.01	0.03	17.00	0.15	78.00	0.03	15.00	0.07	41.00	97.00	77.00	0.05	41.00	7.00	65.00
		G5@1	2.29	0.08	0.25	97.00	1.23	0.05	0.22	84.00	0.57	0.02	0.07	32.00	0.44	0.02	0.06	3.00

* All values are in ppm unless otherwise indicated
* Ca wt% values were measured via microprobe
* Hyphens indicate where no measurement was taken
* Sample codes beginning with "*" were measured during the in-situ analysis

Table DR-1: Trace element geochemisry of vein calcite

Station	Sample number	Point analysis	Pb206 (ppb)	σPb206	Pb207 (ppb)	σPb207	Pb208 (ppb)	σPb208	Th232 (ppb)	σTh232	U238 (ppb)	σU238	ΣREE	Eu/Eu*
XX	PEC-15-11	G1@1	0.11	0.01	0.10	0.01	0.10	0.01	62.00	29.00	1.44	39.00	759.27	15998.79
		G2@2	0.03	46.00	0.03	48.00	0.04	53.00	416.00	71.00	1.33	49.00	583.10	0
		G3@1	1.46	0.16	1.45	0.16	1.46	0.16	174.00	33.00	6.10	14.00	1111.08	0
		G4@1	0.07	91.00	0.15	0.02	0.04	57.00	0.02	17.00	27.80	61.00	32.94	0.23
		G5@1	0	21.00	0	2.00	0	16.00	4.00	2.00	0	16.00	1185.44	37381.44
		G6@1	54.00	22.00	45.00	2.00	0	19.00	0	24.00	0	2.00	825.01	0
XXV	PEC-15-26	G1@1	0.45	0.05	0.43	0.05	0.43	0.05	37.00	19.00	63.00	23.00	1537.95	0.35
		G1@2	58.00	22.00	0	22.00	0	18.00	0	2.00	0	2.00	644.21	2.08
		G2@1	0	24.00	0	22.00	0	19.00	0	18.00	0	14.00	816.53	3960.27
		G3@1	0	23.00	0	22.00	0	18.00	0	23.00	0	16.00	987.02	0
		G4@1	6.00	27.00	91.00	26.00	85.00	24.00	0	25.00	41.00	21.00	928.41	3356.72
		G5@1	0	38.00	0.01	45.00	77.00	36.00	0	57.00	41.00	35.00	79.35	0.46
		G5@2	0.02	52.00	0	4.00	69.00	36.00	0	31.00	0	29.00	317.12	0
XXVI	PEC-15-30	G1@1	44.00	2.00	0	2.00	56.00	18.00	153.00	3.00	1.83	5.00	22.51	0.15
		G2@1	0	22.00	66.00	2.00	0	18.00	0	26.00	0	18.00	1051.19	259.47
		G3@1	0.85	0.10	0.91	0.10	1.94	0.22	0.01	31.00	320.00	0.07	75.94	0
		G3@2	0.22	0.03	0.18	0.02	0.16	0.02	0.02	14.00	318.00	0.07	88.85	0.17
		G4@1	1.43	0.55	1.25	0.51	1.03	0.45	0.05	0.05	510.00	0.17	11.06	0
		G5@1	63.00	2.00	63.00	21.00	42.00	16.00	65.00	24.00	54.00	0.01	3.24	0.14
		*1	0.05	0.02	0.06	0.02	0.04	0.02	37.00	19.00	193.00	0.01	99.74	0.14
		*2	0.10	0.02	0.09	0.02	0.04	0.02	64.00	28.00	511.00	0.02	22.00	0.12
		*3	0.29	0.03	1.35	0.07	0.08	0.01	0.73	0.03	837.00	0.04	191.90	0.13
		*4	0.05	0.02	0.05	0.02	0.04	0.01	24.00	14.00	30.70	42.00	113.56	0
XXIX	PEC-15-32A	G1@1	0.02	44.00	0.03	52.00	0.04	52.00	0.09	49.00	15.80	35.00	25.64	0.21
		G2@1	0.03	52.00	0.01	41.00	0.02	38.00	0.02	15.00	232.00	76.00	1044.64	0.36
		G2@2	0	38.00	0	37.00	0	32.00	0	41.00	0.69	26.00	6.79	0.31
		G3@1	0	45.00	0	45.00	97.00	39.00	95.00	48.00	92.00	44.00	235.93	0.69
		G4@1	0.02	47.00	0	46.00	0	39.00	772.00	99.00	12.00	49.00	74.58	0.28
		G5@1	0	66.00	0.01	63.00	0	57.00	0	65.00	0	74.00	96.72	0.28
		G6@1	0.90	0.11	0.81	0.09	0.75	0.09	0.03	47.00	46.00	0.01	8.25	0.16
	PEC-15-32B	G1@1	0.01	19.00	48.00	17.00	89.00	17.00	0.24	89.00	19.90	11.00	13.46	0.19
		G1@2	53.00	18.00	0	15.00	42.00	16.00	0.10	4.00	12.86	76.00	5.76	0.19
		G2@1	0.01	2.00	0	17.00	0	16.00	0.12	5.00	3.55	43.00	32.64	0.20
		G3@1	0	23.00	0.01	24.00	87.00	21.00	0	22.00	0	13.00	631.16	3510.78
		G4@1	58.00	18.00	0	18.00	0	15.00	57.00	18.00	4.00	16.00	106.89	0.22
		G5@1	0	18.00	39.00	16.00	0	14.00	0.04	18.00	12.11	74.00	53.40	0.16

* All values are in ppm unless otherwise indicated
* Ca wt% values were measured via microprobe
* Hyphens indicate where no measurement was taken
* Sample codes beginning with "*" were measured during the in-situ analysis

Table DR-2: U-Pb geochronology data of vein calcite

Sample	Point analysis	Analysis								Standardized Concordia					Ages (Ma)					
		$^{207}Pb/^{206}Pb$	σ2	$^{206}Pb/^{238}U$	σ2	^{238}U (Kcps)	Th/U	U (ppm)	^{206}Pb (ppm)	$^{207}Pb/^{235}U$	σ2	$^{206}Pb/^{238}U$	σ2	RhoXY	Model Age	σ2	$^{206}Pb/^{238}U$	σ2	$^{207}Pb/^{235}U$	σ2
PEC-15-2A	1	0.695	0.072	0.1925	0.0170	43	1.78	0.23	0.057	23.585	3.209	0.2479	0.0219	0.64842	281.4	144.7	1427.8	112.0	3251.4	126.7
	6	0.274	0.016	0.0174	0.0005	28	0.05	0.16	0.004	0.840	0.055	0.0223	0.0006	0.43284	101.8	4.1	142.4	4.0	619.3	30.2
	7	0.280	0.021	0.0154	0.0005	84	0.00	0.48	0.009	0.759	0.062	0.0197	0.0007	0.4344	88.9	4.6	125.9	4.5	573.2	35.5
	8	0.663	0.041	0.1814	0.0094	2	0.05	0.01	0.002	21.187	1.724	0.2325	0.0121	0.63847	318.3	78.7	1347.8	62.9	3147.2	76.8
	9	0.479	0.036	0.0255	0.0012	8	0.00	0.05	0.002	2.151	0.191	0.0327	0.0015	0.51307	94.2	10.6	207.2	9.3	1165.4	60.1
	10	0.177	0.014	0.0135	0.0004	48	0.00	0.27	0.005	0.422	0.036	0.0173	0.0005	0.37026	92.7	3.5	110.8	3.5	357.3	25.4
	11	0.336	0.020	0.0153	0.0005	26	0.00	0.15	0.003	0.913	0.063	0.0197	0.0006	0.4594	79.9	4.1	126.0	3.9	658.4	32.9
	12	0.384	0.041	0.0185	0.0011	85	0.02	0.49	0.012	1.261	0.152	0.0238	0.0014	0.4794	87.1	9.4	151.8	8.7	828.5	66.6
	13	0.321	0.024	0.0170	0.0006	182	0.00	1.05	0.023	0.970	0.081	0.0219	0.0008	0.4544	91.3	5.5	139.7	5.2	688.2	41.1
	16	0.699	0.042	0.1523	0.0074	62	0.48	0.37	0.072	18.810	1.458	0.1958	0.0096	0.6312	212.3	67.0	1152.8	51.4	3032.1	72.8
	18	0.644	0.087	0.0626	0.0059	346	0.15	2.07	0.166	7.115	1.177	0.0805	0.0076	0.5734	124.0	58.1	498.9	45.4	2125.9	139.9
	20	0.552	0.016	0.0725	0.0015	16	0.08	0.10	0.009	7.080	0.256	0.0934	0.0019	0.5620	212.9	13.1	575.7	11.2	2121.6	31.8
	21	0.439	0.038	0.0181	0.0009	10	0.01	0.06	0.001	1.408	0.142	0.0234	0.0012	0.4968	75.1	8.2	148.8	7.4	892.2	58.6
	22	0.595	0.066	0.0888	0.0070	4829	0.13	28.07	3.215	9.360	1.265	0.1145	0.0090	0.5795	221.0	62.7	699.1	51.7	2373.9	118.8
	23	0.730	0.074	0.0759	0.0057	79	0.35	0.46	0.045	9.814	1.233	0.0979	0.0073	0.5957	82.7	59.0	602.2	42.9	2417.5	111.2
	24	0.617	0.067	0.0803	0.0062	169	0.30	0.96	0.100	8.785	1.171	0.1036	0.0080	0.5790	181.5	57.7	635.5	46.5	2315.9	116.5
	25	0.673	0.075	0.0730	0.0059	1	0.28	0.01	0.001	8.715	1.203	0.0943	0.0076	0.5848	122.7	58.5	580.6	44.7	2308.7	120.3
PEC-15-2C	2C_1	0.575	0.066	0.0289	0.0021	2	0.01	0.00	-	3.309	0.453	0.0419	0.0031	0.5380	88.5	23.5	264.9	19.1	1483.1	102.6
	2C_2	0.295	0.035	0.0187	0.0011	5	0.07	0.00	-	1.094	0.144	0.0270	0.0016	0.4435	118.6	10.3	172.0	9.9	750.5	68.2
	2C_4	0.296	0.030	0.0152	0.0007	9	0.01	0.01	-	0.886	0.099	0.0218	0.0011	0.4416	95.8	7.0	139.3	6.8	644.1	52.2
	2C_5	0.373	0.039	0.0223	0.0013	4	0.03	0.00	-	1.630	0.196	0.0319	0.0018	0.4777	119.8	12.2	202.5	11.4	981.9	73.5
	2C_6	0.421	0.039	0.0370	0.0020	5	0.48	0.01	-	3.066	0.330	0.0531	0.0029	0.5039	178.0	19.2	333.5	17.6	1424.1	79.9
	2C_8	0.331	0.022	0.0235	0.0008	10	0.08	0.01	-	1.526	0.115	0.0337	0.0012	0.4623	137.9	7.7	213.6	7.3	940.8	45.6
	2C_9	0.541	0.047	0.0286	0.0016	3	0.02	0.00	-	3.043	0.313	0.0410	0.0022	0.5304	98.0	16.5	259.2	13.8	1418.5	76.3
	2C_10	0.410	0.042	0.0235	0.0014	4	0.02	0.00	-	1.892	0.223	0.0337	0.0020	0.4911	116.6	13.3	213.8	12.2	1078.2	76.1
	2C_11	0.406	0.033	0.0243	0.0011	6	0.06	0.01	-	1.939	0.182	0.0349	0.0016	0.4905	121.5	10.9	220.9	10.0	1094.6	61.4
PEC-15-5A	5A_2	0.777	0.009	1.0515	0.0180	4	3.47	0.00	0.004	160.451	3.294	1.5052	0.0258	0.8333	681.4	103.3	5920.1	65.9	5162.4	20.6
	5A_8	0.860	0.015	5.3896	0.3075	0	32.92	0.00	0.002	909.459	54.321	7.7054	0.4396	0.9552	0.0	0.0	13949.7	317.6	6918.8	59.0
	5A_9	1.034	0.012	5.1590	0.2066	1	9.16	0.00	0.004	1044.800	43.705	7.3562	0.2946	0.9573	0.0	0.0	13685.7	223.3	7059.5	41.7
	5A_10	0.865	0.013	4.2879	0.1892	1	12.70	0.00	0.003	726.639	33.921	6.1093	0.2696	0.9454	0.0	0.0	12644.0	239.9	6691.2	46.4
	5A_11	0.839	0.014	3.6816	0.1672	1	12.77	0.00	0.002	604.598	29.321	5.2414	0.2381	0.9368	-244.8	525.9	11804.7	241.4	6504.8	48.2
	5A_12	1.150	0.021	2.8536	0.1330	1	15.19	0.00	0.002	641.526	32.085	4.0594	0.1893	0.9322	0.0	0.0	10451.2	236.7	6564.9	49.7
	5A_13	1.710	0.040	1.0343	0.0434	1	16.39	0.00	0.001	345.085	16.581	1.4716	0.0618	0.8741	0.0	0.0	5833.1	159.2	5936.6	47.8
	5A_18	0.814	0.008	4.5402	0.1233	2	10.42	0.00	0.007	720.507	20.694	6.4598	0.1756	0.9462	1067.8	373.1	12954.3	149.9	6682.6	28.8
	5A_20	1.163	0.057	3.0886	0.4030	0	9.34	0.00	0.002	700.400	97.541	4.3900	0.5728	0.9369	0.0	0.0	10859.3	651.0	6653.9	133.4

Table DR-2: U-Pb geochronology data of vein calcite

Sample	Point analysis	Analysis								Standardized Concordia					Ages (Ma)					
		$^{207}Pb/^{206}Pb$	σ2	$^{206}Pb/^{238}U$	σ2	^{238}U (Kcps)	Th/U	U (ppm)	^{206}Pb (ppm)	$^{207}Pb/^{235}U$	σ2	$^{206}Pb/^{238}U$	σ2	RhoXY	Model Age	σ2	$^{206}Pb/^{238}U$	σ2	$^{207}Pb/^{235}U$	σ2
PEC-15-8	27	0.424	0.022	0.0225	0.0007	22	1.50	0.13	0.004	1.690	0.100	0.0290	0.0008	0.4956	96.6	5.8	184.2	5.3	1004.9	37.1
	28	0.424	0.022	0.0225	0.0007	22	1.50	0.13	0.004	1.690	0.100	0.0290	0.0008	0.4956	96.6	5.8	184.2	5.3	1004.9	37.1
	30	0.342	0.019	0.0193	0.0006	24	0.12	0.14	0.003	1.174	0.074	0.0249	0.0007	0.4648	99.6	4.8	158.7	4.6	788.3	34.0
	31	0.392	0.028	0.0244	0.0010	11	0.15	0.06	0.002	1.701	0.139	0.0315	0.0013	0.4864	113.1	8.5	200.1	7.8	1008.8	51.4
	32	0.405	0.036	0.0216	0.0011	15	0.38	0.09	0.003	1.550	0.157	0.0278	0.0014	0.4885	97.0	9.4	177.0	8.7	950.5	61.2
	33	0.283	0.020	0.0179	0.0006	20	0.10	0.12	0.003	0.902	0.072	0.0232	0.0008	0.4379	103.7	5.3	147.6	5.1	652.7	38.0
	34	0.405	0.034	0.0221	0.0010	140	0.03	0.85	0.024	1.591	0.151	0.0286	0.0013	0.4890	99.8	9.0	181.8	8.3	966.8	57.9
	32	0.217	0.014	0.0158	0.0005	21	0.09	0.16	0.003	0.609	0.044	0.0204	0.0006	0.3999	102.6	3.8	130.4	3.7	483.1	27.2
	33	0.519	0.029	0.0281	0.0010	9	1.20	0.07	0.002	2.596	0.171	0.0363	0.0013	0.5252	92.7	9.2	230.1	7.8	1299.5	47.4
	34	0.372	0.021	0.0213	0.0007	14	0.66	0.10	0.003	1.414	0.092	0.0276	0.0009	0.4774	103.3	5.7	175.4	5.4	894.9	38.0
	35	0.209	0.017	0.0147	0.0005	15	0.06	0.11	0.002	0.551	0.050	0.0191	0.0007	0.3942	96.9	4.4	121.8	4.3	445.9	32.1
	36	0.363	0.022	0.0206	0.0007	13	0.62	0.09	0.002	1.332	0.093	0.0266	0.0009	0.4736	101.6	5.9	169.3	5.5	859.8	40.0
	38	0.273	0.021	0.0179	0.0007	12	0.74	0.09	0.002	0.866	0.073	0.0231	0.0008	0.4326	105.2	5.4	147.0	5.3	633.2	39.1
	39	0.401	0.037	0.0234	0.0012	5	0.01	0.04	0.001	1.664	0.175	0.0302	0.0015	0.4887	106.0	10.5	191.5	9.7	994.9	65.0
	40	0.338	0.035	0.0179	0.0010	6	0.78	0.05	0.001	1.072	0.126	0.0231	0.0013	0.4619	93.0	8.3	146.9	7.9	739.6	60.2
	41	0.233	0.022	0.0156	0.0007	14	0.20	0.11	0.002	0.645	0.067	0.0202	0.0009	0.4091	98.6	5.5	128.7	5.4	505.5	40.9
PEC-15-25A	21A_2	0.779	0.104	0.2115	0.0253	1	0.07	0.00	-	32.491	5.813	0.3042	0.0364	0.6686	137.3	240.6	1711.9	177.4	3565.3	166.2
	21A_6	0.751	0.045	0.2638	0.0147	1	0.35	0.00	-	39.226	3.196	0.3805	0.0212	0.6845	254.0	137.1	2078.5	98.3	3751.3	78.5
	21A_7	0.604	0.045	0.0459	0.0023	3	0.09	0.00	-	5.486	0.489	0.0662	0.0033	0.5552	124.0	24.7	413.4	19.8	1898.3	74.5
	21A_8	0.882	0.064	0.5833	0.0531	1	0.26	0.00	0.001	101.804	11.866	0.8411	0.0765	0.7808	-284.4	380.8	3934.6	262.6	4704.1	112.6
	21A_10	0.628	0.130	0.3601	0.0723	0	1.38	.	-	44.759	12.909	0.5207	0.1046	0.6964	850.2	549.5	2701.9	428.7	3882.2	261.2
PEC-15-30	46	0.755	0.097	0.0731	0.0070	1	0.03	0.01	0.001	9.787	1.568	0.0940	0.0090	0.5978	57.7	72.6	579.1	52.8	2414.9	140.3
	47	0.778	0.044	0.1735	0.0085	1	0.04	0.01	0.002	23.906	1.791	0.2229	0.0109	0.6524	95.3	80.6	1297.3	57.2	3264.6	71.2
	48	0.814	0.162	0.2224	0.0407	1	0.02	0.00	0.001	32.072	8.659	0.2856	0.0522	0.6774	36.1	331.5	1619.3	256.7	3552.5	243.9
	49	0.734	0.016	0.3368	0.0073	5	0.68	0.04	0.016	43.721	1.353	0.4319	0.0094	0.7057	334.4	55.9	2314.2	42.3	3858.9	30.4
	57	0.810	0.023	0.1760	0.0044	4	0.01	0.04	0.008	25.343	0.973	0.2270	0.0057	0.6579	37.5	42.8	1318.6	30.0	3321.5	37.0
	57B	0.767	0.022	0.2384	0.0064	3	0.07	0.03	0.008	32.542	1.295	0.3074	0.0083	0.6775	156.2	56.2	1728.0	40.8	3566.8	38.7
PEC-15-31A	58	0.160	0.010	0.0154	0.0004	30	0.11	0.27	0.005	0.436	0.030	0.0198	0.0005	0.3586	108.6	3.1	126.4	3.1	367.2	20.9
	59	0.201	0.013	0.0162	0.0005	30	0.10	0.28	0.006	0.577	0.042	0.0209	0.0006	0.3894	107.6	3.8	133.3	3.7	462.3	26.7
	60	0.237	0.020	0.0176	0.0007	11	0.20	0.10	0.002	0.739	0.067	0.0226	0.0008	0.4131	109.9	5.5	144.4	5.4	561.7	38.6
	61	0.498	0.048	0.0305	0.0018	3	1.25	0.03	0.001	2.677	0.302	0.0391	0.0023	0.5213	106.8	16.4	247.5	14.2	1322.1	80.8
	62	0.293	0.019	0.0190	0.0006	22	1.20	0.20	0.005	0.983	0.071	0.0244	0.0008	0.4438	107.3	5.1	155.4	4.9	695.3	36.0
	64	0.492	0.021	0.0280	0.0007	16	0.11	0.15	0.005	2.428	0.121	0.0360	0.0009	0.5189	100.1	6.6	227.8	5.8	1251.0	35.3
	65	0.338	0.028	0.0194	0.0008	8	0.06	0.07	0.002	1.156	0.108	0.0250	0.0011	0.4630	100.9	7.1	159.0	6.8	780.2	50.0
	66	0.174	0.015	0.0159	0.0006	15	0.16	0.14	0.003	0.490	0.046	0.0205	0.0007	0.3700	110.1	4.6	130.8	4.5	404.6	30.9
	69	0.248	0.021	0.0176	0.0007	10	0.10	0.09	0.002	0.767	0.071	0.0226	0.0009	0.4193	108.0	5.7	144.1	5.6	578.3	40.4
	73	0.543	0.049	0.0290	0.0017	3	0.03	0.03	0.001	2.774	0.297	0.0373	0.0021	0.5314	88.5	15.7	235.9	13.2	1348.6	77.7
	81	0.488	0.133	0.0217	0.0035	6	0.05	0.05	0.001	1.869	0.594	0.0279	0.0045	0.5126	78.5	32.8	177.3	28.4	1070.0	195.1
	82	0.409	0.056	0.0266	0.0020	4	0.05	0.03	0.001	1.927	0.301	0.0342	0.0026	0.4932	117.7	17.9	216.7	16.4	1090.5	100.4
	84	0.364	0.040	0.0207	0.0012	4	0.02	0.04	0.001	1.334	0.166	0.0266	0.0016	0.4738	101.4	10.5	169.2	9.8	860.5	70.3